ISSN 2807-0461 (Print)
ISSN 2807-047X (Online)

University of Zadar

PROCEEDINGS

14th Annual Baška GNSS Conference:
Technologies, Techniques and Applications Across PNT

and

The 1st Workshop on
Smart, Blue and Green Maritime Technologies

Under the High Auspicies of

Baška, Krk Island, Croatia

10 – 12 May 2021

14th Annual Baška GNSS Conference:
Technologies, Techniques and Applications Across PNT
and
The **1st** Workshop on Smart, Blue and Green Maritime Technologies

PROCEEDINGS

14th Baška GNSS Conference:
Technologies, Techniques and Applications Across PNT and
The 1st Workshop on Smart Blue and Green Maritime Technologies
PROCEEDINGS

ISSN 2807-0461 (Print) | ISSN 2807-047X (Online)

Published by
University of Rijeka, Faculty of Maritime Studies, Rijeka, Croatia

For the Publisher
Prof Alen Jugović, PhD, Dean
University of Rijeka, Faculty of Maritime Studies, Rijeka, Croatia

Publisher's address
University of Rijeka, Faculty of Maritime Studies
Studentska 2, 51000 Rijeka, Croatia
Phone: +385 (0)51 338 411, Fax: +385 (0)51 336 755
URL: http://www.pfri.uniri.hr/
E-mail: dekanat@pfri.uniri.hr, GNSS_SBGMT@pfri.uniri.hr

Publishing Associates
Terry Moore, PhD, FRIN, FION, President
The Royal Institute of Navigation, London, UK
John Pottle, FRIN, Director
The Royal Institute of Navigation, London, UK

Editors
Assoc Prof David Brčić, PhD,
University of Rijeka, Faculty of Maritime Studies, Rijeka, Croatia
Assoc Prof Marko Valčić, PhD,
University of Zadar, Maritime Department, Zadar, Croatia
Academician Serdjo Kos, PhD, FRIN,
University of Rijeka, Faculty of Maritime Studies, Rijeka, Croatia

Photo credits
Front page: *Unsettled*, David Brčić

Text design
Tempora, Rijeka

Print
AKD d.o.o. Zagreb

14th Annual Baška GNSS Conference:
Technologies, Techniques and Applications Across PNT

and

The 1st Workshop on Smart, Blue and Green Maritime Technologies

Under the High Auspicies of

PROCEEDINGS

University of Zadar

Baška, Krk Island, Croatia

10 – 12 May 2021

International Programme and Organising Committee

John R Pottle, Director, The Royal Institute of Navigation, London, UK, *Chair*; **David Brčić**, University of Rijeka, Faculty of Maritime Studies, Croatia, *Co-Chair*; **Hrvoje Gold**, University of Zagreb, Faculty of Transportation and Traffic Sciences, Croatia, *Co-Chair*; **Serdjo Kos**, FRIN, University of Rijeka, Faculty of Maritime Studies, Croatia, *Co-Chair*; **Jasna Prpić-Oršić**, University of Rijeka, Faculty of Engineering, Croatia, *Co-Chair and Chair of Smart, Blue and Green Maritime Technology Workshop*; **Marko Valčić**, University of Zadar, Maritime Department, Zadar, Croatia, *Co-Chair and Conference Programme Chair*; **Franc Dimc**, University of Ljubljana, Faculty of Maritime Studies and Transport, Portorož, Slovenia; **Luka Grubišić**, University of Zagreb, Faculty of Science, Department for Mathematics, Zagreb, Croatia; **Tomislav Kos**, University of Zagreb, Faculty of Electrical Engineering and Computing, Zagreb, Croatia; **Tomislav Josip Mlinarić**, University of Zagreb, Faculty of Transport and Traffic Sciences, Zagreb, Croatia; **Nenad Sikirica**, Krapina University of Applied Sciences, Krapina, Croatia; **Clare Stead**, The Royal Institute of Navigation, London, UK, *Communications & Events Manager*; **Josip Vuković**, University of Zagreb, Faculty of Electrical Engineering and Computing, Zagreb, Croatia; **Srđan Žuškin**, University of Rijeka, Faculty of Maritime Studies, Rijeka, Croatia; **Mirano Hess**, University of Rijeka, Faculty of Maritime Studies, Rijeka, Croatia; **Mario Muštra**, University of Zagreb, Faculty of Transportation and Traffic Sciences, Croatia; **Barbara Pongračić**, iOLAP, Rijeka, Croatia; **George Shaw**, General Lighthouse Authority, London, UK; **Zeljko Marušić**, University of Zagreb, Faculty of Transport and Traffic Sciences, Zagreb, Croatia; **Mariusz Specht**, Gdynia Maritime University, Department of Transport and Logistics, Gdynia, Poland; **Danijel Šugar**, University of Zagreb, Faculty of Geodesy, Zagreb, Croatia

List of Reviewers

Andrej Androjna (University of Ljubljana, Faculty of Maritime Studies and Transport, Portorož, Slovenia); **Mate Barić** (University of Zadar, Maritime Department, Zadar, Croatia); **Bilal Beldjilali** (Agence Spatiale Algerienne, Department of Space Geodesy, Algiers, Algeria); **Jasmin Ćelić** (University of Rijeka, Faculty of Maritime Studies, Rijeka, Croatia); **Franc Dimc** (University of Ljubljana, Faculty of Maritime Studies and Transport, Portorož, Slovenia); **Serdjo Kos** (University of Rijeka, Faculty of Maritime Studies, Rijeka, Croatia); **Lovro Maglić** (University of Rijeka, Faculty of Maritime Studies, Rijeka, Croatia); **Đani Mohović** (University of Rijeka, Faculty of Maritime Studies, Rijeka, Croatia); **Josip Orović** (University of Zadar, Maritime Department, Zadar, Croatia); **Marko Perkovič** (University of Ljubljana, Faculty of Maritime Studies and Transport, Portorož, Slovenia); **Jasna Prpić-Oršić** (University of Rijeka, Faculty of Engineering, Rijeka, Croatia); **Mariusz Specht** (Gdynia Maritime University, Department of Transport and Logistics, Gdynia, Poland); **Boris Sviličić** (University of Rijeka, Faculty of Maritime Studies, Rijeka, Croatia); **Danijel Šugar** (University of Zagreb, Faculty of Geodesy, Zagreb, Croatia); **Sanjin Valčić** (University of Rijeka, Faculty of Maritime Studies, Rijeka, Croatia); **Srđan Vujičić** (University of Dubrovnik, Maritime Department, Dubrovnik, Croatia); **Josip Vuković** (University of Zagreb, Faculty of Electrical Engineering and Computing, Zagreb, Croatia)

CONTENTS

PREFACE

The satellite navigation can no longer be observed on its own. It is represented almost everywhere, with basic and advanced services implemented in all segments of everyday life.

The book you have in front of you contains selected papers from the 2021 Baška event, which took place in the period from 10 to 12 May, in Baška on the island of Krk, Croatia. This year's event had a special connotation for several reasons. After the 2020 corona outbreak and the consequent lockdown, and given that the measures were still globally present, the gathering was held in a hybrid form, using multiple remote communication platforms, combined with *in situ* attendance. The organisation and realisation of the hybrid event as a whole were challenging, but we believe it was managed smoothly, constructively and to the satisfaction of all participants. In one way or another – shoulder to shoulder, or interacting through screens across the globe.

The event comprised two segments. *The Annual Baška GNSS Conference*, the core event, was held for the fourteenth time, meaning for the fourteenth year in a row. It brought together a range of academic community members, students, professionals and enthusiasts, who presented their research results in the field of satellite navigation, and beyond.

The second part was a novelty. For the first time, the *Workshop on Smart, Blue and Green Maritime Technologies* took place. The vision of the Workshop was (and still is) to enhance current and future navigation applications to a broader research area, with a focus on technologies and solutions for safer, more reliable and greener shipping. The traditional conference concentrated on more application-oriented means and related improvements of existing, as well as the build-up of emerging maritime technologies.

During the conference, 22 scientists presented the results of their research. In addition to specialist sections, eight invited lectures were held by world-renowned experts and scientists in the field of satellite navigation and new maritime technologies. The event was attended by approximately 70 participants. Virtual discussions were held after each section during both conference and the workshop events. We coined the term *'virtual coffee break'*, which proved to be an excellent way of communication and further networking. The results could already see the light of day in 2022, in the same place, at about the same time.

The event was jointly organised by the Royal Institute of Navigation, London, the Faculty of Maritime Studies and Faculty of Engineering of the University of Rijeka, the Faculty of Transport and Traffic Sciences of the University of Zagreb, and the University of Zadar, Maritime Department. The whole event was held under the high auspices of the European Academy of Sciences and Arts, Salzburg, and the Croatian Academy of Engineering, Zagreb.

Perhaps it is needless to say, but we are genuinely proud of the successful realisation of the event, especially nowadays, when scientific conferences have become rarer and even ceased owing to well-known reasons. Our decision on organising the event in the first place, and then holding it 'live' (at least partially), proved to be justified, right and necessary as well, given that the spirit of the conference was maintained. It seems that we succeeded, both during the Baška days, as well as here, in presenting the research outputs in a published form.

Many people should be given credit for this event, starting with organisers, members of our international and local committees, hotels' (extra kind) personnel, reviewers, but most of all, the contributors. The authors are the true reason why are you reading this, dear reader. And maybe, next time, it could be you.

Editors

14th Annual Baška GNSS Conference:
Technologies, Techniques and Applications Across PNT and
The **1st** Workshop on Smart, Blue and Green Maritime Technologies

PROCEEDINGS

University of Zadar

A BENCHMARK OF THE GPS+GALILEO F9P RECEIVER

Damien Rivoal[1*], Quentin Bossard[2], David Bétaille[2]

Abstract. *Still very few publications relate test results of multi-constellation receivers since Galileo satellites massive launch by Ariane 5, leading to more than 20 operational space vehicles in orbit. One can refer to automotive receivers and smartphones test bench made during the European COST action SaPPART (Satellite Positioning Performance Assessment for Road Transport), but this was GPS only or GPS+Glonass. This article gives an overview of a test carried out in the city of Nantes, France, and its suburban area, with a brand new receiver, F9P, of the automotive range of Ublox. The dual constellation configuration GPS+Galileo is tested. This receiver is benchmarked with respect to the previous generation of Ublox LEA6T.*

Key words: *GPS; Galileo; receiver; performance; road transport*

[1] Enac, Signal processing and Navigation (SigNav Toulouse, France)
[2] Ifsttar, Components and Systems (CoSys Nantes, France)
[*] Corresponding author: David Bétaille (david.betaille@ifsttar.fr)

University of Zadar

1 CONTEXT, METHODOLOGY AND EXPERIMENTAL SET-UP

1.1 Context

Still very few publications relate test results of multiconstellation receivers since Galileo satellites massive launch by Ariane 5 in end-2016, end-2017 and mid-2018, leading to more than 20 operational space vehicles in orbit. One can refer to automotive receivers and smartphones test bench made during the European COST action SaPPART (**COST 2018**) (Satellite Positioning Performance Assessment for Road Transport), but this was GPS only or GPS+Glonass (**Betaille *et al.*, 2017**).

The context is that of two consecutive projects, called INTURB for Urban Integrity, and Urban E-map, both in which 3D city model aiding has been investigated. The former one proved the interest of classifying LOS vs NLOS satellites (Non-Line-Of-Sight) using such model, whilst the second proposed map matching on an enhanced map representing all lanes and all modes (cars, buses, cycles, pedestrians) in order to improve the use of 3D computing.

1.2 Methodology

The methodology consisted in reproducing, with the new Ublox F9P series, the trajectories previously done in 2014 with the Ublox LEA former series. These trajectories included rural and urban parts, around and in Nantes, and they lasted approximately 2 hours. Due to long term changes in the GPS constellation at the time of the different tests, both Ublox LEA and F9P series will be embedded in the new campaign. The experiment was planned in 2019.

The objective here is twofold: first, compare the LEA and F9P series in terms of positioning accuracy when tracking the GPS satellites only, and second, assess the improvement thanks to the Galileo satellites on positioning accuracy, those being actually tracked by new F9P multiconstellation multifrequency receivers. Note that the multifrequency capability is not studied in this experimental campaign.

1.3 Experimental set-up

The test took place on Wednesday August 14, 2019. The acquisition was made with the VERT vehicle (Véhicule d'Essais et de Référence en Trajectographie) shown in **Figures 1** and **2**. The reference trajectory has been calculated from a hybridization between the GNSS signals received on-board and the vehicle gyroscope and wheel speed sensors, with the same equipment and method as usual in the Geoloc lab, in particular for the 2014 test for Urban Integrity (INTURB) project and also for the 2017 SaPPART campaign. The acquisition and calculation of the reference trajectory have been carried out by the Geoloc team of Ifsttar. VERT is the Vehicle for Experimental Research on Trajectory of IFSTTAR (**Betaille *et al.*, 2008**): the reference trajectory considered as the ground truth is provided, in this experimental set-up, by a tactical inertial measurement unit (iXSea LandINS) coupled to GNSS PPK (GPS+Glonass Novatel DL-V3 calculated with a local permanent GNSS station, the one of Nantes Metropole).

Figure 1. Experimental set-up in the Vehicle for Experimental Research on Trajectory.

Figure 2. Antennas on the roof top of the VERT.

(a) (b)

Figure 3. Model of antenna connected to each F9P receiver (a) and to the LEA6T receiver (b).

The specimens under test were prepared by the CoSys team (where Damien Rivoal was part of, during his internship). Throughout the journey, the acquisition of satellite signals was done using multiband antennas. Two Ublox F9P multiconstellation multifrequency receivers were used, each with its own antenna. These receivers output NMEA frames and raw data. One receiver was dedicated to GPS signals only, and the other to GPS and Galileo signals. This double acquisition will allow – after processing the raw data or directly from NMEA frames – to assess the contribution of the Galileo constellation on positioning accuracy.

Another receiver, Ublox LEA6T, which the lab used formerly for several experiments in particular in 2014, was also installed on-board the vehicle.

Antennas used were multiband Ublox ANN-MB for both F9Ps. The LEA6T was connected to a patch antenna ANN-MS.

Both F9P and LEA6T devices were configured in default mode. Only settings needed for raw data output and NMEA sentences, at 5Hz, were modified (and GPS only for one F9P).

1.4 GNSS data acquisition

GNSS data were acquired at a frequency of 5Hz. Two breaks which lasted approximately 600s were made in order to ensure safe log-in of the F9Ps by a laptop running Ucenter data logger (v19.03), which resulted in splitting the data files into three, each of a duration of approximately 1 hour. This was not needed for the LEA6T, which could be logged continuously and without any trouble on another laptop running Ucenter v8.16.

The data files to process are:

- One file of GPS measurements recorded for the LEA6T;
- Three files of GPS measurements recorded for one F9P;
- Three files of GPS and Galileo measurements recorded by the other F9P.

GPS times are converted into UTC times of day, removing also the current 18 leap seconds. Occasionally, data frames may be missing at start or stop of the different acquisitions.

The **highest start time** and **lowest stop time** between RINEX and GGA is underlined hereafter.

The chronogram of the acquisitions is given in **Table 1**.

Table 1. Chronogram of the data acquisition of the different receivers on 14 August 2019: start and stop times are aligned onto 23671.80 and 32390.60, respectively, common to all data files.

LEA6T_2019_08_14.ubx, converted into RINEX 2.10 with RTKCONV 2.4.2

```
 2019    8   14   6   26 18.8010000    GPS    TIME OF FIRST OBS = 23160.80
 2019    8   14   9   21  8.8000000    GPS    TIME OF LAST OBS  = 32520.80
```

$GPGGA,062603.80 (23163.80) to $GPGGA,090200.80 (32520.80)

F9P_190814_063424.ubx + 190814_073911.ubx + 190814_084055.ubx, GPS only, converted into RINEX 2.10 with RTKCONV 2.4.3

```
 2019    8   14   6   34 49.8000000    GPS    TIME OF FIRST OBS = 23671.80
 2019    8   14   7   28  4.2010000    GPS    TIME OF LAST OBS
```

$GPGGA,063431.80 (23671.80) to $GPGGA,072746.20 (26866.20)

```
 2019    8   14   7    9 34.5990000    GPS    TIME OF FIRST OBS
 2019    8   14   8   31  1.0000000    GPS    TIME OF LAST OBS
```

$GPGGA,073916.60 (27556.60) to $GPGGA,083042.80 (30642.80)

```
 2019    8   14   8   41 19.4020000    GPS    TIME OF FIRST OBS
 2019    8   14   9    0  8.8030000    GPS    TIME OF LAST OBS  = 32390.80
```

$GPGGA,084101.20 (31261.20) to $GPGGA,085950.60 (32390.60)

F9P_190814_063120.ubx + 190814_073712.ubx + 190814_083900.ubx, GPS+Galileo, converted into RINEX 3.03 with RTKCONV 2.4.3

```
 2019    8   14   6    1 54.7890000    GPS    TIME OF FIRST OBS = 23496.80
 2019    8   14   7   29 23.3900000    GPS    TIME OF LAST OBS
```

$GPGGA,063136.60 (23496.60) to $GPGGA,072905.20 (26945.20)

```
 2019    8   14   7   37 43.8020000    GPS    TIME OF FIRST OBS
 2019    8   14   8   32  9.0030000    GPS    TIME OF LAST OBS
```

$GPGGA,073725.60 (27445.60) to $GPGGA,083151.00 (30711.00)

```
 2019    8   14   8   39 30.0020000    GPS    TIME OF FIRST OBS
 2019    8   14   9    0 39.6020000    GPS    TIME OF LAST OBS  = 32421.60
```

$GPGGA,083911.80 (31151.80) to $GPGGA,090021.40 (32421.40)

[STATIC]	]MOVE OUT[	[MOVE URB]	]STATIC[	[MOVE URB]	]STATIC]	]MOVE OUT]
[23163.80 23889]	]23889 24828[	[24828 26824]	]26824 27667[	[27667 30627]	]30627 31381]	]31381 32520.80]
[23671.80 23889]	]23889 24828[	[24828 26824]	]26824 stop 27667[	[27667 30627]	]30627 stop 31381]	]31381 32390.60]
[23496.80 23889]	]23889 24828[	[24828 26824]	]26824 stop 27667[	[27667 30627]	]30627 stop 31381]	]31381 32421.40]

Only the kinematic sketches (in green in **Table 1**) will be considered for performance analysis, respectively in rural and urban conditions. The static sketches (initial and on the way during which both stops were made, in red in **Table 1**) are not processed later on. The corresponding time windows have been defined graphically at starts and stops of the vehicle.

The rural part contains 9742 epochs (~33min) at 5 Hz and the urban part 24782 (~1h23min). Except the two breaks, no frame is missing for F9P GGA logging, whilst a few are missing for LEA6T, both in rural (8 missing) and urban parts (1 missing).

1.5 Former LEA6T data acquisition in Nantes

Another file of GPS measurement was recorded formerly on Thursday February 27, 2014, for the LEA6T. Note that it was during winter (whereas during summer in 2019, with different foliage and possibly multipath) and under different constellations.

GPS times are converted into UTC times of day, removing also the 16 leap seconds in 2014. The chronogram of the acquisition is given in **Table 2**.

Table 2. Chronogram of the data acquisition of the different receivers on 27 February 2014.

2014_02_27_LEA6T.ubx, converted into RINEX 2.10 with RTKCONV 2.4.2

```
 2014    2   27    8   3413.0010000   GPS    TIME OF FIRST OBS = 30837.00
 2014    2   27   10   2215.2010000   GPS    TIME OF LAST OBS  = 37319.20
```

$GPGGA,083357.00 (30837.00) to $GPGGA,102159.20 (37319.20)

[STATIC]	]MOVE OUT[	[MOVE URB]	]MOVE OUT]
[30837.00 31127]	]31127 31977[	[31977 36432]	]36432 37319.20]

The rural part contains 8685 epochs (~29min) at 5 Hz and the urban part 22276 (~1h14min). A few GGA frames are missing: 32 and 54 in rural and urban parts, respectively.

The trajectory carried out during the 2019 test is represented in a local tangent plane (using latitude and longitude of a monument located on lab site) on **Figures 4** and **5**.

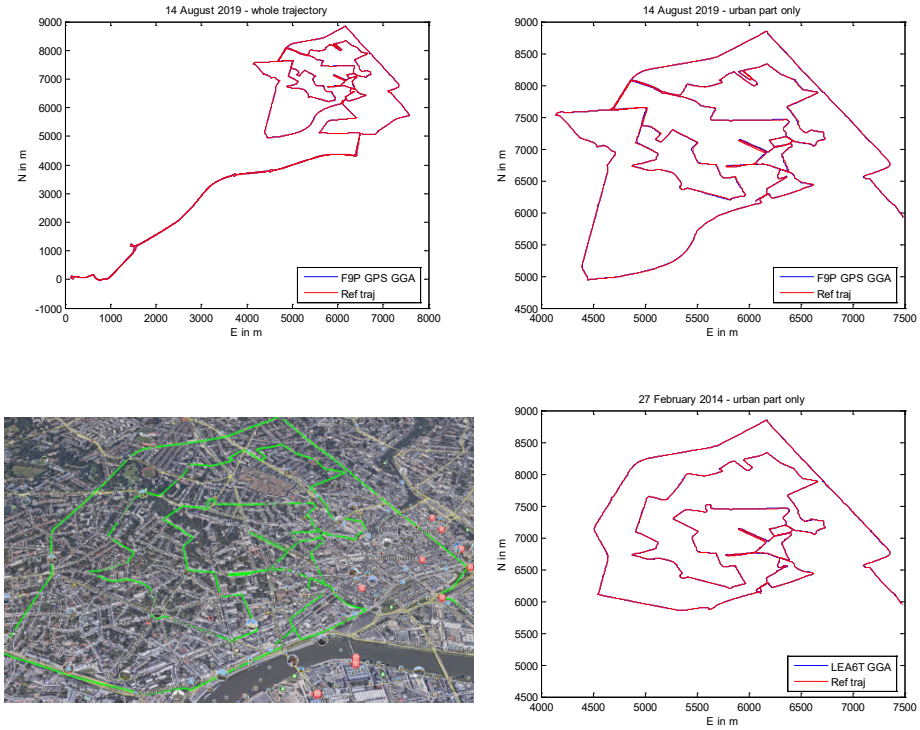

Figure 4. Whole plane trajectory, August 14, 2019, and in downtown Nantes for F9P GPS: the bottom right subframe shows the urban part collected in 2014, February 27.

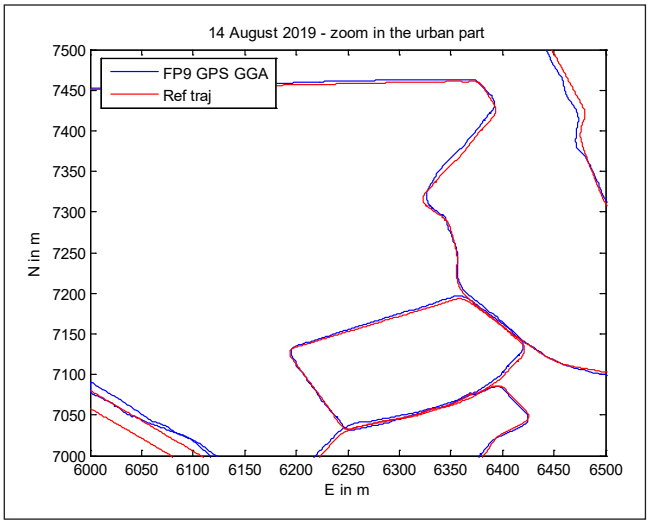

Figure 5. Zoom in downtown Nantes for F9P GPS, August 14, 2019.

Several major detours can be observed compared to the initially planned trajectory similar as the former test in 2014 with LEA6T. (This was due to numerous works along the west part of the travel.)

Figure 5 is a zoom in downtown Nantes, where plane errors are visible. They can reach tens of meters in severe urban canyons.

2 RESULTS BASED ON NMEA FRAMES

First investigations were made on the basis of the GGA frames. They indeed contain the navigation solutions computed by the manufacturer of the equipment (latitude and longitude) along with timing, which enables the computation of the horizontal distance with respect to the VERT reference trajectory, this being interpolated at the same timing.

2.1 Accuracy

The analysis compares city centre vs suburban and rural areas, which are part of the total travel (in between the Ifsttar lab and the city centre). The static parts have been removed. **Table 3** is based on GGA frames, i.e. on navigation solutions computed by Ublox.

Table 3. Median plane errors (in m) in the different parts of the trajectory.

Receiver	Urban part	Suburban and rural parts
LEA6T (2014)	1.59	0.95
LEA6T	2.04	1.59
F9P GPS	2.67	1.20
F9P GPS+Galileo	1.46	0.89

2.2 Number of satellites

Table 4 is still based on NMEA frames, and it reports the average number of satellites, signal-to-noise ratios (CN0) and HDOP (Horizontal Dilution Of Precision) extracted from the GGA frames during each part.

Table 4. Average number of satellites, CN0 and HDOP per epoch in the different parts of the trajectory.

Receiver	Urban part	Suburban and rural parts
LEA6T (2014)	avg. 8.24 sat. / 43.18dB / 1.28	avg. 8.81 sat. / 45.44dB / 1.02
LEA6T	avg. 7.31 sat. / 41.84dB / 1.33	avg. 8.94 sat. / 42.85dB / 1.08
F9P GPS	avg. 6.69 sat. / 40.48dB / 1.25	avg. 6.90 sat. / 42.33dB / 1.32
F9P GPS+Galileo	avg. 11.44 sat. / 39.80dB / 0.99	avg. 11.66 sat. / 41.09dB / 0.94

These satellites were actually used in the navigation solutions (among those tracked). CN0 can be extracted from the GSV frames, which were also logged during the tests.

2.3 Discussion

Based on the NMEA frames, the discussion is threefold:

First, a question is raised concerning the accuracy of the LEA6T: there is an important difference between the accuracies of the two data sets (2014 and 2019).

In the rural part: the number of satellites is almost the same. The median HDOPs are both close to 1.00. But the average CN0 is 45.44dB in 2014, versus only 42.85dB in 2019. The ranging noise stochastic model from (**Wieser and Brunner, 2000**) and already used by (**Zhu, 2018**) for Ublox LEA6T gives:

$$\sigma^2 = m\,(10^{-CN0/10} - 10^{-55/10}) \qquad (1)$$

From experience, CN0 has 55dB maximum value. And the parameter m should be adjusted to match the actual plane accuracy. m=45000 makes sense, giving median plane accuracies of 1.19m, versus 1.53m, for 2014 and 2019 data sets, respectively.

Thus, the difference in CN0 can explain the difference in accuracy.

In the urban part: median HDOPs are close to 1.25, and average CN0 are 43.18dB and 41.84dB, respectively. Using the same model, this makes 1.68 m, versus 1.94 m, for 2014 and 2019 data sets, respectively.

The second point concerns the F9P tracking GPS only: it seems this receiver experiences multipath with severe impact in the urban environment. Whereas the

other receivers have half a meter increase of the median plane error compared to the rural environment, the increase is here much more: 1.5m. The number of satellites tracked, which – if low – mechanically degrades the HDOP, and the perturbation in ranging with buildings around, cannot explain this degradation of the accuracy by itself.

The diminution of the number of satellites used between the rural and urban environments is not more important for F9P than for LEA6T. A hypothesis could be that the LEA6T used to apply a rather severe FDE (fault detection and exclusion) algorithm, compared to F9P. Presumably, Ublox makes use of sequential Extended Kalman Filter (EKF) innovation-based FDE (**Joerger and Pervan, 2011**), but this is not publicly documented. Degraded measurements remaining in the F9P solution, with one constellation only (GPS), could cause large errors.

The last point would be as follows. The best accuracy obtained corresponds to using both GPS and Galileo constellations. In rural environment, the median plane error is below one meter (0.89 m) and close to 1.5 m in the city of Nantes with the F9P receiver.

3 RESULTS BASED ON RAW DATA

3.1 Computation of the position of the GNSS satellites

Ephemeris for both GPS and Galileo constellations (among others) were downloaded from https://igs.bkg.bund.de/root_ftp/MGEX/BRDC_v3/2019/226/, namely brdm2260.19p.Z file. These broadcasted ephemerides gather GPS+GLO+GAL+BDS+QZSS+IRNSS+SBAS satellites, and they were merged by DLR from streams of about 35 stations, until 2020 (https://www.igs.org/mgex/data-products). For 2014, nmcu0580.14n collected in the Nantes permanent station was downloaded from IGN. Hopfield tropospheric with Essen and Froome parameters and broadcasted ionospheric correction terms have been applied (*).

3.2 Computation of the ranging errors

Based on the reference trajectory, as well as on the broadcasted ephemeris and atmospheric corrections, receiver-to-satellites ranging errors have been computed, fixing the receiver clock term with the highest satellite in elevation. (Its error

becomes consequently null). Note that whereas LEA6T keeps its clock drift within 1ms, it can exceed 10ms for F9P (**Figure 6**).

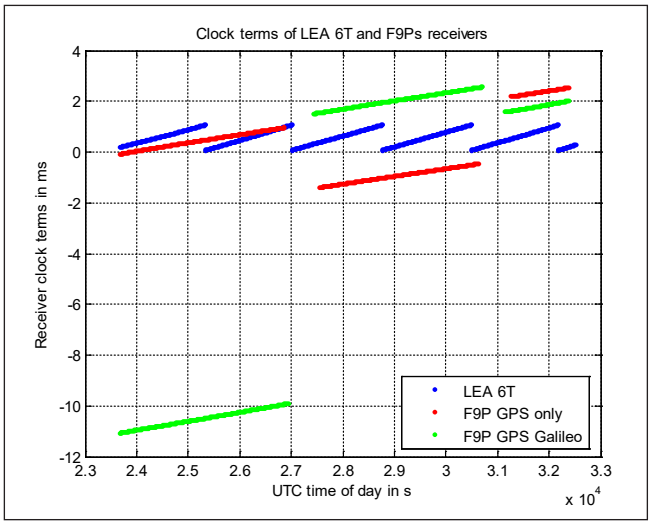

Figure 6. Clock terms of LEA6T and F9Ps receivers.

These errors are represented in histograms in **Figures 7 to 10** next.

Each figure displays urban (left) versus rural (right) parts, and histograms for ranging errors (top) and signal-to-noise ratios (bottom).

At first visual inspection, there is obviously a difference between urban and rural ranging errors, in terms of symmetry in the distribution as well as in terms of amplitude of the errors. Positive queues in the distribution are clearly visible in the city of Nantes, irrespective of the receivers and the constellations used.

One can notice that the Gaussian queues have an order of magnitude of several tens of m in urban environment, which is much more than in rural environment. This is the same magnitude as tropospheric corrections, but occasionally these errors may be much larger. (Note that the order of magnitude of ionospheric corrections is only of several m.) Since these corrections are applied, the large errors observed are therefore significant of non-line-of-sight satellite tracking. Histograms of CN0 are also given with CN0 average value (in red). CN0 between 30-35dB are clearly over represented in urban environment, which makes a bump in their distribution, not visible in rural environment.

Table 5 gathers urban parts in 2014 (22276 epochs for LEA6T) and 2019 (24782 epochs in 2 sketches for LEA6T and F9P receivers). Note that the number of satellites which were registered is slightly different from those reported in the NMEA solutions which actually passed Ublox's FDE.

Table 5. Median ranging errors showing dissymmetric histograms in urban environment.

LEA6T 2014	LEA6T 2019
166033 ranges (1 epoch with no range log) - 22275 epochs => 143758 ranging errors 7.45 sat. / epoch	165653 ranges - 24782 epochs => 140871 ranging errors 6.68 sat. / epoch
median(err) = 0.89m (*vs 0.61m in rural**) 2.5 percentile = -3.84m (*vs -3.61m in rural*) 97.5 percentile = 33.30m (*vs 8.62m in rural*)	median(err) = 0.87m (vs 0.28m in rural) 2.5 percentile = -4.54m (vs -4.47m in rural) 97.5 percentile = 35.69m (vs 19.04m in rural)
errors are 65% positive	errors are 63% positive

F9P GPS 2019	F9P GPS GALILEO 2019
188614 ranges (2 epochs with no range log) - 24780 epochs => 163834 ranging errors 7.61 sat. / epoch	319483 ranges - 24782 epochs => 294701 ranging errors 12.89 sat. / epoch
median(err) = 2.12m (vs 0.93m in rural) 2.5 percentile = -3.00m (vs -1.67m in rural) 97.5 percentile = 49.95m (vs 34.74m in rural)	median(err) = 1.27m (vs -0.01m in rural) 2.5 percentile = -2.99m (vs -3.09m in rural) 97.5 percentile = 42.71m (vs 26.42m in rural)
errors are 80% positive	errors are 73% positive

(* It appears that the solar activity, impacting ionospheric effect, was high in 2014 and low in 2019, which justified the use of broadcasted vs seasonal alpha – beta parameters in 2014.)

Statistics, and particularly the 97.5 percentiles, confirm the dissymmetry and the distribution of the ranging errors. These percentiles are systematically much larger in Nantes than out of Nantes. In a few words, errors are generally positive, whereas it should be equally distributed around zero. This characterizes multipath impact on ranging in the urban environment.

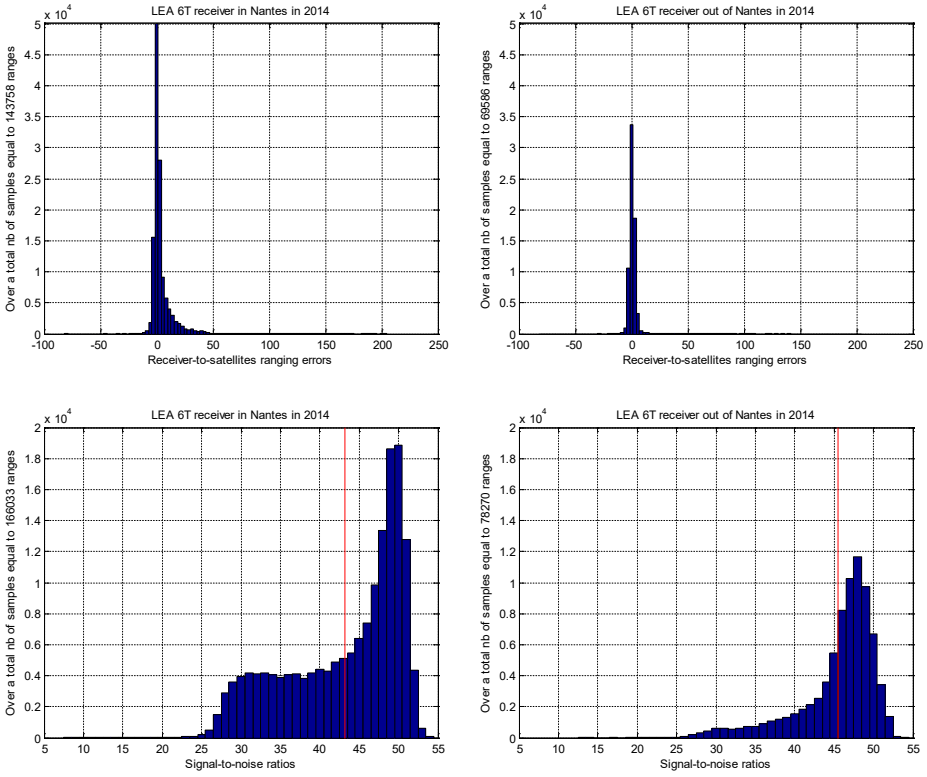

Figure 7. LEA 6T ranging errors and CN0 (2014) in (left) and out of Nantes (right).

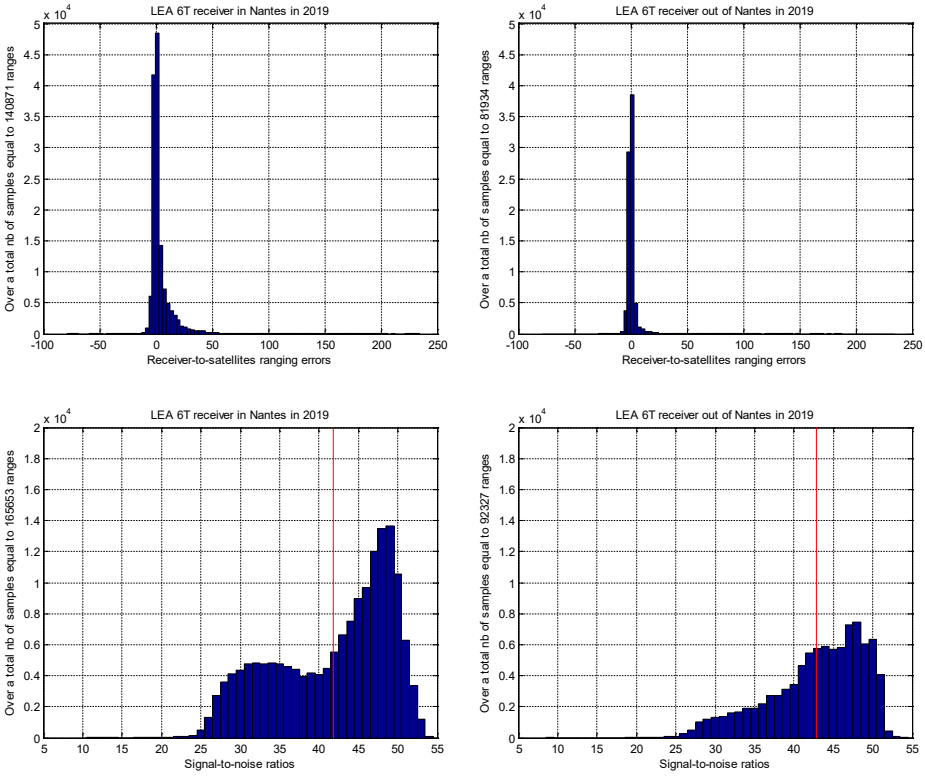

Figure 8. LEA 6T ranging errors and CN0 (2019) in (left) and out of Nantes (right).

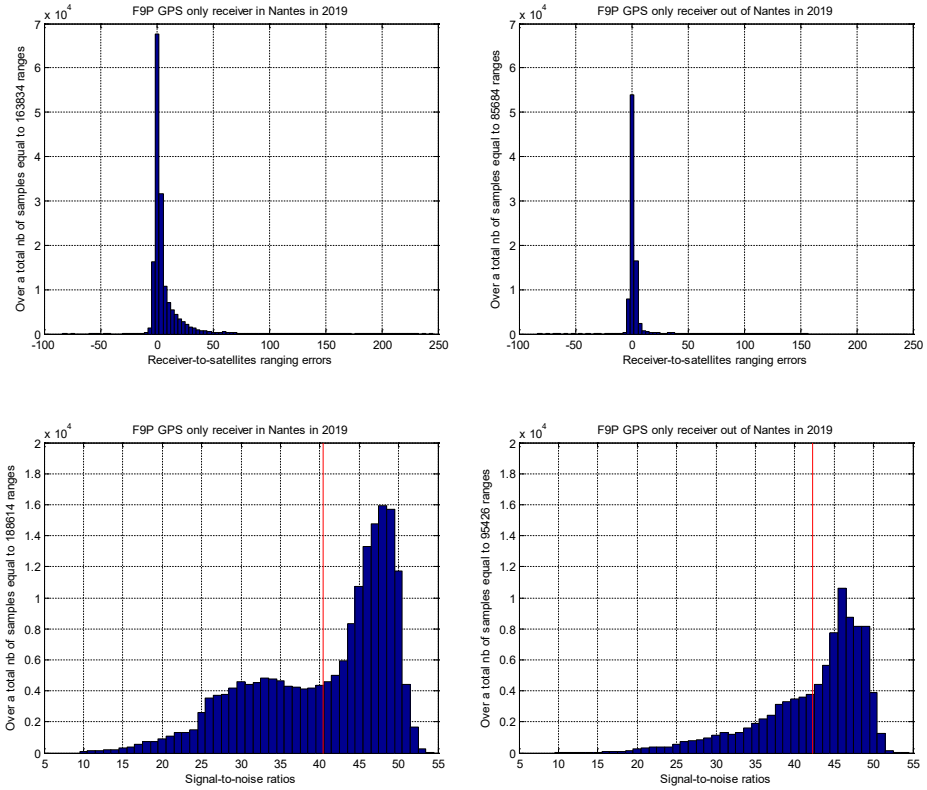

Figure 9. F9P ranging errors and CN0 (GPS) in (left) and out of Nantes (right).

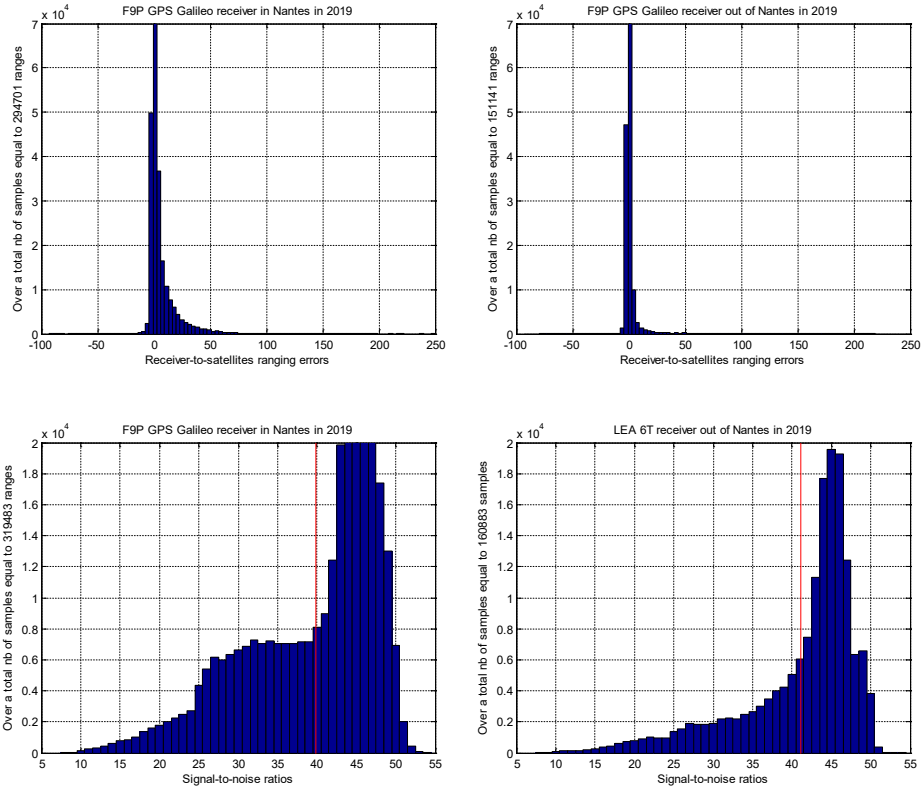

Figure 10. F9P ranging errors and CN0 (dual GPS Galileo) in (left) and out of Nantes (right).

4 CONCLUSIONS AND PERSPECTIVES

To conclude, despite urban perturbations, the F9P median plane accuracy assessed in this campaign is around 1.5 m, with a clear advantage of sharing GPS and Galileo constellations. Out of the city, the F9P median plane error is below 1 m. The potential improvement by 3D city model is challenged for further research, with the aim of approaching the median plane error obtained in rural and suburban environments (less than 1 m).

We have clearly identified ranging errors in the urban environment, for GPS observations as well as Galileo. We are currently trying to model and correct them, using 3D city modelling. Next step in this research will be to try to explain the observed ranging errors with local 3D map, and apply the process of downweighting and correction.

Acknowledgments

This work has been funded by the Ministry responsible for transport in France, DGITM (General Directorate for Infrastructure, Transport and the Sea), in the frame of the project named Urban E-map. A particular thanks to the Geoloc team of Ifsttar for its cooperation.

REFERENCES

Bétaille D., *et al.* (2008). How to produce a reference trajectory for studying GNSS errors in urban environments. *European Navigation Conf.* 22 – 25 April 2008, Toulouse, France.

Bétaille D., Stern A., Ortiz M. and Ruotsalainen L. (2017). Autonomous vehicles: get necessary redundancy in positioning with enhanced GNSS and maps. *ITS World Congress*. 29 October – 2 November 2017, Montreal, Canada.

COST Action TU1302 (2015-2018). SaPPART White Paper (TMI1), Handbook (TMI2), and Guidelines (TMI3): *Assessment of positioning performance in ITS applications*. Ifsttar, Collection Techniques et Méthodes. ISBN 978-2-85782(-706-1), (-727-6), and (-740-5).

Joerger M. and Pervan B. (2011). Integrity risk of Kalman Filter-based RAIM. *23rd International Technical Meeting of the Satellite Division of the Institute of Navigation (ION GNSS)*. 19 – 23 September 2011, Portland, Oregon, USA.

Wieser A. and Brunner F. K. (2000). An extended weight model for GPS phase observations. *Earth, planets and space*, 52.

Zhu, N. (2018). *GNSS propagation channel modelling in constrained environments: Contribution to the improvement of the geolocation service quality*. Doctoral dissertation, Univ. de Lille.

ASSESSMENT OF EGNOS CORRECTION MESSAGES FOR CIVIL AVIATION IN ALGERIA WITHOUT RIMS STATION

Beldjilali Bilal*, Kahlouche Salem

Abstract. *The European Geostationary Navigation Overlay Service (EGNOS) is developed by the European Space Agency (ESA) initially to provide an augmentation service to the Global Positioning Service (GPS). The principal goal of this system is to improve the accuracy given by the GPS alone and give the necessary integrity required for the civil aviation navigation operation. In this context, the aim of this work is to analyze the actual performance of the EGNOS system for civil aviation in Algeria in terms of availability through protection levels based on alarm limits. It should be noted that there is no, until now (2021), a Ranging and Integrity Monitoring Station (RIMS) in Algeria. The study in this work is based on the analysis of four (4) GPS sites in Algeria (from the north to the south), the results show that the positions are improved in all the 4 sites (ARZEW, M'sila, Ouargla and In-salah), especially for the two sites in the north (ARZEW and M'sila). On the other hand, it should be noted that the only site that ensures the integrity of the APV I required for civil aviation is the ARZEW site in the far north of Algeria. The results obtained confirm that the installation of a RIMS station in Algeria is necessary for the use of the EGNOS system in civil aviation.*

Key words: *EGNOS; GPS; civil aviation; APV I; precision; integrity; RIMS station*

Department of Space Geodesy, Center of Space Techniques, Algerian Space Agency, Arzew, Algeria

* Corresponding author: Beldjilali Bilal (bel.bilal@yahoo.fr)

University of Zadar

1 INTRODUCTION

GNSS systems are proprietary systems and their operators do not guarantee continuous availability. In the event of errors or breakdowns, users are not immediately informed and the aeronautical operators of those systems do not guarantee continuity of service. To meet the demand of these users, it was necessary to implement complementary systems to GNSS which made it possible to remedy certain shortcomings or improve their performance while continuing to benefit from technological and operational progress. These complementary systems called augmentation systems, consisting either of terrestrial or space-based infrastructures (**ESA, 2018**; **Kaplan and Hegarty, 2006**).

Spatial augmentation systems consist of terrestrial relay stations and geostationary satellites that receive signals from GPS satellites and transmit corrected time and distance measurements, greatly increasing the accuracy of the measurements. The special feature of these systems is that the frequency band and modulation of the data link signals are identical to those of the GPS signals. In addition, the SBAS signal is broadcast by geostationary satellites covering very large areas. Currently, many systems are available: EGNOS for Europe, WAAS for the United States, MSAS for Japan and China's SNAS system. India has also committed to implement its own GAGAN system and also Algeria is in the final steps to make its one SBAS system fully operational (**Beldjilali and Benadda, 2017**; **ESA, 2019**).

2 RIMS STATION

On the ground, EGNOS comprises a network of 40 RIMS stations, continuously observing GPS satellites signals (L1, L2 and L5) in addition to GLONASS L1 frequency and SBAS geostationary satellites also on L1. These observations are sent to the Mission Centers (MCC), which check their quality and process them. Mission centers calculate orbits, clocks, ionospheric parameters and check data consistency to calculate quality criteria. This makes it possible to create an integrity message and generate differential corrections. These messages are sent to three geostationary satellites which retransmit them to the user (**Beldjilali, Kahlouche and Tabti, 2020**; **Marila, 2016**; **Manila, 2018**; **Fruehauf, 2004**; **Beldjilali, Tabti and Kahlouche, 2020**). The **Figure 1** illustrates the location of EGNOS RIMS station in addition to its actual coverage area.

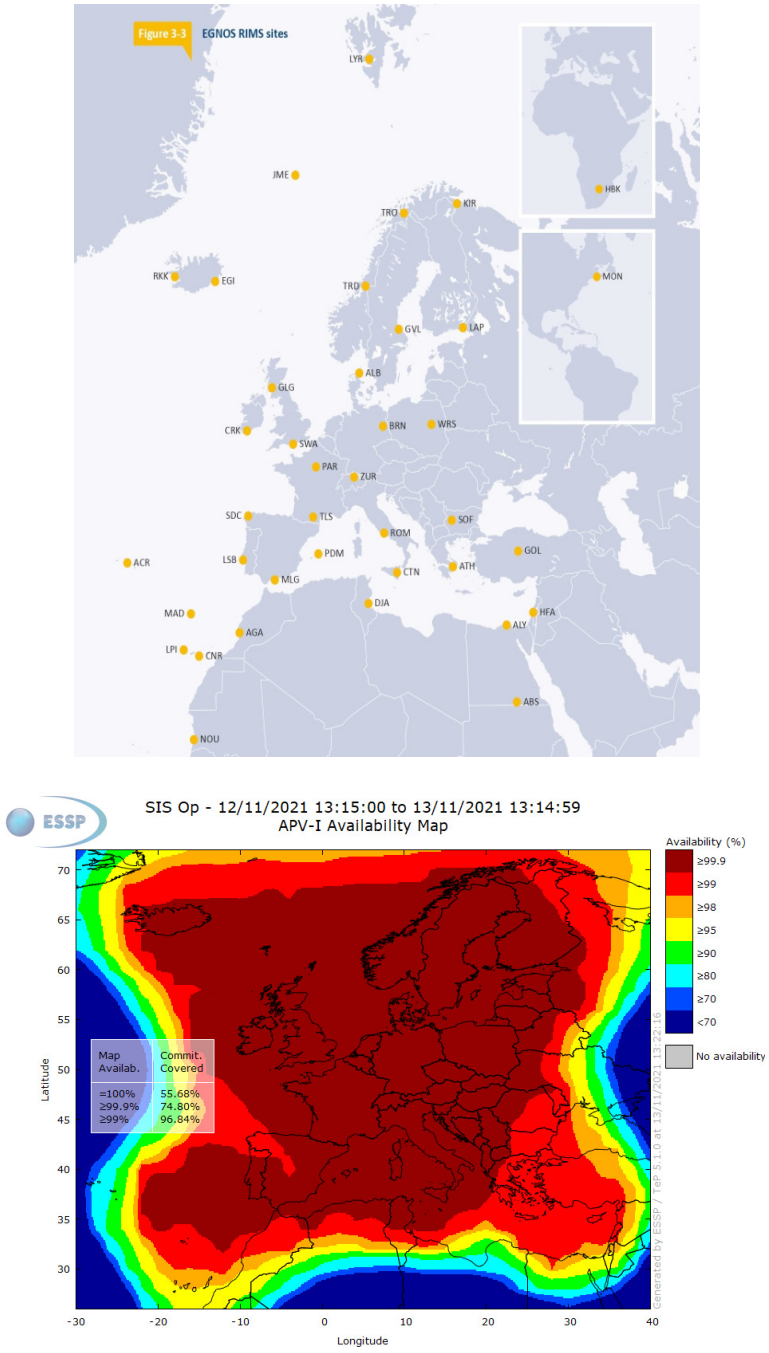

Figure 1. RIMS stations localization (up) and EGNOS coverage area (bottom) for civil aviation (**ESA 2011**)

3 CIVIL AVIATION REQUIREMENTS

Aircrafts used much navigation equipment which needs numbers of requirement to be able for using in civil aviation. The International Civil Aviation Organization (ICAO) is responsible for establishing the standards for radio navigation aids, including the ones concerning GNSS. The ICAO defines three main approaches and landing categories and they are classified as follows (**ESA 2018**):

- Non-Precision Approaches and landing operations (NPA),
- Approaches and landing operations with vertical guidance (APV),
- Precision approaches and landing operation (PA).

The next figure (**Figure 2**) shows the approach phase as divided according with the ICAO:

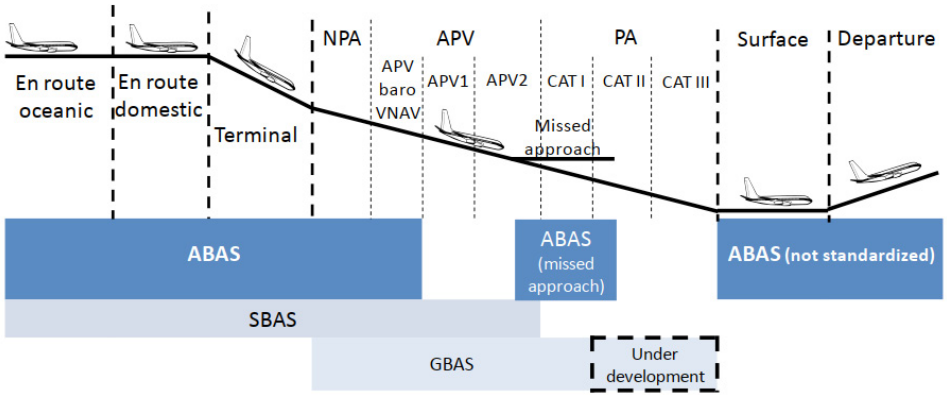

Figure 2. Civil aviation steps with SBAS approach. (**ESA 2011**)

Table 1. Civil aviation requirement.

Operation	Horizontal accuracy (95%)	Vertical accuracy (95%)	Time to Alert	Availability
En-route	3.7 Km	N/A	5 min	0.99 to 0.99999
En-route Terminal	0.74 Km	N/A	15 s	0.99 to 0.99999
NPA	220 m	N/A	10 s	0.99 to 0.99999
APV-I	16 m	20 m	10 s	0.99 to 0.99999
APV-II	16 m	8 m	6 s	0.99 to 0.99999
CAT-I precision approach	16 m	6 to 4 m	6 s	0.99 to 0.99999

Table 1 summarizes the requirement of the ICAO for each flight phase in terms of Accuracy, Time to Alert and Availability.

4 EGNOS MESSAGES

The EGNOS system broadcasts its messages on the L1 band (1575.42 MHz) with a rate of 250 bits per second. It uses the same modulation as the GPS L1 signal, but with a flow 5 times higher. So every second a 250 bit message is available to the user in the following format (**Fruehauf, 2004**; **Beldjilali, Tabti and Kahlouche, 2020**):

- 8 preamble bits; is a single 24-bit word (01010011- 10011010 -11000110), distributed over three successive messages which makes it possible to synchronize the start of the data (during the acquisition phase),
- 6 bits to identify the type of message (from 0 to 63),
- 212 bits of current EGNOS correction,
- 24 bits of parity; to ensure that the data was not corrupted during transmission.

A total of 63 types of messages can be transmitted, but for the moment only 20 are defined and 18 are used by EGNOS (**ESA, 2011**; **Shuanggen, 2012**; **Cwiklak, Grzegorzewski and Adamski, 2014**; **Salomon 2020**). A brief description of these messages is presented in **Table 2**:

Table 2. EGNOS messages description.

Message	Description	Duration (s)
1	PRN mask	120
2-5	Fast Correction	6
6	Integrity Information (EDREI)	120
7	Degradation factor for quick fixes	120
9	GEO satellite position parameters (X, Y, Z, time, etc.)	120
10	Degradation settings	120
12	UTC SBAS time	300
17	Position parameters of GEO satellites (Almanac)	300
18	Mask of the ionospheric grid	300
24	Fast fixes / slow fixes	120
25	Slow fixes	120
26	Ionosphere delays	300

5 STUDY AREA

To carry out our work and achieve our goals, the position quality will be analyzed at 4 different sites located in different altitude in Algeria (**Figure 3**) in order to test the relevance of the EGNOS correction for civil aviation.

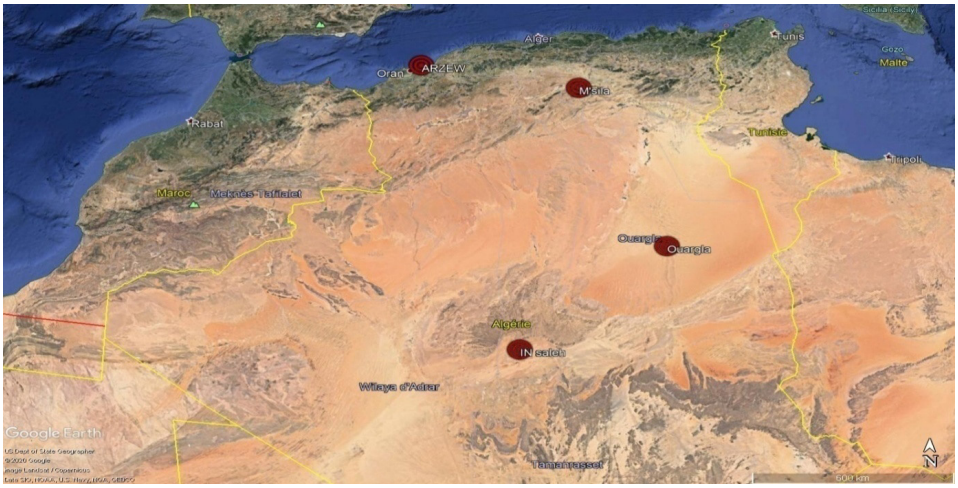

Figure 3. Locations of the chosen sites for the study.

In the first case, the position will be computed using GPS alone, while in the other case, the pseudo range will be corrected using EGNOS correction. The EGNOS corrections message used in this work are obtained from the (fttp://serenad-public.cnes.fr) which is based on the FTP service; this is a historical site that containing EGNOS ground station data, SBAS messages, and raw data in various formats for download. The collected data was analyzed using the gLAB software tool suite. This is a flexible software tool to provide high accuracy GNSS positioning for processing and analysis of GNSS data. This utility handles the decoding and processing of SBAS data.

6 APPLICATION OF CORRECTIONS

The EGNOS system allows corrections to the pseudo-distances of satellites to be transmitted to users in the service area via a network of stations. These corrections allow the receiver to compensate for errors such as the inaccuracy of

ephemerides and satellite clocks, or delays imposed on the GPS signal by the ionospheric and tropospheric layers. The user collects all of the differential correction messages and calculates the corrected pseudo-distance corrections l_{corr} based on the pseudo distance measured l_{meas} for each satellite, this correction is given by (**Salvatori, 2014**):

$$l_{corr}(t) = l_{meas}(t) + RC_{fast}(t) - RC_{iono}(t) + RC_{tropo}(t) + RC_{clock}(t) \quad (1)$$

RC_{fast} Quick correction: used to correct the errors which varies quickly (rapid variations of the ephemeris errors and clock for GPS satellites), transmitted in message types 2 to 5, calculated by (**Salvatori, 2014**):

$$PR_{corrected}(t) = PR_{measure}(t) + PRC_f(t_{0f}) + RRC(t - t_{0f})(m) \quad (2)$$

$$RRC(t_{0f}) = \frac{PRC_{f\ current} - PRC_{f\ previous}}{t_{0f\ current} - t_{0f\ previous}}(m) \quad (3)$$

where t is the time of applicability (s), and t_{0f} is the time of applicability of the most recent message (s), PRC_f is the rapid correction (m), and RRC is the variation of correction (m).

RC_{iono} Ionospheric correction; used to estimate the ionospheric error on each receiver/satellite within line of sight, the receiver must identify the points of penetration of the ionosphere IPP (Ionospheric Pierce Point). The ionospheric correction is given by:

$$RC_{iono} = \left[1 - \left(\frac{R_e cosE}{R_e + h_I}\right)^2\right]^{-1/2} \times \tau_{IPP} \quad (4)$$

where E is the elevation angle of the satellite relative to the user (radians); Re is the approximate radius of the Earth (6378.1363 km); h_I is the height of the maximum electron density (350 km); τ_{IPP} is the delay of the IPP, which it is calculated by this equation:

$$\tau_{IPP} = \sum_{i=1}^{4} w_i \times \tau_{IGPi} \quad (5)$$

τ_{IGPi} is the broadcast grid point vertical delay values at the i^{th} corner of the IGP grid, and w_i is the weighting function of IGP grids as a function of its latitude and longitude.

$$\begin{aligned}(x_{pp}, y_{pp}) &= x_{pp}\ \ y_{pp}\\ (x_{pp}, y_{pp}) &= (1 - x_{pp})\ \ y_{pp}\\ (x_{pp}, y_{pp}) &= (1 - x_{pp})\ (1 - \ y_{pp})\\ (x_{pp}, y_{pp}) &= x_{pp}\ (1 - \ y_{pp})\end{aligned} \tag{6}$$

with: $x_{pp} = \frac{\lambda_{pp} - \lambda_1}{\lambda_2 - \lambda_1}$ and $y_{pp} = \frac{\varphi_{pp} - \varphi_1}{\varphi_2 - \varphi_1}$

where φ_{pp} and λ_{pp} are the latitude and longitude of IPP, respectively. λ_1 is longitude of IGPs west of IPP; λ_2 is longitude of IGPs east of IPP, φ_1 is latitude of IGPs south of IPP; φ_2 is latitude of IGPs north of IPP.

RC_{tropo} **Tropospheric correction;** the user estimates it by spatial and temporal interpolation using a model defined by the MOPS standards (Minimum Operational Performance Standards), The estimation of the tropospheric delay then takes the following form:

$$RC_{tropo} = -\left(d_{hyd} + d_{wet}\right)\frac{1.001}{\sqrt{0.002001 + sin^2(E_i)}} \tag{7}$$

RC_{tropo} tropospheric delay estimate; E_i is the elevation angle of a particular satellite; d_{hyd} represents dry contribution to the zenith delay; and d_{wet} is the wet contribution to the zenith delay.

RC_{clock} **Clock correction**:The pseudo distance correction factor is given by:

$$RC_{clock}(\mathrm{t}) = \delta\Delta T_{sat}(\mathrm{t}) \cdot c \tag{8}$$

where c is the speed of light.

$$\delta\Delta T_{sat}(t) = \delta a_{f0} + \delta a_{f1}(t - t_0) \tag{9}$$

δa_{f0} and δa_{f1} are correction parameters at time t_0.

The following figures (**Figures 4** and **5**) give a comparison between the positions calculated from the GPS data alone and by the application of the EGNOS correction messages for the same period.

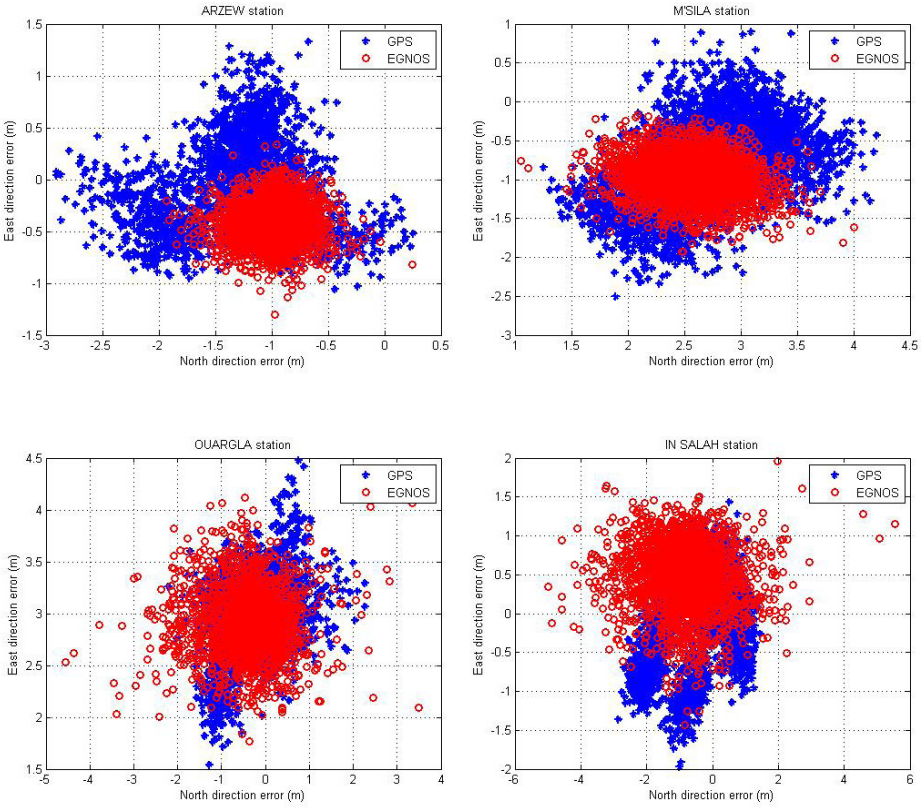

Figure 4. Northing and Easting error calculated from GPS and GPS & EGNOS data.

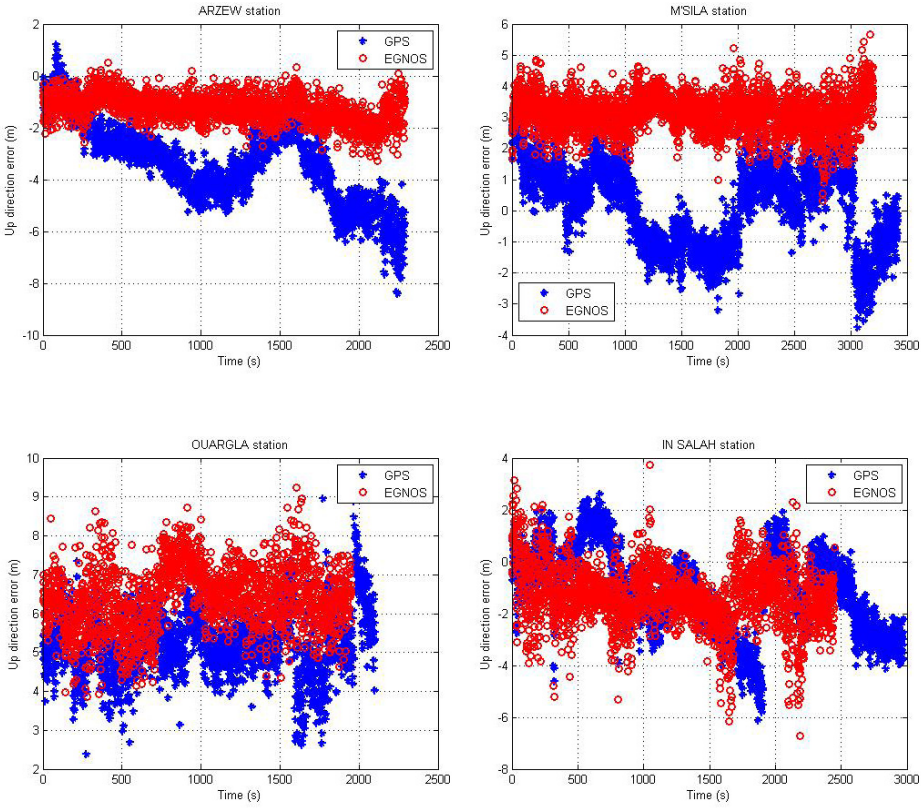

Figure 5. UP error calculated from GPS and GPS & EGNOS data.

The previous figures summarize the errors variation between the two solutions (GPS and GPS+EGNOS) for all sites used in this study. The EGNOS corrections influence are clearly observed, for our study area the positions are improved significantly, and we can conclude that the accuracy obtained can by EGNOS correction can be used for all flight phase until APV I which need a precision of 16 m in planimetry and 20 m in altimetry.

7 INTEGRITY INFORMATION

As defined by the ICAO "*Integrity is a measure of confidence in the accuracy of the information provided by the system. Integrity includes the ability of a system to provide instantaneously valid warnings to users (alert) when the system cannot be used for the intended operation*". Four parameters (**Figure 6**) characterize the notion of integrity (**ESA, 2018**):

- The alarm limit (VAL / HAL – Vertical / Horizontal Alarm Limit),
- The protection level (VPL / HPL – Vertical / Horizontal Protection Level),
- The risk of integrity (HMI – Hazardously Misleading Information),
- The alarm delay (TTA – Time To Alarm).

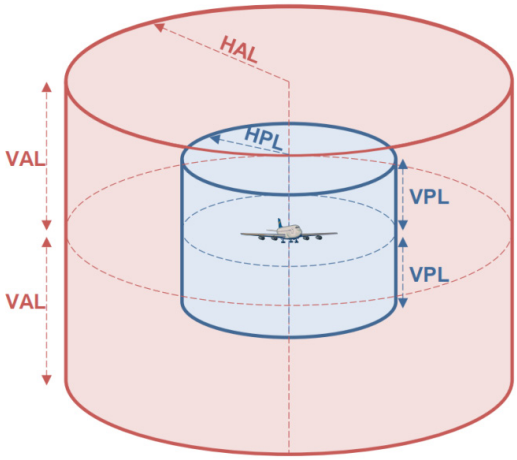

Figure 6. Integrity information given by EGNOS.

The horizontal and vertical protection level calculation is given by:

$$HPL = K_h \times d_a \tag{10}$$

$$VPL = K_v \times d_v \tag{11}$$

K_h and K_v are the coefficient of proportionality, for civil aviation; *Kh* is fixed at 6; and *Kv* is fixed at 5.33 for the PA (precision approach) phases. This parameter can nevertheless be modified for other applications, for example land or maritime, thus allowing to have reduced HPL for higher probabilities of non-integrity (**Salvatori, 2014**).

d is the vertical or horizontal variance of the estimated position as a function of matrix **G** and **W**:

$$\mathbf{G}_i = [-cosEl\ sin\ Azi \quad -cosEl\ cos\ Az \quad -sinEl \quad 1]$$
$$\boldsymbol{W} = \begin{bmatrix} 1/\sigma_1^2 & 0 & \dots & 0 \\ 0 & 1/\sigma_2^2 & \dots & 0 \\ \vdots & \vdots & \dots & \vdots \\ 0 & 0 & \dots & 1/\sigma_N^2 \end{bmatrix} \tag{12}$$

σ_i is the sum of the variances for each satellite (m) it is calculated by:

$$\sigma_i^2 = \sigma_{i,flt}^2 + \sigma_{i,UIRE}^2 + \sigma_{i,air}^2 + \sigma_{i,tropo}^2 \tag{13}$$

$\sigma_{i,\ flt}$ is the variance of the residues of the slow and fast corrections (m); $\sigma_{i,\ UIRE}$ is the variance of the residues of the ionospheric corrections (m); $\sigma_{i,\ air}$ is the variance of the errors of the airborne receiver (m); and $\sigma_{i,\ tropo}$ is the variance of the residues of the tropospheric corrections (m).

The protection level calculation is given in **Figures 7** and **8**.

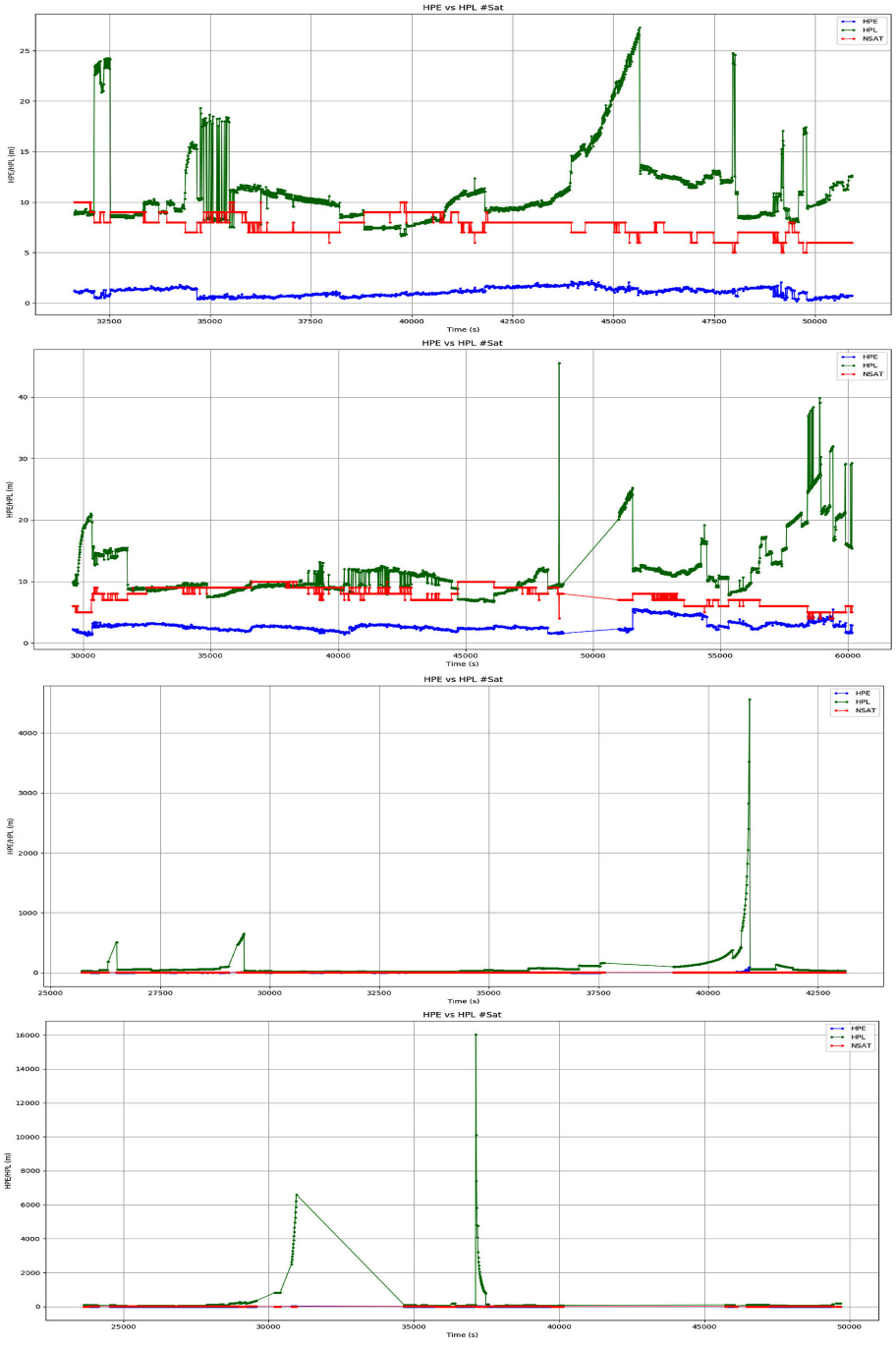

Figure 7. HPE and HPL for the 4 sites.

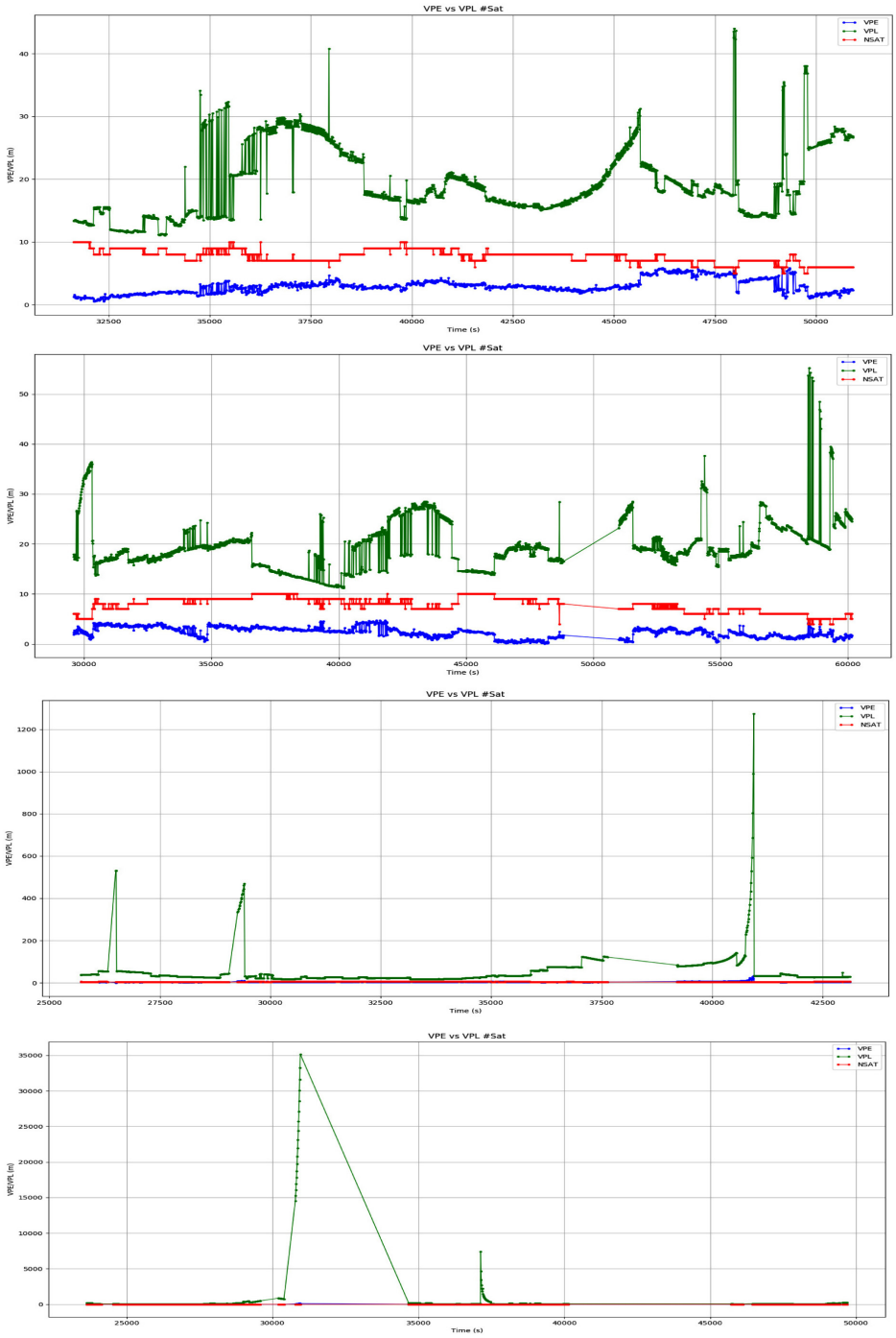

Figure 8. VPE and VPL for the 4 sites.

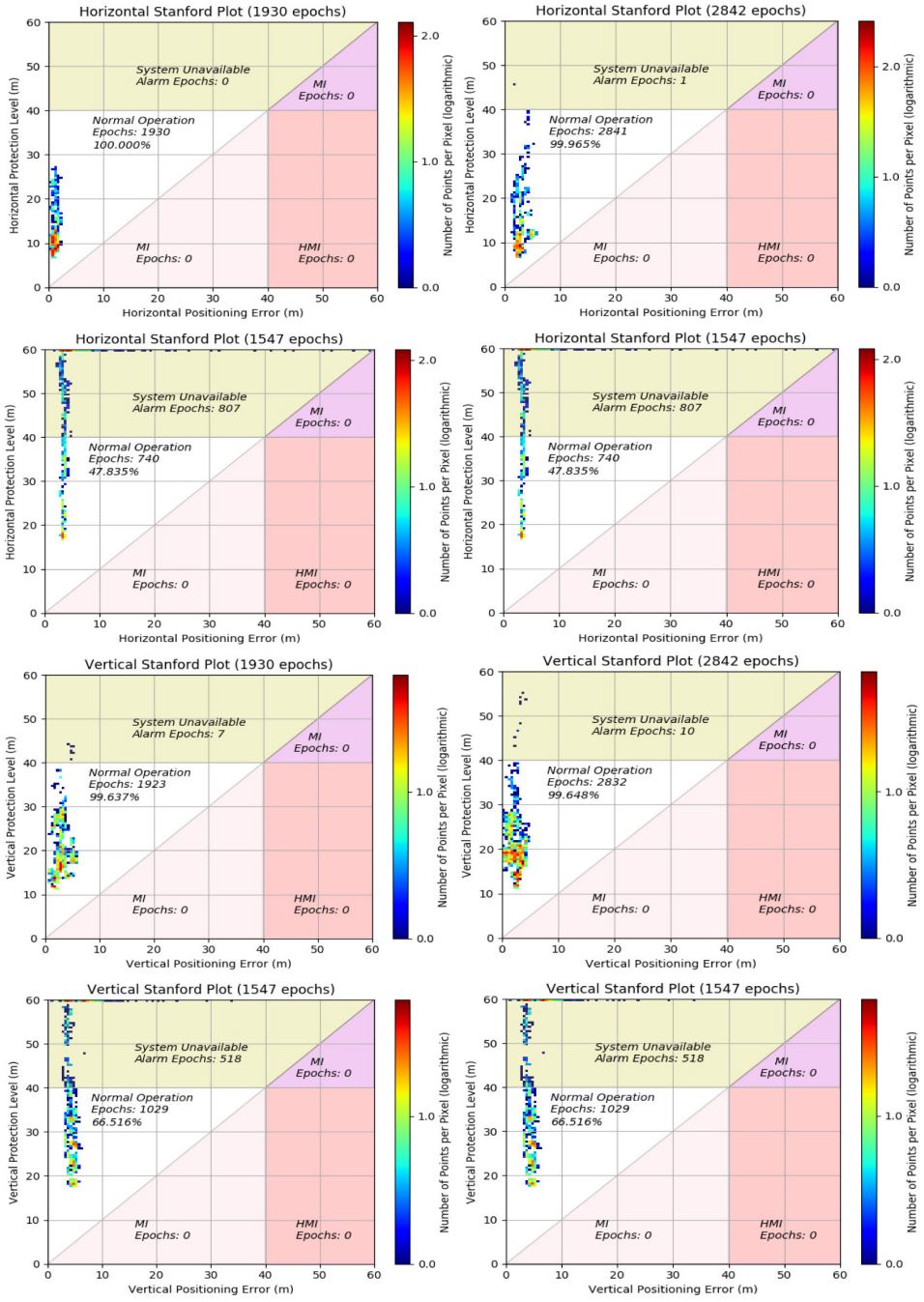

Figure 9. Stanford Plot for Horizontal and Vertical Protection Level.

From the results illustrated above, it can be concluded that only one site meets the requirements of ICAO phase APV I which is the ARZEW site in the extreme north of Algeria. For others sites, the HPL and VPL respectively exceed the 40 m and 50 m required for the APVI phase.

The availability required by ICAO for all phases of flight must be greater than 99.99%. In our case, this value is respected for both the vertical and horizontal components from the first site in the extreme north of Algeria only for the APV1 phase.

8 CONCLUSION

EGNOS system currently covers most of Europe and North Africa, with varying coverage areas depending on the service. In this work, we have analysed the EGNOS performance for4 sites in Algeria excluding the RIMS station. In the context of this work, the APV I approach is investigated. The accuracy and integrity for ARZEW, M'sila, Ouargla and In-salah are also analysed. The main conclusions drawn from the analyses carried out are:

– EGNOS performance results at the ARZEW site confirmed accuracy and integrity according to ICAO APV I flight phase, which is critical for aviation applications. However, at the other sites, the horizontal and vertical protection levels can reach 60 m and 80 m, which is higher than the horizontal and vertical alarm limits (40 m and 50 m). This is explained by the distance of these sites from the grid RIMS.

– The addition of RIMS stations in Algeria will certainly improve the geographical distribution of RIMS stations and increase the homogeneity of the network for the EGNOS system. These stations could extend the availability performance significantly beyond the original reference network regions.

– EGNOS performance may vary at different sites and maybe degraded in areas at the edge of system coverage.

REFERENCES

Beldjilali B. and Benadda B. (2017). *Real time software based L1 C/A GPS receiver*. Seminar on Detection Systems Architectures and Technologies. Algiers, Algeria.

Beldjilali B., Kahlouche S. and Tabti L. (2020). Assessment of EGNOS performance for civil aviation flight phase in the edge coverage area. *International Journal of Aviation, Aeronautics, and Aerospace*. 7(3).

Beldjilali B., Tabti H., and Kahlouche S. (2020). *Performance of the European Geostationary Navigation Overlay Service for Civil Aviation in North Algeria*. 8th International Conference on Defence systems: Architectures And Technologies (DAT'2020). Constantine, Algeria.

Cwiklak J., Grzegorzewski M. and Adamski M. (2014). *Studies of EGNOS suitability for air navigation in Poland*. IEEE Chinese Guidance, Navigation and Control Conference. Yantai, China.

ESA (2018). *Aviation User Needs and Requirements Outcome of the European GNSS, User Consultation Platform*. Report No GSA-MKD-AV-UREQ-230069. European Space Agency.

ESA (2011). *User Guide for EGNOS Application Developers*. Report No ED 2.0, 15/12/2011.

ESA (2019). *EGNOS Safety of Life (SoL)*. Service Definition Document. Issue 3.3. European Space Agency.

Fruehauf H. (2004). *WAAS, EGNOS, MSAS, and SNAS for telecom sync applications*. 2004 18th European Frequency and Time Forum. Guildford

Kaplan E.D. and Hegarty C.J. (2006). *Understanding GPS Principles and Applications*. Norwood: Artech House INC, Second Edition.

Manila M. (2018). *Civil aviation regulations air navigation services*. Aeronautical Telecommunications.

Marila S. (2016). Performance comparison of differential GNSS, EGNOS and SDCM in different user scenarios in Finland. European Navigation Conference (ENC). Helsinki, Finland.

Salomon H. (2020). Performance of EGNSS-Based Timing in Various Threat Conditions *IEEE Transactions on Instrumentation and Measurement.* 69(5).

Salvatori P. (2014). *Augmentation and Integrity Monitoring Network and EGNOS performance comparison for train positioning*. 22nd European Signal Processing Conference (EUSIPCO). Lisbon, Portugal.

Shuanggen J. (2012). *Global Navigation Satellite Systems – Signal, Theory and Applications*. Rijeka: InTech web.

CYBER SECURITY CHALLENGES FOR SAFE NAVIGATION AT SEA

Andrej Androjna[1*], Marko Perkovič[1], Ivica Pavić[2]

Abstract. *This paper provides an overview of cyber threats and actual incidents in the maritime sector, identifying nowadays challenges related to safe navigation. The vulnerabilities of satellite navigation systems, particularly the Global Positioning System (GPS) and the Automatic Identification System (AIS), receive special attention. For this article, a systematic literature review was conducted, complemented by an analysis of recent cyber-attacks and their influence on safe navigation. The analysis show vulnerabilities of maritime navigational systems against cyber threats and generation of erroneous position information. The maritime industry is neither immune to cyberattacks nor fully prepared for the risks associated with the use of modern digital systems. Maintaining seaworthiness in the face of the impact of digital technologies requires a shift in mindset to direct more attention and resources toward cybersecurity and a robust cybersecurity framework.*

Key words: *maritime cyber; cybersecurity; the safety of navigation; shipboard systems; Automatic Identification System (AIS); jamming and spoofing*

[1] Faculty of Maritime Studies and Transport, University of Ljubljana, 6320 Portorož, Slovenia; marko.perkovic@fpp.uni-lj.si

[2] Faculty of Maritime Studies, University of Split, 21000 Split, Croatia; ipavic71@pfst.hr

[*] Corresponding author: andrej.androjna@fpp.uni-lj.si

University of Zadar

1 INTRODUCTION

Today's global maritime sector depends increasingly on digitalization, integration of operations, and automation (**Androjna *et al.*, 2020**). Cyber technologies plays a significant role in contemporary shipborne systems, especially in the fields of safety, security, navigation, cargo handling operations and marine environment protection. These technologies have integrated IT (Information Technology) and OT (Operational Technology) onboard ships through networking and connectivity to the Internet (**World Economic Forum, 2020**; **Marineinsight, 2000**; **Middleton *et al.*, 2014**; **Chybowski *et al.*, 2019**; **Dobryakova *et al.*, 2018**; **Hareide *et al.*, 2018**). In the World Economic Forum's Global Risks Report 2020, cyberattacks on critical infrastructure with reference to shipping are rated the fifth top risk in 2020 (**WEF, 2020**). According to Boston Naval Dome's Cyber–attacks on the maritime industry's OT systems have increased by 900 % over the last three years.

The global maritime industry systems depend on satellite navigation that presents a vital part of a wide variety of shipboard, port, and even oil rig systems, especially the GPS and Automatic Identification System (AIS). Of particular concern is the relative ease (**Glomsvoll and Bonenberg, 2017**) by which these systems can be jammed (through denial of reception by a competing signal) or spoofed (through deliberate introduction of a false signal).

This paper presents findings from our paper titled: "AIS Data Vulnerability Indicated by a Spoofing Case-Study", published in Applied Sciences on 28 May 2021 (**Androjna *et al.*, 2021**) and updates regarding the Elba case. It presents vulnerabilities and challenges for safe navigation and shipping with a particular focus on spoofing. The paper confirms that the maritime industry is neither immune nor well prepared for the risks connected with modern digital systems vulnerabilities. Maintaining seaworthiness in the face of the impact of digital technologies requires a shift in mindset to direct more attention and resources toward cybersecurity and a robust cybersecurity framework.

This paper is organized as follows: Section 2 describes the methodology, Section 3 discusses significant findings, Section 4 presents a case study and finally, Section 5 contains a summary and conclusions.

2 METHODOLOGY

For our study (**Androjna *et al.*, 2021**) a systematic literature review followed by a comprehensive, explicit, reproducible and idiosyncratic implicit method of data collection was conducted and structured following the documented guidelines (**Tranfield *et al.*, 2003**; **Grant and Booth, 2009**; **Milner, 2015**). The specific aspect of AIS/GPS spoofing is corroborated by the case study analysis in section 3.1 from the Faculty of Maritime Studies and Transport, University of Ljubljana, regarding a particular AIS spoofing event near Elba Island in late 2019. As part of the research, AIS data were first obtained through cooperation with the Slovenian Maritime Administration, the Italian Coastguard, MarineTraffic and VesselFinder. The archive data was streamed again using the application AIS Network Data Client and played in two different VTS applications Navi-Harbor (Wärtsilä) and Pelagus (Elman). A navigation scenario was then configured in the affected area. The spoofing data AIS is displayed on Electronic Chart Display Information System (ECDIS) and RADAR applications via the ship handling simulator Navi Trainer Pro (Wärtsilä). Finally, using the EMODnet method, a traffic density map was created by using ship positioning data from terrestrial and Satellite-based AIS (S-AIS) data sources, maritime infrastructure, and the SafeSeaNet Ecosystem Graphical Interface application. Data analysis confirmed that typical maritime AIS can be easily spoofed and generate erroneous position information.

3 FINDINGS

This chapter highlights the unique AIS challenges associated with problems in securing ships at sea. It presents findings on AIS vulnerabilities, some of the recent examples of AIS spoofing trajectories, and practical investigations of an AIS spoofing event (**Androjna *et al.*, 2021**).

The last two years of the decade have been remarkable in many ways. While the coronavirus pandemic has disrupted operations worldwide, some global trends have continued unabated. One of these is our increasing reliance on the Global Navigation Satellite System – GNSS (**Buesnel, 2020**; **Androjna and Twrdy, 2020**). In recent years, there have been several disruptive incidents that have caused a stir in the shipping industry, as shown in **Table 1**.

Table 1. An overview of some GNSS spoofing events that affected maritime traffic between the years 2008 and 2020.

Location and Date	Spoofing Incidents Description
The Southern Ocean, 2008–2018	To disguise her illegal fishing operations, M/V Andrej Longov/Sea Breez 1/Ayda/STS-50 committed identity fraud by repeatedly falsifying her registry, producing multiple fake signals, and appearing in nearly 100 different locations simultaneously.
Gulf of Oman/Malaysia, 09/2013	M/V Ramtin was involved in "spoofing" by falsely transmitting her AIS identity during suspicious activities and deceiving authorities at Karachi port under the name of M/V Hamoda.
Ten global locations connected to one of the superpower states, 2016–2019	9883 suspected spoofing incidents.
The Black Sea, 06/2017	Vessel tracking systems placed many vessels near Novorossiysk Commercial Sea Port in the nonsensical location, on the Gelendzhik Airport.
The East China Sea, 28/10/2018	M/V Yuk Tung was involved in "spoofing" by falsely transmitting its AIS identity in a suspicious ship-to-ship transfer and deceiving authorities under the name of M/V Hika, which was anchored in the Gulf of Guinea, more than 7000 m away.
Point Reyes in northern California, 08/2018–06/2019	Ships thousands of miles at sea mysteriously reported GPS positions in ring patterns off the coast of San Francisco.
Eastern Mediterranean and the Red Sea, 2018–2019	Signal interference, loss of erratic AIS/GPS signals.
Strait of Hormuz, 07/2019	A British oil tanker, the Stena Impero, was seized by Iranian forces after the ship was spoofed into changing course into Iranian waters.
Ningbo (China)-Nampo (Democratic People's Republic of Korea), 07–11/2019	The M/V Fu Xing 12 manipulated its identity by employing two AIS on board and using four different ship names to disguise its operations in delivering illegal coal and other resources.
Port of Shanghai, 2018–2019	Fake signals caused ships to appear to be moving in ring patterns at short intervals.
Ponce De Leon Inlet, Florida, 2020	Four visual AtoNs appeared on the map based on fake AIS messages.
Elba Island, 03/12/2019	Deliberate spoofing of the vast number of artificial AIS targets temporarily affected the navigation of ships.
Galapagos, 07/2020	One of the world's largest fleets of fishing nations misreported its location (approximately 10,000 km from its observed location) to conceal illegal fishing activities in the exclusive economic zone (EEZ) around the Galápagos Islands.

Source: **Androjna *et al.*, 2021**

It can be concluded that the original purpose of AIS spoofing to this day is to disguise illegal fishing and other illegal activities at sea, which includes ship spoofing and AIS hijacking. There have also been some examples of Aids to navigation (AtoN) spoofing. In recent years, we have seen GNSS spoofing as part of defense development in a civilian scenario. The AIS spoofing has been deliberately used for electronic warfare and concealment of military activities, just like the eastern Mediterranean and the Red Sea situation (**Androjna *et al.*, 2021**).

At the incident in the Black Sea, the vessel tracking systems placed many vessels near Novorossiysk Commercial Sea Port in the nonsensical location – on the Gelendzhik Airport, as shown in **Figure 1** (**C4ADS, 2019**). That led us to speculate that it could be attributed to one of the tests of satellite spoofing technology by one of the space superpower states. Whether as part of their electronic warfare arsenal or simply as an anti-drone measure to protect very important persons (**Androjna *et al.*, 2020**).

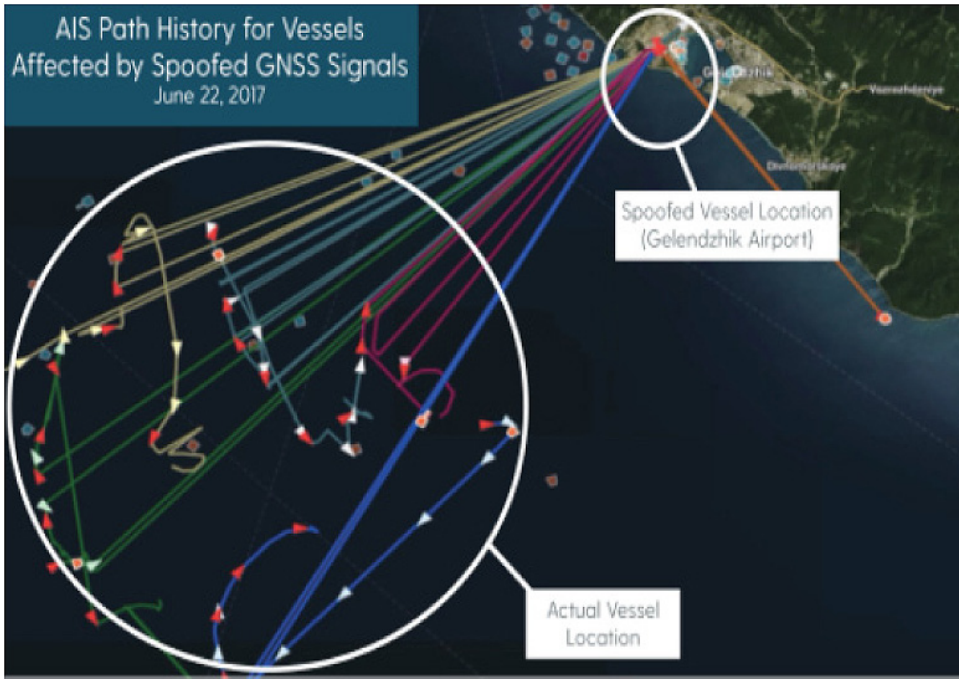

Figure 1. GNSS Spoofing at Gelendzhik Airport.
(Source: **C4ADS, 2019**)

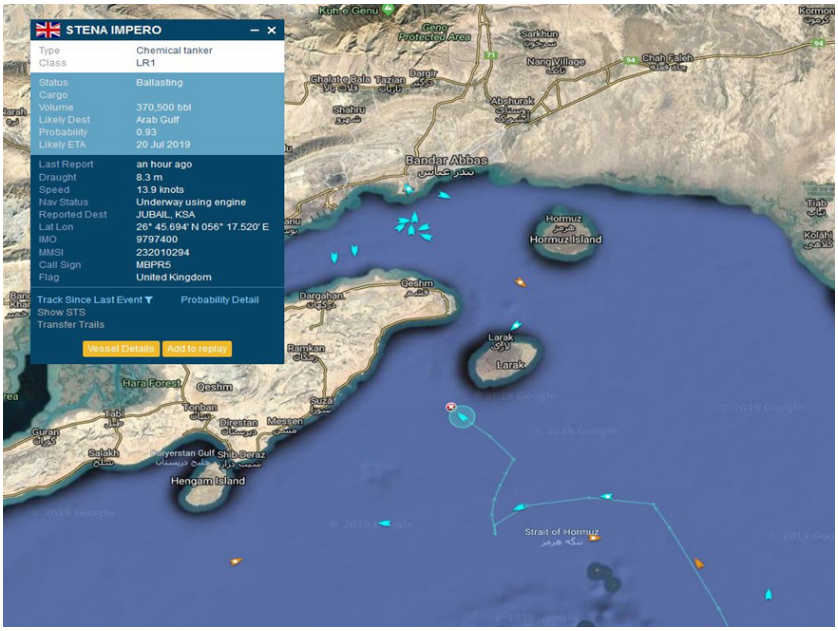

Figure 2. Stena Impero veered off-course.
(Source: **ClipperData, 2019**)

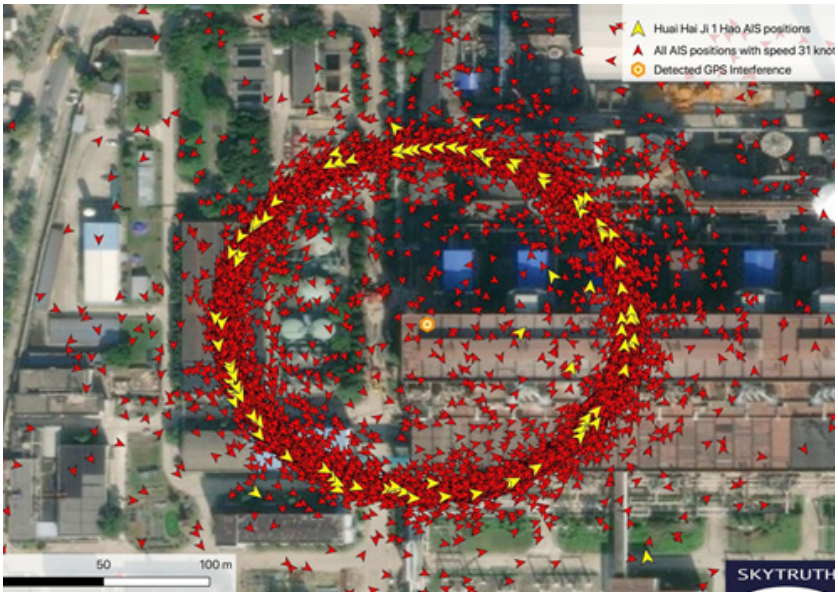

Figure 3. Fake signals caused ships to appear to be moving in ring patterns at short intervals.
(Source: **SkyTruth, 2020**)

An example of GNSS spoofing that had a great impact on the maritime community and international trade occurred in July 2019 in the Strait of Hormuz. Because of the GNSS spoofing British oil tanker the Stena Impero altered the course into Iranian waters (as shown in **Figure 2**), and she was seized by Iranian forces. (**Lloydslist, 2019**). As a result, many of the shipping companies require that their ships sail at a high speed and only during the day while transiting through the Strait of Hormuz. It is important to mention that one-third of the world's oil flows by the sea – about 17 million barrels per day – through the strait, making it one of the essential oil trade routes in the world (**Lloydslist, 2019**).

One more recent example of AIS spoofing occurred in China. Multiple spoofing incidents in more than 20 coastal areas and ports have been reported. The incidents lasted for months. The GNSS signals were congregated into large circles, later dubbed »crop circles«, moving signals shifted to the same position, resulting in a confusing traffic situation for the pilots of ships, as shown in **Figures 3** and **4**. Since the locations of the »spoofing circles« are oil terminals, some sources suggest that it was a matter of covering up the trade of Iranian oil due to international sanctions. (**Insidegnss.com, 2021**; **Maritime-executive.com, 2021**).

Figure 4. Locations of detected GPS manipulation occurring in six Chinese cities in 2019. (Source: **SkyTruth**, **2020**)

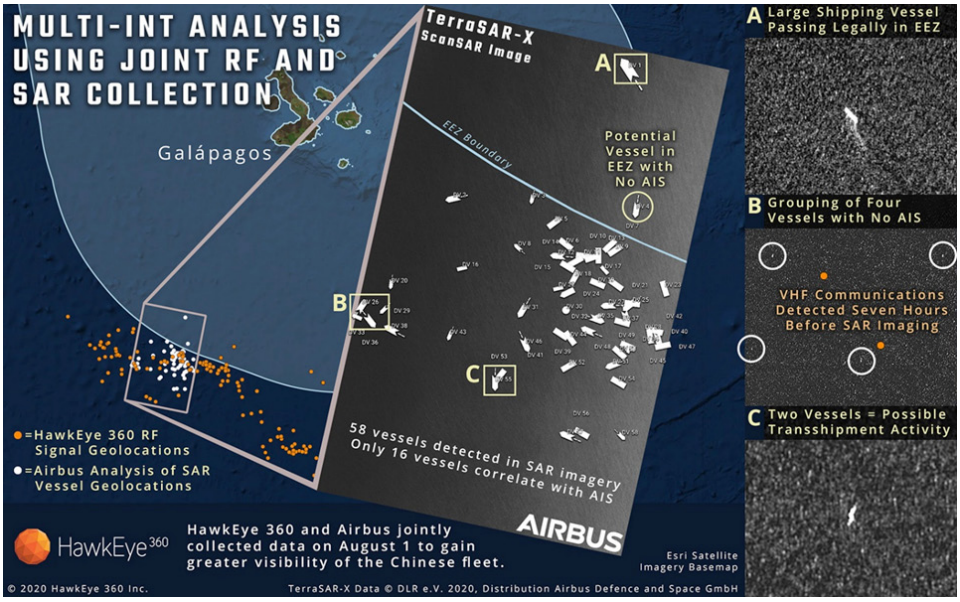

Figure 5. Vessels disappearance from AIS tracking, the Galápagos Islands. (Source: **HawkEye360**, **2020**)

In July 2020, another case of spoofing of AIS signal in the waters of the Galápagos Islands occurred. Fishing vessels located within the EEZ of the Galápagos Islands broadcast positions via AIS on New Zealand or stopped broadcasting an AIS signal to covertly carry out illegal fishing activities in the Galápagos EEZ as shown in **Figure 5** (**HawkEye360**, **2020**).

4 AIS SPOOFING EVENT NEAR ELBA ISLAND – CASE STUDY

In December 2019 an Italian AIS base station experienced a ship-spoofing situation near Elba Island that was visible in the European Maritime Safety Agency (EMSA) Maritime Application, SSN Ecosystem GUI. The first investigation provided by the Italian Coast Guard indicated 870 different vessels were created at two different moments (13:13 and 13:28 hours, respectively) with a duration of 3 min in the first transmission and 2 min in the second. All the tracks appeared in an area of 28 × 21 nautical miles between Elba Island and Corsica with different routes and speeds, rendering the monitoring of the maritime traffic in the area impossible and impacting real vessel transmissions (**Androjna *et al.*, 2021**).

At the Faculty of Maritime Studies and Transport, University of Ljubljana, we have thoroughly investigated the situation to support EMSA's analysis and found 3742 fake ships (861 false tracks with MMSI 24480XXXX) that generated together 5133 reports. By using the European Marine Observation and Data Network (EMODnet) method, a traffic density map is created by using ship positioning data collected from Terrestrial and Satellite AIS data sources, the maritime infrastructure, and the SafeSeaNet Ecosystem Graphical Interface application. It showed a shipping density of up to 45 ships/km2, as shown in **Figure 6** (**Androjna *et al.*, 2021**).

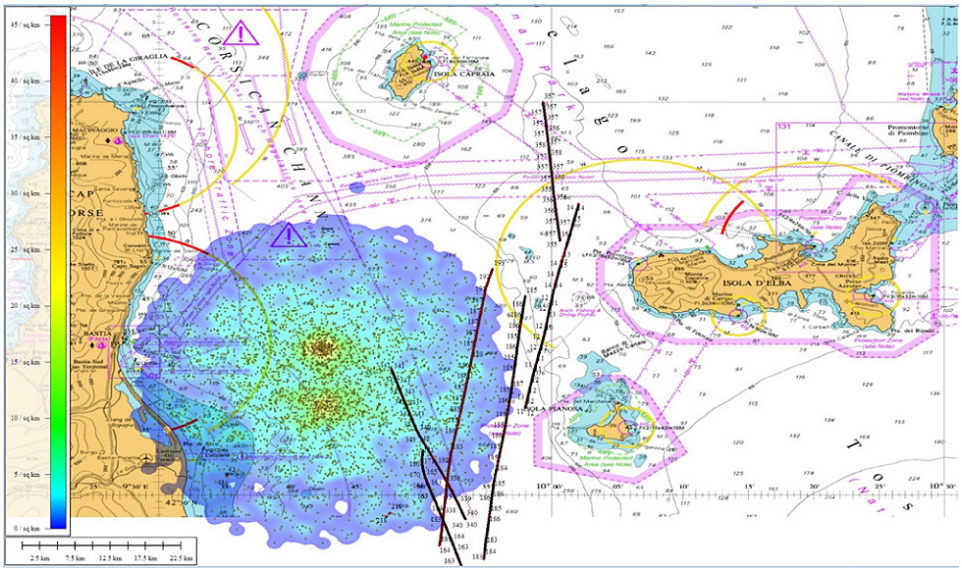

Figure 6. AIS spoofing – shipping density near Elba Island
(Screenshot of Global Mapper, Admiralty Raster Chart background).
(Source: **Androjna *et al.*, 2020**; **Androjna *et al.*, 2021**)

It also shows seven vessels are in a spoofing cloud. During the spoofing event, the broadcasting system was overloaded. Thousands of AIS streams were received and recognized as Dutch-flagged naval units that were artificially generated and had different identification codes, positions, routes, and speeds. There were 3 AIS bursts, and "all" ships were identified as passenger ships (AIS type 60) with a length of 90 meters and a width of 24 meters, without draft and destination information (**Androjna *et al.*, 2021**).

Right at the beginning of spoofing, two exciting AIS targets also appear at the edge of the generated cloud of artificial targets. The first with the invalid Maritime Mobile Service Identity (MMSI) number 999999999, which is quite common around AIS and often associated with navy vessels. The second vessel is a Belize-registered bulk carrier (MMSI 312320000) that has been scrapped since 2016. Individual fishing vessels are known to take on the identity of scrapped vessels. Received data indicates that a spoofing algorithm was run with auto-incrementing MMSI numbers. Possible candidates for this AIS spoofing event are ships with MMSI 999999999, MMSI 312320000 and MMSI 367309390. In this case study, it was not possible to determine the reasons for spoofing and the location of the transmitter that generated the false signals. Furthermore, the simulation of the mentioned spoofing event shows a possible impact on the safety of navigation (**Androjna *et al.*, 2021**).

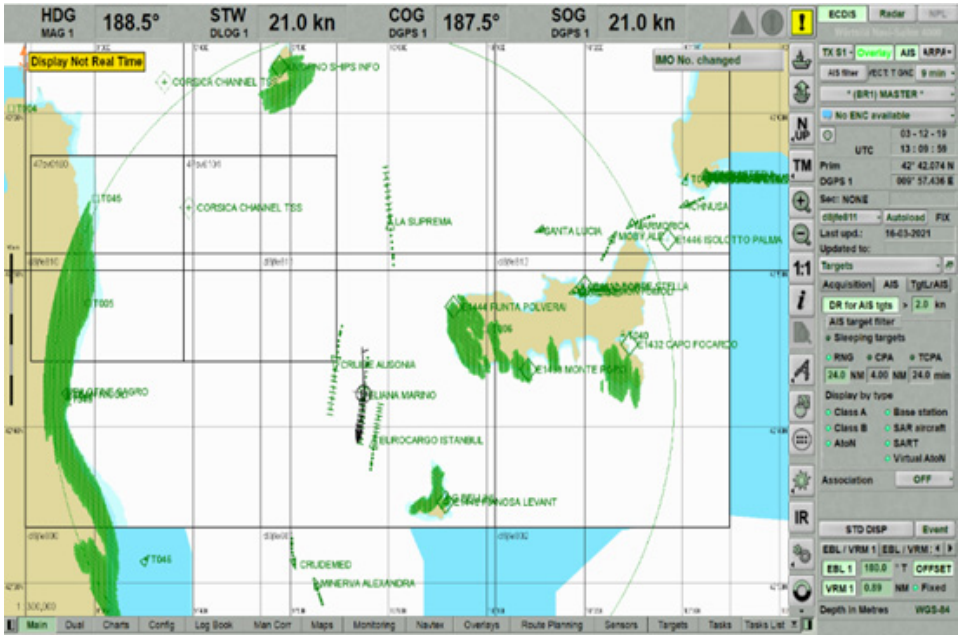

Figure 7. Simulation of the M/V "Eliana Marino" ECDIS display just a minute before the actual spoofing occurrence (Screenshot of Navi-RADAR 4000 ECDIS MFD, Navi-Trainer Professional 5000 Simulator, Wärtsilä).
(Source: **Androjna *et al.*, 2021**)

For this case study, we have picked up M/V "Eliana Marino" within the area covered by the AIS spoofing cloud. We have synchronized the clock with the AIS data, and by using her actual position, course and speed, we were able to simulate what has been seen on her ECDIS screen just a minute before AIS spoofing. **Figure 7** presents the information obtained by the radar (including AIS) overlay display on ECDIS.

Figure 8 presents the first burst of AIS spoofing event displayed on ECDIS with radar overlay and AIS data, in which significant degradation of Maritime situational awareness (MSA) is caused, and 95% of the AIS signal processing load occurs.

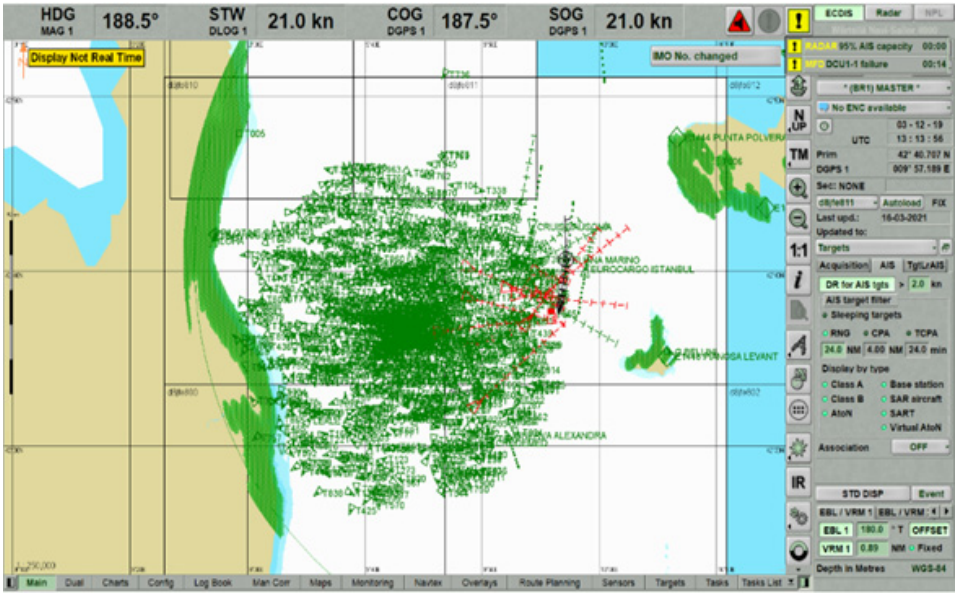

Figure 8. AIS processing overload (Screenshot of Navi-RADAR 4000 ECDIS MFD, Navi-Trainer Professional 5000 Simulator, Wärtsilä).
(Source: **Androjna *et al.*, 2021**)

Consequently, the radar image shows a dangerous situation of M/V »Eliana Marino« on a collision course with more than a dozen other fake M/V, as shown in **Figure 9**.

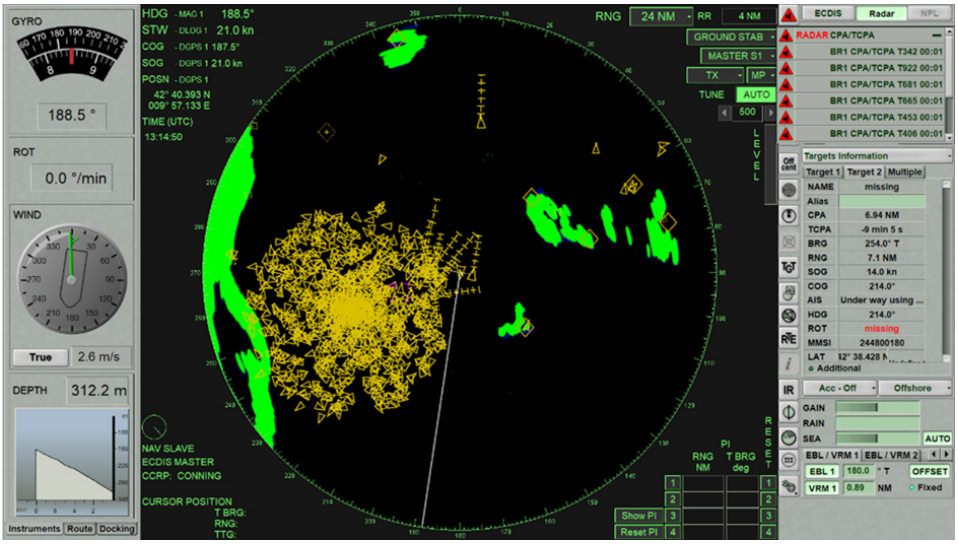

Figure 9. Collision course with the number of ships (Screenshot of Navi-RADAR 4000 ECDIS MFD, Navi-Trainer Professional 5000 Simulator, Wärtsilä). (Source: **Androjna *et al.*, 2021**)

This situation presents a significant risk for navigation since many false signals with collision course and a very short Closest Points of Approaches (CPA) are generated. Consequently, a relatively large number of collision alarms appears, which can further lead to inadequate Officer of the watch (OOW) decisions. An experienced OOW will use in this situation a »raw« radar picture without the AIS data support and enhance sharp visual lookout. Luckily, the AIS spoofing event took place during the daytime and in a favourable navigation area. If it occurred during the night and in a dense maritime traffic area dangerous for navigation, it might have severe consequences on the safety of navigation. Therefore, the OOWs need to be aware of the possibility of AIS spoofing and the possible impact on the MSA (**Androjna *et al.*, 2021**).

5 CONCLUSIONS

In summary, we have pointed out the importance of cybersecurity. GNSS spoofing has been a defense issue for many years and is now beginning to affect shipping. As more devices and autonomous systems rely on GNSS, even more systems could be vulnerable to spoofing attacks. The maritime industry and

shipping are not immune to such cyberattacks, nor is the situation expected to improve soon.

With hackers constantly looking for new ways to spoof and exploit AIS vulnerabilities, there will be several new cybersecurity openings in the future through which systems will be attacked if they are not adequately protected. Our analysis has shown that even a relatively easy to obtain AIS spoofing generator, such as that found near Elba Island, can have an impact on ship security. It was pointed out that many such ships appearing on the screen are primarily a technical problem, clearly projecting a false scenario. Under this mass of data, a ship can be missed, making it essential to use other safe navigation means simultaneously. Given the impact of digital technologies and to maintain seaworthiness, robust cybersecurity frameworks are needed. Disruptions to GNSS-based positioning and navigation have become a global phenomenon. To address a global problem, the GNSS community needs a global solution. The maritime industry needs to be ahead of the game, so manufacturers need to ensure the reliability, resilience, and functioning of multi-sensor systems for safety and liability reasons. Certainly there will always be a temporal challenge involved, as there is in every conceivable contest between fiscal order and criminal or even non-criminal attempts to confound any extant and ultimately arbitrary and –face it—virtually therianthropic process or system; in recognition of this mutable, not to say fickle, circumstance, we restrain ourselves from exhibiting undue confidence in any current solutions or even sojourns towards such, and conclude primarily that more effort need be made, and, frankly, that will always be the case, if the last three or so millennia of history be taken into account.

That said, navigators should never rely on a single source of information and should double-check the data provided by AIS; and, as clearly explained, building resilience against cybercriminals is a never-ending battle.

List of Acronyms

AtoN	Aids to Navigation
AIS	Automatic Identification System
ECDIS	Electronic Chart Display and Information System
EMSA	European Maritime Safety Agency
EMODnet	European Marine Observation and Data Network
GNSS	Global Navigation Satellite System
GPS	Global Positioning System

MMSI	Maritime Mobile Service Identity
MSA	Maritime situational awareness
OOW	Officer of the watch
OT	Operational Technology
PC	Personal Computer
RADAR	RAdio Detection And Ranging

REFERENCES

Above Us Only Stars (C4ADS) – Exposing GPS Spoofing in Russia and Syria. Available on: https://www.c4reports.org/aboveusonlystars, accessed on 27 February 2021).

AIS Ship Tracking Data Shows False Vessel Tracks Circling Above Point Reyes, Near San Francisco. Available online: https://skytruth.org/2020/05/ais-ship-tracking-data-shows-false-vessel-tracks-circling-above-point-reyes-near-san-francisco/, accessed on 27 May 2020.

Androjna, A.; Brcko, T.; Pavic, I.; Greidanus, H. Assessing Cyber Challenges of Maritime Navigation. *J. Mar. Sci. Eng.* **2020**, 8, 776.

Androjna, A.; Perkovič, M.; Pavic, I.; Mišković, J. AIS Data Vulnerability Indicated by a Spoofing Case-Study. *Appl. Sci*. **2021**, 11, 5015.

Androjna, A.; Twrdy, E. Cyber Threats to Maritime Critical Infrastructure. In *Cyber Terrorism and Extremism as Threat to Critical Infrastructure Protection*; Čaleta, D., Powers, F.J., Eds.; Ministry of Defense, Republic of Slovenia, Institute for Corporative Security Studies, Joint Special Operations University: Ljubljana, Slovenia; Tampa, FL, USA, **2020**; pp. 163–170.

Chinese Fishing Fleet Encroaches on the Galapagos Islands: HawkEye360 Monitors the Fleet for Suspicious Behavior and Potential Illegal Fishing. Available online: https://www.he360.com/insight/potential-illegal-fishing-seen-from-space/, accessed on 1 February 2020.

Chinese Fishing Fleet Encroaches on the Galapagos Islands HawkEye360 Monitors the Fleet for Suspicious Behavior and Potential Illegal Fishing. Available online: https://www.he360.com/insight/potential-illegal-fishing-seen-from-space/, accessed on 1 February 2021.

Chybowski, L.; Gawdzinska, K.; Laskowski, R. Assessing the Unreliability of Systems during the Early Operation Period of a Ship—A Case Study. *J. Mar. Sci. Eng*. **2019**, 7, 213.

ClipperData. ClipperData July 19, 2019 – the vessel took an abrupt turn north. Available at: https://twitter.com/ClipperData/status/1152276984355000321, accessed on 22 March 2021.

Dobryakova, L.A.; Lemieszewski, L.S.; Ochin, E.F. GNSS spoofing detection using static or rotating single-antenna of a static or moving victim. *IEEE Access* **2018**, 6, 79074–79081.

Glomsvoll, O.; Bonenberg, L. GNSS Jamming Resilience for Close to Shore Navigation in the Northern Sea. *J. Navig.* **2017**, 70, 33–48.

Grant, M.J.; Booth, A. A Typology of Reviews: An Analysis of 14 Review Types and Associated Methodologies. *Health Inf. Libr. J.* **2009**, 26, 91–108.

Hareide, O.S.; Jøsok, Ø.; Lund, M.S.; Ostnes, R.; Helkala, K. Enhancing Navigator Competence by Demonstrating Maritime Cyber Security. *J. Navig.* **2018**, 71, 1025–1039.

Maritime Cyber-Attacks Increase by 900% in Three Years. Available online: https://www.marineinsight.com/shipping-news/maritime-cyber-attacks-increase-by-900-in-three-years/#, accessed on 20 April 2021.

Middleton, A. Hide and Seek: Managing Automatic Identification System Vulnerabilities: Proceedings of the Marine Safety and Security Council, Coast Guard. J. Saf. Secur. Sea **2014**, 71, 48–50.

Milner, K.A. Systematic Reviews. *Oncol. Nurs. Forum* **2015**, 42, 89–93.

Patterns of GPS Spoofing at Chinese Ports. Available online: https://www.maritime-executive.com/editorials/patterns-of-gps-spoofing-at-chinese-ports, accessed on 2 February 2021.

Seized UK Tanker Likely 'Spoofed' by Iran. Available online: https://lloydslist.maritimeintelligence.informa.com/LL1128820/Seized-UK-tanker-likely-spoofed-by-Iran, accessed on 20 July 2020.

Sinister Spoofing in Shanghai. Available online: https://insidegnss.com/sinister-spoofing-in-shanghai/#:~:text=Someone%20has%20updated%2019th%20century,experts%20have%20never%20seen%20before, accessed on1 February 2021.

Thousands of GMDSS Jamming and Spoofing Incidents Reported in 2020. Available on: https://www.linkedin.com/pulse/thousands-gnss-jamming-spoofing-incidents-reported-2020-guy-buesnel/, accessed on 1 February 2021.

Tranfield, D.; Denyer, D.; Smart, P. Towards a Methodology for Developing Evidence-Informed Management Knowledge by Means of Systematic Review* Introduction: The Need for an Evidence-Informed Approach. Br. *J. Manag.* **2003**, 14, 207–222.

World Economic Forum (WEF). Wild Wide Web—Consequences of Digital Fragmentation. *The Global Risks Report 2020*, 15th Ed. ed. January 2020. Available online: https://www.weforum.org/reports/the-global-risks-report-, accessed on 20 April 2021.

DRONE AS A PART OF MARITIME SEARCH AND RESCUE OPERATIONS

Ivan Panić*, Jasmin Ćelić, Miroslav Bistrović, Antonio Škrobonja

Abstract. *Improving efficiency and response time of Search and rescue (SAR) services can improve victims' chance of survival and prevent unnecessary loss of life. Success rate of SAR operation significantly depends on the response speed and magnitude of the search area. These often include areas with reduced visibility where approach is highly difficult or impossible. This can place SAR teams that are conducting the SAR mission or otherwise helping the victims, in danger. One of the potential solutions that can help with locating and identifying victims in danger, while at the same time reducing time necessary for extracting the victims from harm's way, regardless of the time of day or the terrain is unmanned aerial vehicle (UAV) or drone. SAR missions at sea would benefit greatly from the use of drones equipped with thermal imaging equipment due to the fact that thermal cameras can read temperature measurement very easily and display temperature readings as an image or video in various sea conditions, regardless of the time of the day and night. This paper presents one possible solution to victim recognition in the sea by the use of drone equipped with thermal camera. Low cost solution developed in this paper was tested on several different scenarios. Future work and improvement recommendations are presented.*

Key words: *Search and rescue (SAR); services and operation at sea; unmanned aerial vehicle (UAV); drone; GNSS; thermal camera; horizontal and vertical projections*

University of Rijeka, Faculty of Maritime Studies, Department of Electrical Engineering, Automation and Computing, Studentska 2, 51000 Rijeka, Croatia
University of Rijeka, Faculty of Maritime Studies, Center for Marine Technologies
* Corresponding author: Ivan Panić (ivan.panic@uniri.hr)

1 INTRODUCTION

Unmanned Aerial Vehicle (UAV) or a drone is a remotely piloted or autonomous flying machine that can carry a payload but does not require a pilot on board. Drone technology has long been researched and limited primarily for military purposes, but in recent years public UAV research and development has experienced rapid growth. Improved payload capacity, flight times as well as precision and accuracy in UAV positioning are enabling greater autonomous drone operation and diversifying the potential tasks for which the UAVs can be used (**Krasuski and Wierzbicki, 2021**). This allows drones to be used for tasks that need to be initiated urgently or for those tasks that may be dangerous and perilous for humans to perform. Conventional RGB and thermal imaging systems mounted on drones have been explored, and the technology has been used and implemented in border control, search operations as well as tracking and disaster relief missions (**Csernatoni, 2018**; **Leira, Johansen and Fossen, 2016**; **Quan, Herrmann and Hamdy, 2019**; **Erdelj and Natalizio 2016**). In Australia, drone has been used to successfully transport and deploy an inflatable life raft persons in distress within minutes (**AN, 2021**). It has been shown that drone support in emergency situations, even if it is provided by the non-professional drone operator can be of a great benefit to public safety (**Robakowska *et al.*, 2019**). UAVs have been researched and implemented as a tool for coastal mapping and monitoring, topobathymetry, hydrographic surveys and measurements (**Genchi *et al.*, 2020**; **Nikolakopoulos *et al.*, 2018**; **Specht *et al.*, 2020a**; **Specht *et al.*, 2020b**).

Low cost UAV/USV solution for topobathymetry was presented in (**Genchi *et al.*, 2020**) where it was shown that UAVs can be used for shallow water remote sensing, even in turbid tidal environments. In (**Nikolakopoulos *et al.*, 2018**; **Specht *et al.*, 2020a**; **Specht *et al.*, 2020b**) drone and Unmanned Surface Vehicle (USV) has been used for shallow water mapping and survey using Structure From Motion (SFM) photogrammetry and digital surface modelling. It was demonstrated that UAVs can be used to detect and map morphological features in shallow waters.

Relatively high degree of drone's autonomous and remote-control capabilities combined with the increases in maneuverability, mobility and flight time allows for rapid activation, start-up and deployment of the unit in the field. This feature is of particular interest for search and rescue missions (SAR). However, SAR missions are highly stressful and complex for both victims and SAR personnel. The primary goal of SAR is to save lives as quickly and efficiently as possible in the shortest amount of time. Any delay in SAR deployment can significantly

reduce the chance of survival for those at risk (**Lee and Morrison, 2015**). Search and rescue in maritime emergencies is specific as it may involve lost or missing persons, sea vessels, damaged aircraft, etc. (**Xiong, Gelder and Yang, 2020**). The specifics of the maritime environment at the time of deployment SAR have a relatively high potential to negatively impact the success of the mission and reduce the chances of victim survival. In the event of a maritime emergency, the SAR operation must be planned, coordinated, controlled, and commanded as quickly as possible, while taking into account the specific maritime environmental conditions such as wind, waves, and currents at and around the SAR deployment site (**Ghazali *et al.*, 2016**). Conventional imaging devices such as visual RGB cameras have been successfully used in SAR operations as they provide a clear overview and good understanding of the surveyed area at low implementation cost (**FC, 2019**). Cost of the complete RGB and thermally equipped drone SAR solution with 30-minute flight capability is estimated at 28000 USD, which in comparison with conventional systems represents significantly cheaper air reconnaissance method (**Burke *et al.*, 2019**). The rapid deployment, good vertical and horizontal flight capability, and maneuverability of the drone allow for rapid identification and monitoring of victims in maritime environments (**Ghazali *et al.*, 2016**). However, the images captured by a conventional camera are prone to degradation in quality when captured in poor lighting or darkness, limited visibility, or other adverse weather conditions. This increases the complexity of target detection and classification, directly increasing the possibility of false positive or negative target identification. Thermal imagers are not subject to the same problems as conventional camera types and can be used in poor visibility or darkness (**Burke *et al.*, 2019**; **Portenier *et al.*, 2019**). Because of these improvements over conventional imaging systems, it is increasingly being used in SAR missions. In marine and offshore rescue operations, drones equipped with thermal imaging technology would be beneficial in such cases where the victim's body temperature is significantly different from the temperature of the surrounding sea. Integrating thermal technology into a UAV has the potential to increase the search area and decrease the time required for the search. In this way, primary search areas can be quickly covered and ruled out, while reducing the required search time improves the victim's chances of survival. Remote or autonomous operation of drones can reduce some of the potential hazards to SAR personnel in cases where it would be dangerous or risky to perform these tasks in person.

Machine learning systems for human body identification and classification as part of drone-based search and rescue missions can identify and recognize

human bodies even when only part of the human body is clearly visible (**Quan, Herrmann and Hamdy, 2019**; **Rodin *et al.*, 2018**). The main problem with computer vision systems based on machine learning is that the precision and accuracy of the classification model strongly depends on the large amount of representative training data. When the number of input data points is small or the data is not fully representative, the classification accuracy of a machine learning algorithm may decrease significantly (**Brain, Webb, 2000**; **Ponce *et al.*, 2006**). In such cases, it may be beneficial to use simpler methods for object recognition (**Burke *et al.*, 2019**).

2 MATERIALS AND METHODS

2.1 Proposed method

Success of the maritime SAR operations greatly depends on the fast response time and the ability of the SAR personnel to locate and identify the victims irrespective of the time of the day and the weather conditions on site. This paper proposes a method of victim identification and classification using the drone equipped with RGB/thermal camera as presented on **Figure 1**.

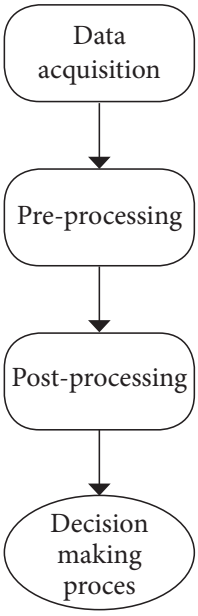

Figure 1. Proposed method for human body detection.

Pre-calibration is performed on the imaging equipment mounted on the drone before the actual flight. This takes into account the camera focus, image, clarity, sharpness, brightness and thermal contrast. This improves the quality of the images captured as well as the accuracy and precision of the thermal imaging camera's temperature measurement. After pre-calibration, the drone can lift the imaging payload and survey the location of interest. During flight, the RGB and thermal cameras are active and continuously recording. Image quality is monitored and the system is automatically recalibrated as needed. Conventional visible RGB as well as thermal HD video is continuously captured and recorded locally on the drone. Video feedback is sent back to the user via the transceiver unit on the flight controller.

All further image and data processing are performed on the drone mounted processing board. Image preprocessing is used to simplify further image analysis. Before image preprocessing, the size of the input image can be changed or reduced, which can reduce the time required for further processing. Individual images are extracted from both RGB and thermal video and preprocessed as grayscale images, after which adjustments to brightness and contrast are be made. Thermal images can be displayed in grayscale or in different color palettes, where pixels representing specific temperature data points are assigned a unique color or shading related to the recorded thermal energy (**TFER, 2021**). Colored images are converted to gray (k) such that the value of individual pixels is determined with respect to the value of the RGB colors (red (r), green (g), and blue (b), respectively) while taking into account horizontal (x) and vertical (y) coordinates, according to the NTSC standard (**Pascale, 2003**).

$$k(x,y) = 0{,}299 \cdot r(x,y) + 0{,}587 \cdot g(x,y) + 0{,}114 \cdot b(x,y) \quad (1)$$

Contrast enhancing procedures are performed on grayscale image in order to emphasize the displayed objects. Thermal camera orientation, distance between the camera and the target can significantly reduce thermal contrast. Contrast enhancement techniques become even more important if the camera is capturing scenes with inherently low thermal contrast (**Thillainayagi and Kumar, 2019**). In maritime environments, sun glint reflected from the surface of the water, and subsurface illumination have negative impact on image quality. These issues can be reduced or eliminated by drone flight planning and image postprocessing (**Joyce *et al.*, 2018**). After the adjustments are made to brightness and contrast, image is binarized and converted to bitmap format. Image binarization procedure

assigns values of 0 or 255 (black or white) to the individual image elements with respect to some threshold. Threshold can be calculated globally for the entire image or locally where the threshold calculation takes into account local image element as well as adjacent elements. Image was binarized using the Adaptive Thresholding technique (**Bradley and Roth, 2007**) where the gray scale color intensity of each pixel is compared to the average intensity of the surrounding pixels, $\overline{k(x,y)}$ with respect to the threshold parameter θ. Threshold setting can be set or adjusted during the pre-calibration phase.

$$g(x,y) = \overline{k(x,y)} \cdot \frac{100-\theta}{100} \tag{2}$$

$$0 \leq \theta \leq 100 \tag{3}$$

If the color intensity value of the current pixel is θ percent lower than the average value, color of that pixel, $p(x,y)$, is set to black, otherwise, pixel color is set to white.

$$p(x,y) = \begin{cases} 255 \; if \;\; g(x,y) > k(x,y) \\ 0 \quad if \;\; g(x,y) \leq k(x,y) \end{cases} \tag{4}$$

Adaptive Thresholding technique was used as it provides good results in cases where the image consists of primarily background pixels, which increases human identification method robustness with respect to changes in illumination from the water surface technique (**Bradley and Roth, 2007**). As a part of post-processing, horizontal and vertical image projections are performed on individual bitmaps as shown on **Figure 2**. Projection profile represents a function that maps binarized image values into a one-dimensional array, or histogram. The values of the histogram are the sums of white pixels along a particular image direction. This mapping can be calculated separately for both vertical and horizontal image axis, referred to as Vertical Projection profile, $V_p(x)$, and Horizontal Projection profile, $H_p(x)$, respectively.

$$V_P(x) = \sum_{y=0}^{y_n-1} p(x,y) \tag{5}$$

$$H_P(y) = \sum_{x=0}^{x_n-1} p(x,y) \tag{6}$$

Both, vertical and horizontal projections serve as base features upon which any further classification can be performed.

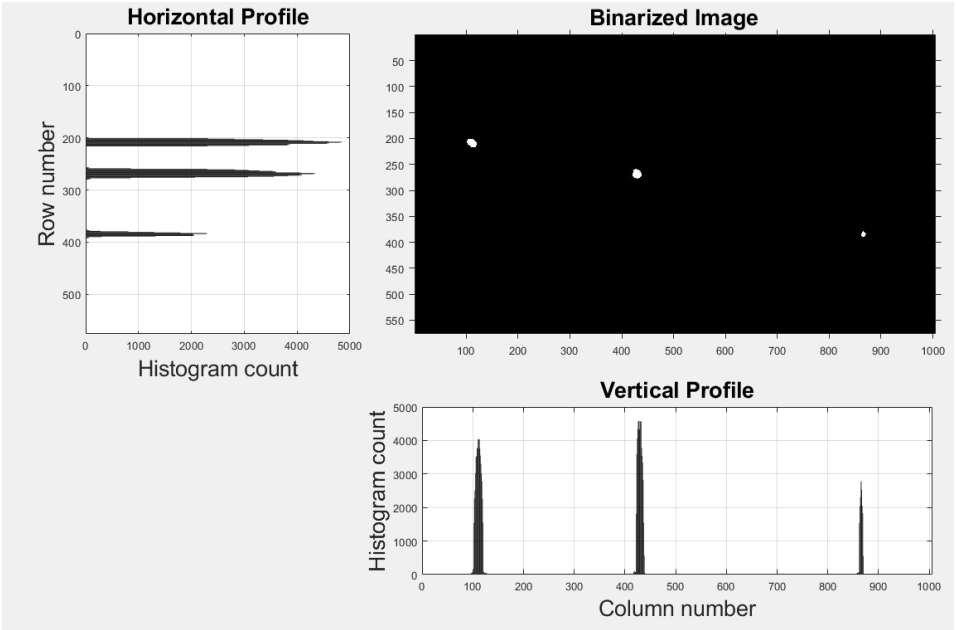

Figure 2. Human head candidate detection and localization based on Vertical and Horizontal Projection profiles.

Coordinates of the potential victim candidate are represented by the rows and columns of the respective projections on **Figure 2**. All three white dots represent potential victim. Leftmost two dots are in reality, metallic buoys while the third, right dot is human volunteer. Image with detected objects that potentially represent victim's head are further analyzed according to the drone height with respect to the surface below, and the shape and regularity of the measured object. Expert based classifier is used where human head shape, size, regularity and proportions are taken into an account.

2.2 Hardware setup

Hardware setup consists of a remotely operated drone with flight controller, dual-type visible/thermographic high-definition camera and laptop computer as shown on **Figure 3**.

Figure 3. Hardware setup.

Custom-built variant of Jazz Hexacopter drone was used for data acquisition (**JC, 2021**). Drone is equipped with six brushless direct current motors (BLDC) that can support up to 2.5 kilograms of mass per axis. Hexagonal placement of motors increases the drone's overall lift capability and enables the user to mount and use heavier equipment. Additional motors enable safer flight as the drone flight stability is increased. Furthermore, increase in the number of propulsion motors gives the drone operator additional opportunities to safely land the drone, even in case of single motor propulsion failure. In order to address marine specific environment, propulsion motors used on the drone are weather resistant under IP56 rating with completely sealed bearings. This can prevent fluid, such as rain or salt spray entering in between the bearing races and facilitating corrosion. Image quality is one of the primary concerns when considering the use of thermographic drone in marine SAR operations. In order to use thermal imaging camera on a drone it is necessary to mount the equipment on a drone securely while considering the propeller and propulsion motor vibration as well as structural vibrations (**Li *et al.*, 2017**).

Imaging equipment is mounted on two-axis gimbal coupled with custom-built antivibration frame and mount in order to increase image quality (**Micropilot, 2013**). Hexacopter drone is equipped with FLIR Duo Pro R High-Definition dual sensor thermal camera. This type of thermal camera was chosen as it provides conventional and thermographic imaging capabilities in the same body with relatively small dimensions and weight. FLIR Duo Pro R weighs only 325 grams but provides high definition imaging capabilities with thermal frame rate of 9 Hz in the spectral band between 7.5 and 13.5 μm. Relative measurement accuracy of thermal camera is 5 °C between -25 °C and 135 °C, and 20°C between -40°C and +550°C.

Conventional camera has visible sensor resolution of 4000×3000 pixels with 56°×45° field of view, while the thermal camera has 13 mm thermal lens with field of view of 45°×37° and can capture thermal images with resolution of 640×512 pixels. Dual-type camera was chosen instead of two separate cameras as the dual type camera has the advantage of reducing the necessary drone lift capabilities as well as overall payload size and power requirement. FLIR Duo Pro R is equipped with global navigation satellite system with GPS and GLONASS connectivity. Flight controller operating at 5.8 GHz was used to operate the drone and camera. Conventional visible and thermographic video feedback was received in real time on the laptop computer via transmitter and receiver pair together with geotagging information.

In order to perform controlled sweep of the area under supervision, drone must have inbuilt systems that enable spatial orientation. This can primarily be done with Inertial Measurement Units (INS) or feature based navigation (**Lu *et al.*, 2018**), although it can be simplified with GNSS self-positioning. Hexacopter was following preselected waypoints on its flight path. This procedure is time insensitive and does not take into account limited drone flight time, but its advantages are simplicity and versatility of use. Hexacopter uses geodetic coordinate system for its waypoint tracking as it coincides with NMEA code standard. Primary waypoint geopositioning data such as latitude, longitude and height can be additionally supplemented with drone heading and speed between particular waypoints. Drone speed can be adjusted, and different heading and speed settings can be preprogrammed in case of individual waypoints. This is of a particular interest in cases where conventional maritime SAR flight patterns are used, as presented on **Figure 4**.

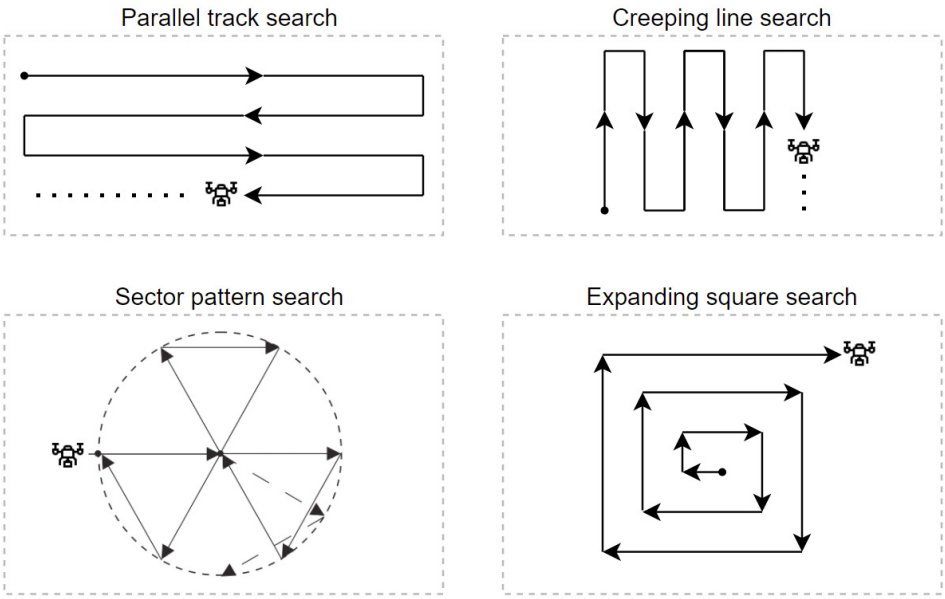

Figure 4. Search patterns for maritime SAR.
(Source: **IMO, 2016**)

During the flight, Hexacopter navigation system receives current geodetic coordinates from the drone mounted GNSS receiver and compares them with the desired drone position defined by the preprogrammed waypoints. Waypoint tracking procedure still depends on SAR personnel and drone operator expertise in order to select appropriate flight pattern and trajectory with respect to the particular SAR mission.

3 RESULTS

In order to test the proposed method, a simulated marine SAR scenario was performed in the coastal region of the Kvarner bay. Drone operation was performed according to all the necessary regulations that govern drone use in Republic of Croatia and European Union (**EC, 2019**; **MMPI, 2018**). Victim in need of a rescue was simulated by a volunteer trained in diving and maritime safety. Over the duration of the simulated scenarios, weather was clear with air temperature between 14 °C and 15 °C and atmospheric pressure of 1009 hPa. In order to perform the scenario in a controlled and safe manner, volunteer was dressed in a diving suit prior to being placed in the water with qualified personnel on standby and ready to

assist in case of emergency. Measured seawater temperature was 13 °C. Diving suit was used in order to reduce the volunteers emitted body heat and mask his temperature signature. In this way conducted scenarios are more representative of divers in a need of rescue as well as persons using maritime immersion suits.

Prior to initial flight, full image calibration was performed on both RGB and thermal cameras. Brightness and color contrast were both calibrated on the RGB camera. Thermal contrast of the thermal camera was checked and adjusted with respect to the nominal dry human body temperature of 36.6 °C. Drone was initially positioned at 10 meters above the sea surface and flown according to predetermined waypoints. Volunteer was placed in the sea in close vicinity to three sea buoys. Two buoys were metallic and only half submerged, while the third, rubber buoy was almost completely submerged. Volunteer was instructed to simulate two scenarios. In the first scenario, volunteer was calmly floating on the back with only the head protruding above the surface of the water. In the second scenario, volunteer was instructed to simulate the state of rough sea by continuously flailing his arms and legs. Secondary benefit of this was that it also simulates the state of panic and distress in a potential victim or the victim's attempt to be more visible. Both scenarios were repeated several times. With each repetition of the simulated scenario, drone's height was increased by 10 meters, up to a total of 50 meters. Representative images for both scenarios have been selected for drone heights of 10 and 50 meters and are presented on **Figure 5**.

At drone height of 10 meters above the sea surface, RGB images show the volunteer's entire body clearly and volunteer's facial features can be easily recognized and identified. Focal view of both cameras is not wide enough to capture any of the buoys at 10 meters drone height. On the thermal images, in both scenarios, only the facial heat signature is visible with slight discoloration of the surrounding sea water. Disturbance of the sea water in second scenario is not captured by the thermal camera. Thermal visibility of the volunteer's face is increased only because the volunteer's sudden movements are reducing the distance to the thermal camera.

At drone height of 50 meters, RGB camera is capturing the volunteer as well as all three sea buoys in close vicinity. Even with RGB camera's greater field of view and sensor resolution, increase in camera height had a clear negative impact on the visibility and clarity of the volunteer's image. Unfavorable atmospheric conditions and poor weather can only further reduce the RGB image quality (**Specht *et al.*, 2020b**).

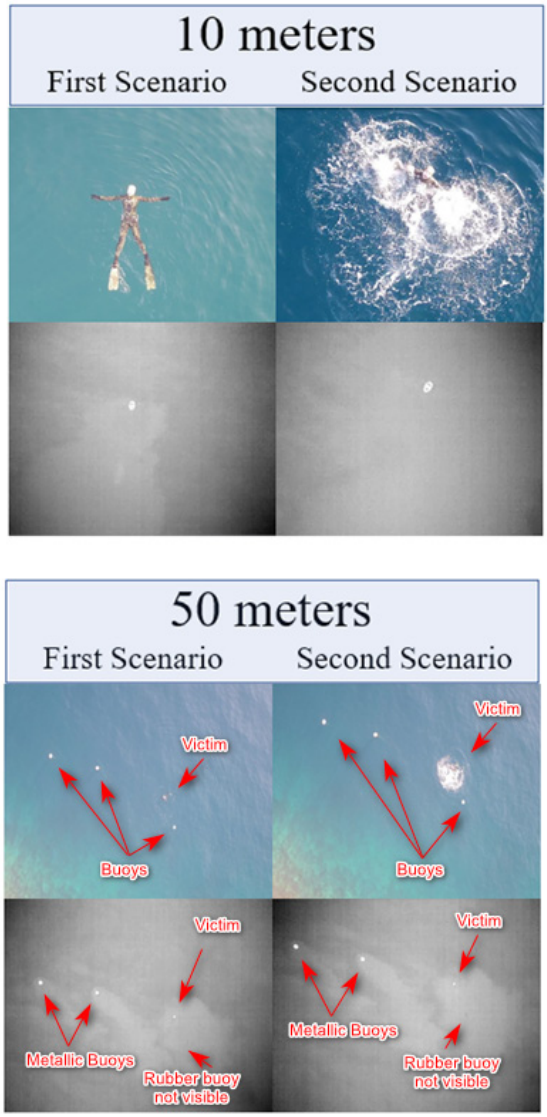

Figure 5. Representative RGB and thermal images for first and second scenario at drone heights of 10 and 50 meters.

Thermal contrast of the volunteer's face remains the same for thermal images taken at drone height of 10 meters as well as 50 meters irrespective of the tested scenario. Thermal camera is still able to capture the volunteer but of the three buoys, only two are visible. Last, rubber buoy is almost completely submerged,

with thin layer of seawater flowing above the buoy. Lower thermal emissivity of the rubber buoy together with temperature equalizing effect of the surrounding sea water has reduced its thermal contrast below the range that can be registered by the FLIR Duo Pro R camera.

4 CONCLUSION

Conducted study has presented possible use of the thermal/RGB camera equipped drone in maritime SAR activities. Even in cases when it is necessary to consider poor visibility, low lighting, darkness or even maritime specific environmental conditions like as rough sea or sea glint, thermal/RGB camera equipped drone can provide good quality images suitable for further processing and feature extraction. Thermal/RGB drone camera configuration together with the use of GNSS geolocation system, can increase success in saving human lives and provide opportunities for successful SAR mission when time of deployment is of a particular interest. Disadvantages that can diminish the value of this approach are most prominently, still relatively short flight time of the current UAV's and maneuverability and flight sensitivity in adverse weather conditions, such as storms. For continued research, it would be advisable to compare the appropriate drone flight patterns with respect to possible flying altitudes in order to determine which are the best suited for maritime SAR operations and develop software that will achieve complete UAV autonomy, with the intent of fully automatic mission start with safe return on the dynamically moving vessel.

ACKNOWLEDGMENTS

This research was supported by University of Rijeka, Faculty of Maritime Studies, Center for Marine Technologies.

REFERENCES

Abc News (AN). (2021). Dramatic drone rescue of 2 Australian swimmers billed as a first; The drone, also recording every second, dropped an inflatable pod. Available from: https://abcnews.go.com/International/drone-rescue-australian-swimmers-billed/story?id=52429138, accessed 18 April 2021.

Bradley, D. and Roth, G. (2007). Adaptive Thresholding using the Integral Image. Journal of Graphics Tools, 12 (2), pp. 13–21.

Brain, D., Webb, G. I. (2000) On the Effect of Data Set Size on Bias and Variance in Classification Learning On the effect of data set size on bias and variance in classification learning. In: Proceedings of the Fourth Australian Knowledge Acquisition Workshop, pp. 117–128. Sydney, Australia.

Burke, C., McWhirter, P. R., Veitch-Michaelis, J., McAree, O., Pointon, H. A. G., Wich, S. and Longmore, S. (2019). Requirements and Limitations of Thermal Drones for Effective Search and Rescue in Marine and Coastal Areas. Drones, 3(4), 78. Available from: https://www.mdpi.com/2504-446X/3/4/78, accessed 13. April 2021.

Burke, C., Rashman, M., Wich, S., Symons, A., Theron, C. and Longmore, S. (2019). Optimizing observing strategies for monitoring animals using drone-mounted thermal infrared cameras, International Journal of Remote Sensing, 40 (2), pp. 439–467.

Csernatoni, R. (2018). Constructing the EU's high-tech borders: FRONTEX and dual-use drones for border management, European Security, volume. 27, Issue 2, pp. 175–200.

Erdelj M. and Natalizio, E. (2016). UAV-Assisted Disaster Management : Applications and Open Issues, ICNC 2016: International Conference on Computing, Networking and Communications, pp. 1–5. 15-18 February 2016, Kauai, Hawaii, USA.

European Commission (EC). (2019). (EU) 2019/945: DELEGIRANA UREDBA KOMISIJE (EU) 2019/945 od 12. ožujka 2019. o sustavima bespilotnih zrakoplova i o operatorima sustava bespilotnih zrakoplova iz trećih zemalja. EU.

FreightComms Trade and Regulations (FCTR). (2019). EMSA RPAS drone service to boost maritime surveillance in Croatia. Available from: https://www.freightcomms.net/emsa-rpas-drone-service-to-boost-maritime-surveillance-in-croatia/, accessed 18 April 2021.

Genchi, S.A., Vitale, A.J., Perillo, G.M.E., Seitz, C. and Delrieux, C.A. (2020). Mapping Topobathymetry in a Shallow Tidal Environment Using Low-cost Technology. Remote Sensing, 12, 1394. Available from: https://www.mdpi.com/2072-4292/12/9/1394/htm, accessed 17. April 2021.

Ghazali, S. N. A. M., Anuar, H. A., Zakaria S. N. A. S. and Yusoff Z. (2016). Determining position of target subjects in Maritime Search and Rescue (MSAR) operations using rotary wing Unmanned Aerial Vehicles (UAVs). ICICTM 2016: International Conference on Information and Communication Technology, pp. 1–4. 16-17 May 2016, Kuala Lumpur, Malaysia.

International Maritime Organization (IMO) and International Civil Aviation Organization (ICAO). (2016). IAMSAR Manual: International Aeronautical and Maritime Search and Rescue Manual Volume III. London: IMO, Montreal: ICAO.

Jazz-copter j.d.o.o. (JC) (2021). Jazz Hexa – Jazz-copter. Available from: http://www.jazz-copter.com/jazz-hexa/uncategorised/jazz-hexa, accessed 14 April 2021.

Joyce, K. E., Duce, S., Leahy, S. M., Leon, J. and Maier, S. W. (2018) Principles and practice of acquiring drone-based image data in marine environments. Marine and Freshwater Research, 70 (7), pp. 952–963.

Krasuski, K. and Wierzbicki, D. (2021). Application the SBAS/EGNOS Corrections in UAV Positioning. Energies 2021, 14, 739. Available from: https://www.mdpi.com/1996-1073/14/3/739, accessed May 2020.

Lee, S. and Morrison, J. R. (2015). Decision support scheduling for maritime search and rescue planning with a system of UAVs and fuel service stations, ICUAS: 2015 International Conference on Unmanned Aircraft Systems, pp. 1168–1177. 9 June 2015, Denver, Colorado, USA.

Leira, S., Johansen T. A. and Fossen T. I. (2016). Tracking of Marine Surface Objects from Unmanned Aerial Vehicles with a Pan / Tilt Unit using a Thermal Camera and Optical Flow, ICUAS 2016: International Conference on Unmanned Aircraft Systems, pp. 107–117. 7-10 June 2016, Arlington, VA, USA.

Li, Z., Lao, M., Phang, S.K., Hamid, M.R., Tang, K. and Lin, F. (2017). Development and Design Methodology of an Anti-Vibration System on Micro-UAVs. IMAV 2017: International Micro Air Vehicle Conference and Flight Competition, pp. 223–228. 18-22 September 2017 Toulouse, France.

Lu, Y., Xue, Z., Xia, G. and Zhang, L. (2018). A survey on vision-based UAV navigation. Geo-spatial Information Science, 21(1), pp. 21–32.

Ministarstvo mora, prometa i infrastrukture (MMPI) (2018). NN 104/2018: Pravilnik o sustavima bespilotnih zrakoplova, Zagreb: Ministarstvo mora, prometa i infrastructure Republike Hrvatske.

Nikolakopoulos, K., Lampropoulou, P., Fakiris, E., Sardelianos, D. and Papatheodorou, G. (2018). Synergistic Use of UAV and USV Data and Petrographic Analyses for the Investigation of Beachrock Formations: A Case Study from Syros Island, Aegean Sea, Greece. Minerals, 8 (11), 534. Available from: https://www.mdpi.com/2075-163X/8/11/534/htm, accessed 16. April 2021.

Pascale, D. (2003). A Review of RGB Color Spaces … from xyY to R'G'B'. Montreal: the BabelColor Company. Available from: https://www.babelcolor.com/index_htm_files/A%20review%20of%20RGB%20color%20spaces.pdf, accessed 18. April 2021.

Ponce, J., Berg, T. L., Everingham, M., Forsyth, D.A., Hebert M., Lazebnik, S., Marszalek, M., Schmid, C., Russell, B. C., Torralba, A., Williams, C. K. I., Zhang, J. and Zisserman, A. (2006). Dataset Issues in Object Recognition. In: Ponce J., Hebert M., Schmid C., Zisserman A. (eds) Toward Category-Level Object Recognition. Lecture Notes in Computer Science, vol 4170, pp. 29–48. Springer, Berlin, Heidelberg.

Portenier, C., Ott, B., Wellig, P. and Wunderle, S. (2019). Cloud detection and visibility estimation during night time using thermal camera images, In: Stein, K. U., Schleijpen, R. (eds.). Proceedings Volume 11158: SPIE Security + Defence; Target and Background Signatures V, pp. 5. 9-12 September 2019, Strasbourg, France.

Quan A., Herrmann C., and Hamdy S. (2019). Project Vulture: A Prototype for Using Drones in Search and Rescue Operations, DCOSS: 15th International Conference on Distributed Computing in Sensor Systems, pp. 619–624. 29-31 May, Santorini, Greece.

Robakowska, M., Ślęzak, D., Tyrańska-Fobke, A., Nowak, J., Robakowski, P., Żuratyński, P., Ładny, J., Nadolny, K. (2019). Operational and Financial Considerations of Using Drones for Medical Support of Mass Events in Poland. Disaster Medicine and Public Health Preparedness, 13 (3), pp. 527–532.

Rodin, C. D., de Lima L. N., de Alcantara Andrade, F. A., Haddad, D. B., Johansen, T. A. and Storvold, R. (2018). Object Classification in Thermal Images using Convolutional Neural Networks for Search and Rescue Missions with Unmanned Aerial Systems, IJCNN 2018: International Joint Conference on Neural Networks, pp. 1–8. 8-13 July 2018, Rio de Janeiro, Brazil.

Specht, C., Lewicka, O., Specht, M., Dąbrowski, P. and Burdziakowski, P. (2020a). Methodology for Carrying out Measurements of the Tombolo Geomorphic Landform Using Unmanned Aerial and Surface Vehicles near Sopot Pier, Poland. Journal of Marine Science and Engineering, 8 (6), 384. Available from: https://www.mdpi.com/2077-1312/8/6/384, accessed 18. April 2021.

Specht, M., Specht, C., Mindykowski, J., Dąbrowski, P., Maśnicki, R. and Makar, A. (2020b). Geospatial Modeling of the Tombolo Phenomenon in Sopot using Integrated Geodetic and Hydrographic Measurement Methods. Remote Sensing, 12 (4), 737. Available from: https://www.mdpi.com/2072-4292/12/4/737, accessed 18. April 2021.

Micropilot (2013). Isolating Components from UAV Vibration. Available from: https://www.micropilot.com/pdf/isolating-components-uav-vibration.pdf, accessed 17 April 2021.

Teledyne FLIR Extech Raymarine Itc. (TFER) (2021). Your Perfect Pallete. Available from: https://www.flir.com/discover/ots/outdoor/your-perfect-palette/, accessed 18 April 2021.

Thillainayagi, R. and Kumar, K.S. (2019). Hybrid bi-dimensional empirical mode decomposition based enhancement technique for extreme low contrast UAV thermal images. Sādhanā, 44 (147), pp 1–11. Available from: https://www.ias.ac.in/article/fulltext/sadh/044/06/0147, accessed 17. April 2021.

Xiong, W., Gelder, P. H. A. J. M. and Yang, K. (2020). A decision support method for design and operationalization of search and rescue in maritime emergency. Ocean Engineering, 207 (2020) 107399, Available from: https://www.sciencedirect.com/science/article/pii/S0029801820304285, accessed 18. April 2021.

ECOLOGICAL SUSTAINABILITY OF MARITIME TRANSPORT WITH AN EMPHASIS ON THE SURFACE CURRENT ROUTING AS A PART OF THE VOYAGE PLANNING OPTIMIZATION

Maro Car*, Miho Kristić, Nermin Hasanspahić, Srđan Vujičić

Abstract. *The world economy and globalization depend heavily on transporting goods by sea since global trade is predominantly seaborne. Therefore, great efforts and resources are invested in developing modern technologies to improve the safe and expeditious transportation of goods. Nevertheless, the negative impact of shipping on the environment has been ignored for a long time. The maritime industry adversely affects the environment and human health in many different ways. Thus, stakeholders need to find ways to reduce or eliminate its negative impact. Sustainable shipping is the goal of all stakeholders, but the system's complexity makes it challenging to find the optimal solution. The introduction of new green technologies along with the optimization of ship management systems, and the training of seafarers on sustainability are possible solutions to reduce the environmental impact of shipping. In this paper, the authors analyzed voyage planning with surface currents and estimated reductions in fuel consumption taken into account, and thus reducing harmful gasses emissions. This case study involved the analysis of a cruise ship voyage from Miami (USA) to Norfolk (USA). A brief overview of the IMO e-Navigation concept that is being developed is also presented, and its*

University of Dubrovnik, Maritime Department, Dubrovnik, Croatia
* Corresponding author: Maro Car (mcar1@unidu.hr)

University of Zadar

complete application is expected to facilitate voyage planning using surface and tidal currents and enable cost savings and environmental protection.

Key words: *voyage planning; Gulf stream; optimization; fuel-saving; energy efficiency*

1 INTRODUCTION

Maritime transport remains the cornerstone of international transport and trade since around 80 % of all goods are shipped by sea (**Statista 2021**). The number of ships and their size is increasing. New technologies that increase the efficiency of maritime transport and safety emerge. However, one of the negative aspects, or side effects, of shipping is its impact on the marine environment and society globally. Shipping pollutes the marine environment in several ways, such as air pollution, spills from ships, solid waste, garbage, ballast water, noise pollution, and ship-breaking. International maritime transport accounts for about 2.7 % of global CO_2 emissions (**Walker *et al.*, 2019**) and approximately 20 % of waste and residue discharges into the sea (**Badurina, Cukrov and Dundović, 2017**). According to some studies, shipping emissions are responsible for approximately 60,000 cardiopulmonary and lung cancer deaths annually worldwide (**Corbett *et al.*, 2007**). Another aspect of shipping emissions is global warming, accelerated by greenhouse gases from ships. Since environmental awareness became a popular term, and people are becoming "green-oriented", international shipping requires transformation. Its stakeholders are becoming increasingly aware of the involved risks and environmental footprint of the transportation process. Key industries depend on societies, and ecological modernization is usually presented as a proper way to make them environmentally and ecologically sustainable. Thus, international shipping needs to be oriented towards environmentally friendly systems and technologies. It is indispensable to adopt and implement measures to reduce the negative effect on the marine environment. International maritime transport and logistic stakeholders must take necessary steps and use all available means to reduce a negative impact on the environment. Due to the increased demand for "green shipping", several measures are imposed as effective solutions (**Hasanspahić *et al.*, 2020**).

The International Maritime Organization (IMO) has recognized the problem and adopted resolutions and protocols to address the adverse impact of shipping on the environment. Various forms of pollution from ships are regulated by the International Convention for the Prevention of Pollution from Ships (MARPOL).

In Annex VI of the Convention, the IMO presented measures to reduce air pollution from ships. Mandatory technical and operational energy efficiency measures are included in the chapter adopted in 2011. The goal of these measures is to augment energy efficiency in a cost-effective method (**IMO, 2017**). The Ship Energy Efficiency Management Plan (SEEMP) is introduced as an operational measure to establish a methodology to manage individual ship or fleet energy efficiency performance over time (**Čampara, Hasanspahić and Vujičić, 2018**). For that purpose, the Energy Efficiency Operational Indicator (EEOI) is used as a monitoring instrument. The EEOI enables companies to monitor the fuel efficiency during operation and the effect of any changes, like voyage planning optimization (including weather and surface current routing), trim and draft optimization or speed optimization (**Tran, 2017**).

Sustainability is the focus of all shipping stakeholders. It includes three key elements or pillars: environmental, economic, and social. The environmental element deals with reducing the negative environmental impacts of shipping, while the economic element minimizes costs and profit growth. The social element deals with community well-being, including better working and living conditions and improved labour regulations (**Shin *et al.*, 2018**). According to (**Shin *et al.*, 2018**), there are three main objectives of sustainability in shipping:

- Minimize economic costs,
- Mitigate adverse impact on the environment,
- Enhance social justice, and improve working conditions.

All three elements interact with each other and form sustainable shipping. Disbalance between these elements leads to non-sustainability. As already stated, there are many adverse effects of non-sustainable shipping, like greenhouse gas (GHG) emissions. Maritime transport needs to balance all three elements to achieve social and environmental safety and gain economic profit. However, it is a demanding task for international shipping stakeholders to achieve economic and social benefits and make a positive impact on the environment. Measures aimed at reducing the negative impact of maritime transport on the environment usually imply additional costs. This is unpopular amongst stakeholders as it reduces profit. The environmental element has been in the spotlight during the last three decades due to the climate change caused by the GHG emissions that reduce the quality of life. As mentioned earlier in the paper, several measures could be implemented to reduce emissions, but most of them are costly. Shipping companies, which for the most part bear all costs for implementing mitigating

measures, unwillingly pay and thus seek more favourable options. The increase of companies' costs consequently increases freight costs. The best answer would be to implement measures that bear no additional costs and positively impact the environment. The solution could be found in operational measures, namely voyage optimization using strong surface currents. This paper focuses on the reduction of emissions by the application of operational measures. Voyage planning optimization, including surface current routing, is elaborated upon.

Lo and McCord formulated the routing problem as an adaptive, probabilistic dynamic program. Information elements included were aged synoptic ocean current information, localized information by ships and state transition probabilities of current changes obtained from historical data. Numerical simulation was conducted in the Gulf Stream area, and it indicated the promise of their formulation for the strong current routing problem (**Lo and McCord, 1998**). **Kobayashi, Asajima and Sueyoshi** (**2011**) proposed a new weather routing framework considering ship's motions, surface currents, wind and waves through time-domain computer simulation. The navigation route is optimized for minimum fuel consumption, and although it is longer than the great circle route, the authors confirmed that less fuel is used during a voyage. **Armstrong** (**2013**) described measures minimizing fuel consumption and reducing carbon emissions. Operational optimization (including route optimization), technical optimization and commercial optimization measures used by Teekay shipping are elaborated. **Chang *et al.*** (**2015**) provided global maps of strong ocean currents focusing on Western Boundary Currents. The authors argue that these currents with rates of 2-3 knots could significantly reduce ships' fuel consumption with low sailing speed (25-50 % reduction for speed of 6 knots). In their paper, **Chen, Shiotani and Sasa** (**2015**) studied the Kuroshio current effect using simulations on ships navigating in the area. They found that significant fuel and time savings could be achieved with optimal voyage planning, including strong ocean currents and waves interaction. **Mannarini and Carelli** (**2019**) introduced ship routing model VISIR-1.b. The authors presented a case study, a route from the Chesapeake Bay to the Mediterranean Sea and vice versa. They found that the ship routing model can save between 2 % and 12 % monthly, 1 % to 4 % being saved using currents. **Perera and Guedes Soares** (**2017**) gave an overview of ship weather routing and safe handling in future of shipping. The authors argue that two approaches combined by selecting an optimal route, introducing safety measures and using forecasted and actual weather conditions can improve shipping safety. **Chang *et al.*** (**2013**) focused on the Kuroshio current, which has

an average flow speed of two knots. The authors proposed ship routing utilizing Kuroshio current on the northbound route (Taipei to Tokyo) and avoiding it on the southbound route. In the case of "super slow steaming "container ship navigating with the speed of 12 knots, it was found that savings in transit time on the northbound route (utilizing current) could be about 1.8 %, but much higher savings could be achieved on the southbound route, 5.7 % in transit time. The authors also proposed that the detailed Kuroshio current energy-saving route could be built into Electronic Chart Display System (ECDIS) and facilitate energy-saving navigation. Yang *et al.* proposed a ship's speed optimization model for a fixed route that distinguishes a ship's speed through water (STW) and speed over ground (SOG) (**Yang *et al.*, 2020**). It can determine fuel consumption and passage time accurately because it takes surface currents into account. The study results showed that a proposed model could enable savings of 2.2 % of fuel used and reduce 26.12 tons of CO_2 emissions for 280 hours long voyage of an oil product tanker ship. **Wang *et al.* (2020)** presented a novel joint optimization method of the ship's navigating route and speed, considering multiple environmental factors. The authors conducted a case study, and results showed that the proposed method is effective and optimal navigating route and speed could be achieved under complex environmental conditions. It showed that 17 tons of fuel could be saved for a single voyage (about 4 %) (**Wang *et al.*, 2020**).

2 METHODOLOGY

In this paper, a case study was done on a sea voyage of a cruise ship between Miami (USA) as a departure port and Norfolk (USA) as an arrival port. The Gulf stream is used as a tool for voyage optimization in terms of fuel-saving and reduced harmful gasses emissions. Gulf stream details (**Figure 1**) were taken from (**NGIA, 2002**). Only a part of a sea voyage is considered, and it was divided into legs (distances between waypoints). The authors calculated the time needed for passing each of the legs (A-B, B-C, C-D, D-E, E-F and F-G), taking into account the different ship's speed and current effect. The Gulf stream rate is steady throughout the whole year. However, during June and July, it reaches its peak force in the NNE direction with an average current speed between 1.5 and 3 knots (**Figure 2**) (**NGIA, 2002**). For the purpose of this study, the authors had planned the ship's voyage during July, which is one of the two months with the most significant Gulf stream strength. Two voyage planning options were taken into account: a shorter one partially utilizing ocean surface

current (voyage plan A) and a longer one utilizing ocean current as much as possible (voyage plan B). Adverse weather effects were not taken into account for passage time calculations.

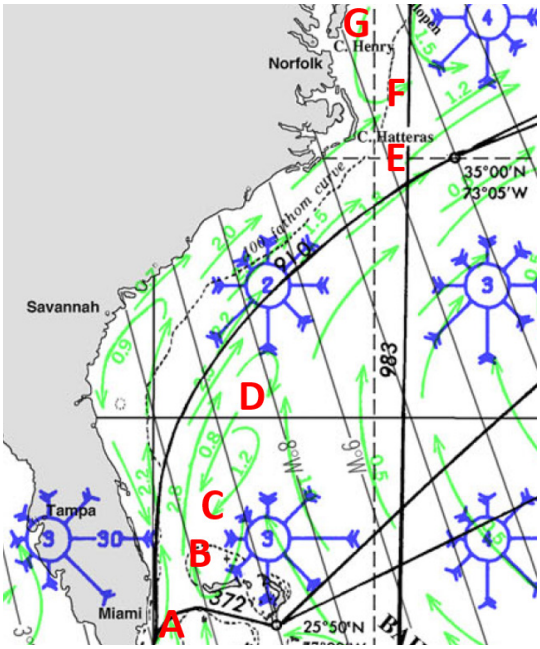

Figure 1. Excerpt of the sea area with particular focus on surface Gulf stream rate and direction. (Source: **NGIA, 2002**)

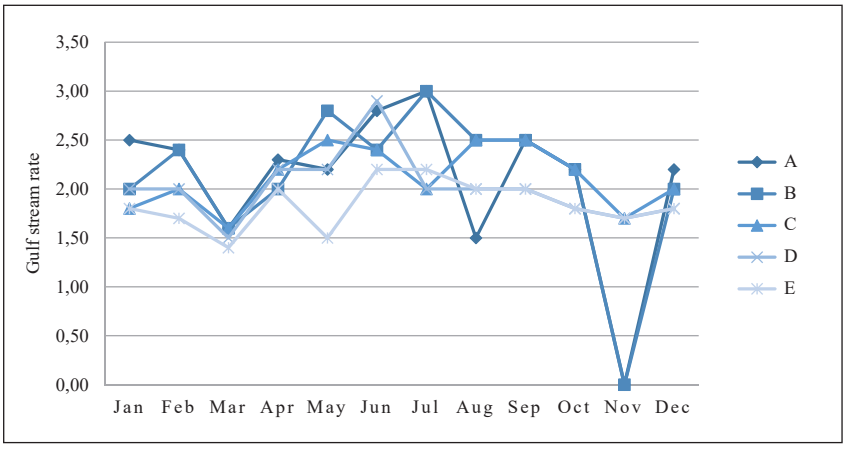

Figure 2. Estimated Gulf stream rate per segment (in knots). (Source: Authors as per **NGIA, 2002**)

Comparing two parts of a voyage regarding the time needed for the passage and fuel consumption gave valuable insight into utilizing strong ocean surface currents and possible savings in time, money, and environment protection. Therefore, the time needed for passing each leg of the voyage segment was calculated using the following formula (1):

$$\Delta t = {}^{D}/_{SOG} \tag{1}$$

where D stands for distance (in nautical miles) and SOG for Speed Over Ground (in knots), which can be calculated using formula (2):

$$\overrightarrow{SOG} = \overrightarrow{STW} + \overrightarrow{SCR} \tag{2}$$

STW stands for Speed Through Water (in knots) and SCR for Surface Current Rate (in knots) in the formula. **Figure 3** presents the effect of surface current rate on the ship's course through water.

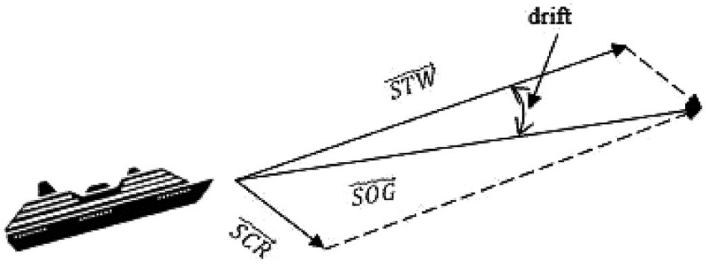

Figure 3. Relations between *SOG*, *STW* and *SCR*.

The total time needed to pass the whole voyage segment can be expressed as a sum of times needed to pass each segment leg, where t represents the steaming time (3).

$$t = \sum_{i=1}^{n} t_i \tag{3}$$

The authors planned a voyage at the University of Dubrovnik on the Kongsberg's Polaris Ship Bridge Simulator approved by DNV Standard for Certification 2.14 for class A. Fuel oil consumption in research was estimated based on available empirical data obtained from a USA based company passenger cruise ship, which is equipped with six diesel generators where each can produce power of 8.5 MW.

3 RESULTS AND DISCUSSION

As previously stated, the voyage segment was divided into legs, and two voyage plans were prepared. One plan (voyage plan A) was as short as possible (considering the safe passing distance from shore) and partially overlapped with the Gulf Stream's direction (**Figure 4a**). The voyage plan A distance was 730 nautical miles (NM) and had seven waypoints marked with numbers from 1 to 7 (**Table 1**). Another plan (voyage plan B) was prepared to utilize the Gulf stream taking into account a safe passing distance from shore (**Figure 4b**). With smart, green planning, a longer route was chosen, but at the same time, it was managed to utilize surface current (up to 3 knots rate) and kept clear of the area of the counter current (-0.8 knots rate). The voyage plan B sailing distance was 736 NM, and it also had seven waypoints (**Table 2**). Five waypoints had the same coordinates in both voyage plans, and the difference between them was waypoints 3 and 4, which were named as 3' and 4' in the voyage plan B.

Figure 4a. Voyage plan A.

Figure 4b. Voyage plan B.

Table 1. Voyage plan A.

WPT	Latitude	Longitude	Leg segment	Leg distance (NM)	Total distance steamed (NM)	The estimated stream rate (kn)
1	25° 46.0' N	080° 03.9' W	A - B	108		+2.2
2	27° 30.0' N	079° 30.0' W	B - C	78	108	0.0
3	28° 40.0' N	078° 50.6' W	C - D	88	186	-0.8
4	30° 00.4' N	078° 10.0' W	D - E	339	274	0.0
5	35° 00.0' N	075° 00.0' W	E - F	80	613	-1.5
6	36° 20.6' N	075° 01.9' W	F- G	37	693	-1.5
7	36° 45.9' N	075° 34.4' W			730	

Table 2. Voyage plan B.

WPT	Latitude	Longitude	Leg Segment	Leg distance (NM)	Total distance steamed (NM)	The estimated stream rate (kn)
1	25° 46.0' N	080° 03.9' W	A - B	108		+2.2
2	27° 30.0' N	079° 30.0' W	B - C	70	108	+2.8
3'	28° 40.0' N	079° 20.6' W	C - D	84	178	+2.8
4'	30° 00.4' N	078° 50.6' W	D - E	357	262	+2.1
5	35° 00.0' N	075° 00.0' W	E - F	80	619	-1.5
6	36° 20.6' N	075° 01.9' W	F- G	37	699	-1.5
7	36° 45.9' N	075° 34.4' W			736	

As shown in **Figure 5**, close to the favourable direction of the Gulf stream, there are areas with counter-current, which were kept clear in voyage plan B because the ship's speed over ground would be reduced.

The time to complete the voyage segment was calculated for both planned voyages using different ship's speeds (**Table 3**).

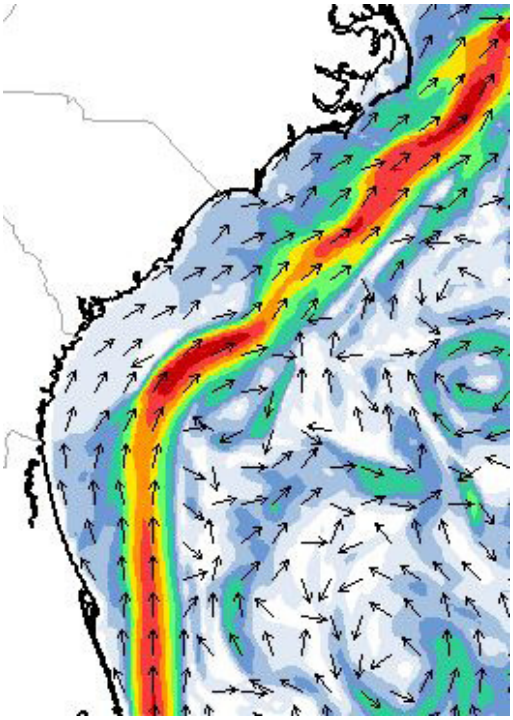

Figure 5. Forecasted Gulf stream rate and direction. (Source: **PW, 2021**)

Table 3. Estimated savings in time using different speed.

Ship's average *STW*	10 kn	12 kn	14 kn	16 kn	18 kn	20 kn
Voyage plan A (segment B-E) estimated steaming time (hours)	51.27	42.61	36.45	31.86	28.28	25.43
Voyage plan B (segment B-E) estimated steaming time (hours)	41.53	35.71	31.34	27.91	25.17	22.90
Difference in estimated steaming time (hours)	9.74	6.90	5.11	3.95	3.11	2.53

As shown in **Table 3**, even choosing the longer route (voyage plan B), with an average speed of 10 knots throughout the voyage, saved 9.74 hours of steaming. With an average speed of 16 knots throughout the voyage, 3.95 hours of steaming were saved, and with an average speed of 20 knots, 2.53 hours were saved. **Figure 6** graphically presents savings in time using voyage plan B instead of voyage plan A. It can be concluded that the lower ship's speed was a time saver.

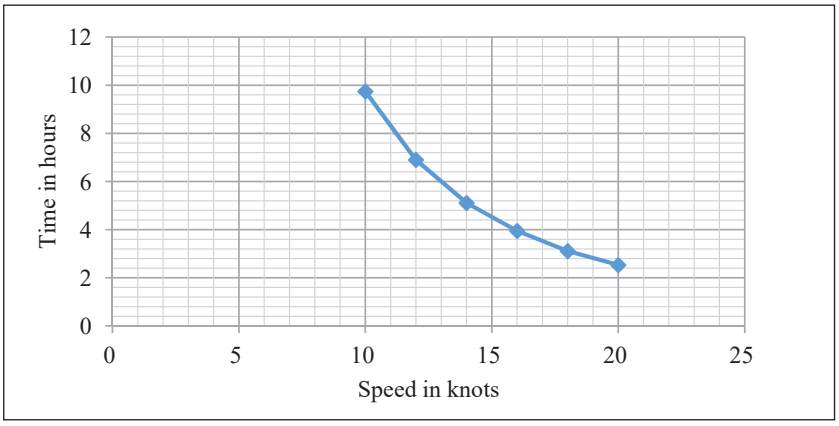

Figure 6. Estimated time saved utilizing surface current with different ship's speed.

The estimated consumption of Low Sulphur Fuel Oil (LSFO) with a sulphur content of <0.5 % for the passenger cruise ship with six diesel generators (8.5 MW each) is presented in **Figure 7**. Estimated consumption was obtained empirically for different ship's speeds (actual average consumption) and used for fuel consumption planning onboard a ship and for fuel management purposes. Based on data obtained from a given ship, estimated savings in fuel oil used during the execution of voyage plan B were calculated (**Figure 8**). To estimate fuel saved for different ship's speeds, empirical fuel consumption was multiplied by the difference in estimated steaming time (**Table 3**).

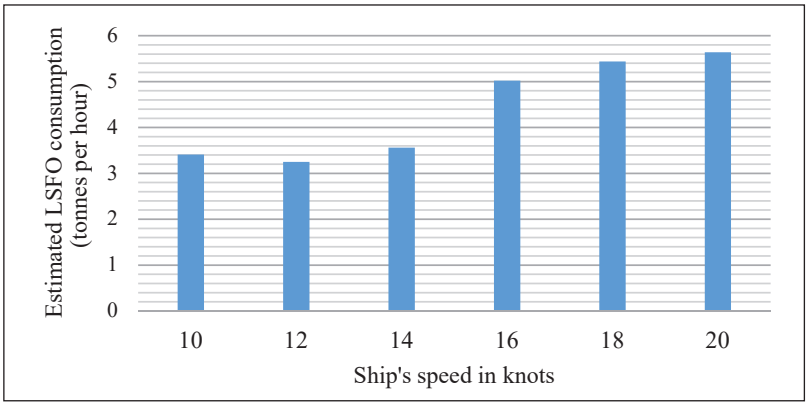

Figure 7. Estimated LSFO consumption of a cruise ship for different speeds. (Source: Private communication)

The benefits of the surface current routing optimization are presented in **Figure 8** and **Figure 9**. As can be seen, if using voyage plan B instead of plan A, a significant amount of fuel oil could be saved. For instance, if steaming with a speed of 18 knots using voyage plan B, it is estimated that 16.9 tons of LSFO could be saved, unlike using voyage plan A (**Figure 8**). Even more fuel could be saved for a lower ship's speed (33.2 tons for a speed of 10 knots).

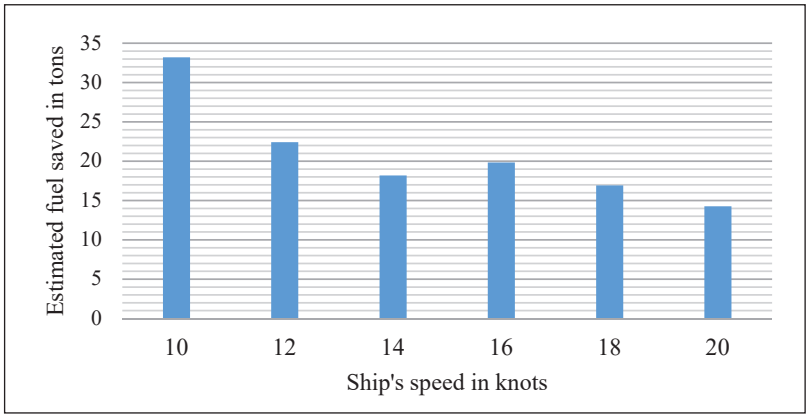

Figure 8. Estimated fuel saved (tons) using voyage plan B. (Source: Authors based on data obtained from a cruise ship)

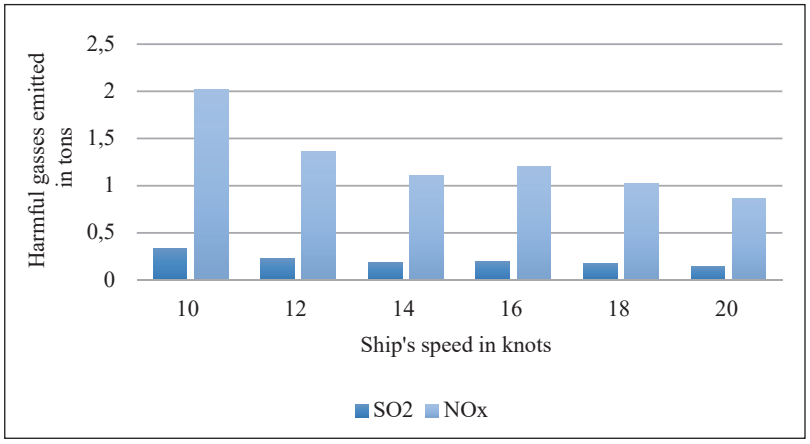

Figure 9. Estimated reduction in emission of harmful gasses to the atmosphere using voyage plan B. (Source: Authors using **Trozzi, 2010**)

Furthermore, less harmful gasses would be emitted into the atmosphere. Reductions in emissions were estimated for different ship's speeds based on the emission factors given in (**Trozzi, 2010**; **Trozzi and De Lauretis, 2020**). According to Trozzi (**Trozzi, 2010**), the emission factor for SO_2 equals 20·S, where S denotes the percentage of sulphur content in fuel. Therefore, SO_2 emissions were calculated based on the following: fuel saved was multiplied by 20*0.5. NO_x emissions were calculated based on the 60.6 kg/tonne emission factor presented by **Trozzi and De Lauretis** (**2020**) (fuel saved was multiplied by NO_x emission factor). As presented in **Figure 9**, for a speed of 20 knots using voyage plan B, the cruise ship would emit 0.86 tons NO_x less and 0.14 tons less of SO_2 than using voyage plan A.

Results obtained confirmed that strong ocean surface currents could be efficiently used for voyage optimization with multiple benefits. For example, steaming time could be reduced, a significant saving in fuel consumption could be achieved, and less harmful gasses would be emitted from ships. Research results are in line with the findings of **Kobayashi, Asayima and Sueyoshi** (**2011**), **Chang *et al.*** (**2015**), **Chang *et al.*** (**2013**), and **Chen, Shiotani and Sasa** (**2015**).

Furthermore, as **Chang *et al.*** (**2013**) suggested, strong ocean surface currents data could be integrated into ECDIS. That could significantly improve voyage planning optimization because the voyage planning officer would have ocean currents data on ECDIS and easily plan voyage utilizing it efficiently. IMO and IHO are developing S-10X Standards, facilitating passage planning and navigation safety by using ECDIS. S-111 Surface Currents Standard is particularly interesting for this research because it will integrate surface currents data in ECDIS, enabling seafarers to optimize voyage planning and safely navigate through areas where strong currents exist (**NOAA, 2021**, **IHO, 2021**).

4 CONCLUSION

Environmentally friendly shipping could be achieved by technological, operational and market-based measures. This paper focuses on operational measures, specifically on voyage planning optimization using strong surface currents. A case study involved the analysis of a cruise ship passage from Miami to Norfolk, whereupon two voyage plans were developed. One plan was shorter (concerning the safety of navigation), while the other plan was longer but utilized the Gulf stream. Calculations were done based on available data on the Gulf

stream and cruise ship's fuel oil consumption. Results confirmed that less fuel would be spent if a longer voyage plan utilizing the Gulf stream was used. Moreover, passage time will be shorter and less harmful gasses will be emitted into the atmosphere.

However, voyage optimization using strong surface currents is not an easy task since the current's set and drift must be carefully assessed and utilized. As seen from our research, if the course is slightly moved aside from the ocean stream, the favourable effect of the sea current could be lost, resulting in the counter-current effect negatively affecting savings and environmental pollution.

To facilitate passage planning tasks for navigation officers, S-100 Standards are being developed. Integration of strong ocean currents data in ECDIS would be beneficial for all shipping stakeholders, as it might result in significant savings in fuel consumption, reduced passage time, reduced emissions of harmful gasses into the atmosphere, and safer navigation.

REFERENCES

Statista. Available online: https://www.statista.com/topics/1367/container-shipping/ (accessed on 5 April 2021).

Walker, T. R., Adebambo, O., Del Aguila Feijoo, M. C., Elhaimer, E., Hossain, T., Johnston Edwards, S., Morrison, C. E., Romo, J., Sharma, N., Taylor, S., Zomorodi, S. (2019). Environmental Effects of Marine Transportation. In Shepard, C. (Eds.) World Seas: An Environmental Evaluation, Volume III: Ecological Issues and Environmental Impacts. pp. 505–530.

Badurina, P., Cukrov, M., Dundović, Č. (2017). Contribution to the implementation of »Green Port« concept in Croatian seaports. Scientific Journal of Maritime Research, vol. 31, pp. 10–17. DOI:10.31217/p.31.1.3.

Corbett, J. J., Winebrake, J. J., Green, E. H., Kasibhatla, P., Eyring, V., Lauer, A. (2007). Mortality from Ship Emissions: A Global Assessment. Environmental Science & Technology, vol. 41 (24), pp. 8512–8518. doi: 10.1021/es071686z.

Hasanspahić, N., Vujičić, S., Čampara, L., Piekarska, K. (2020). Sustainability and Environmental Challenges of Modern Shipping Industry. Journal of Applied Engineering Science, 19 (2021), 2; 369–374. doi: 10.5937/jaes0-28681.

International Maritime Organization. MARPOL Consolidated Edition 2017. International Convention for the Prevention of Pollution from Ships. IMO, London 2017.

Čampara, L., Hasanspahić, N., Vujičić, S. (2018). Overview of MARPOL ANNEX VI regulations for prevention of air pollution from marine diesel engines. SHS Web of Conferences 58, 01004, GLOBMAR 2018.

Tran, T. A. (2017). A research on the energy efficiency operational indicator EEOI calculation tool on M/V NSU JUSTICE of VINIC transportation company, Vietnam. Journal of Ocean Engineering and Science, 2(1), 55–60. doi: 10.1016/j.joes.2017.01.001.

Shin, S.-H., Kwon, O. K., Ruan, X., Chhetri, P., Lee, P. T.-W., Shahparvari, S. (2018). Analyzing Sustainability Literature in Maritime Studies with Text Mining. Sustainability, vol.10 (3522). doi: 10.3390/su10103522.

Lo, H. K., McCord, M. R. (1998) Adaptive ship routing through stochastic ocean currents: general formulations and empirical results. Transp. Res.-A, Vol. 32, No. 7, pp. 547–561.

Kobayashi, E., Asajima, T., Sueyoshi, N. (2011) Advanced Navigation Route Optimization for an Oceangoing Vessel. TransNav International Journal on Marine Navigation and Safety of Sea Transportation. Vol. 5, No. 3. pp. 377–383.

Armstrong, V. N. (2013) Vessel optimization for low carbon shipping. Ocean Engineering 73, pp. 195–207.

Chang, Y.-C., Tseng, R.-S., Chu, P. C., Shao, H.-J. (2015). Global Energy-saving Map of Strong Ocean Currents. Journal of Navigation, 69, 75–92. doi: 10.1017/s0373463315000466.

Chen, C., Shiotani, S., Sasa, K. (2015). Effect of ocean currents on ship navigation in the East China sea. Ocean Engineering, 104, 283–293. doi:10.1016/j.oceaneng.2015.04.062.

Mannarini, G., Carelli, L. (2019). VISIR-1.b: ocean surface gravity waves and currents for energy-efficient navigation. Geoscientific Model Development, 12(8), 3449–3480. doi: 10.5194/gmd-12-3449-2019.

Perera, L. P., Soares, C. G. (2017). Weather routing and safe ship handling in the future of shipping. Ocean Engineering, 130, 684–695. doi: 10.1016/j.oceaneng.2016.09.007.

Chang, Y.-C., Tseng, R.-S., Chen, G.-Y., Chu, P. C., Shen, Y.-T. (2013). Ship Routing Utilizing Strong Ocean Currents. Journal of Navigation, 66(06), 825–835. doi: 10.1017/s0373463313000441.

Yang, L., Chen, G., Zhao, J., Rytter, N. G. M. (2020). Ship Speed Optimization Considering Ocean Currents to Enhance Environmental Sustainability in Maritime Shipping. Sustainability, 12(9), 3649. doi: 10.3390/su12093649.

Wang, K., Li, J., Huang, L., Ma, R., Jiang, X., Yuan, Y., Mwero, N. A., Negenborn, R. R., Sun, P., Yan, X. (2020). A novel method for joint optimization of the sailing route and speed considering multiple environmental factors for more energy efficient shipping. Ocean Engineering, 216, 107591. doi: 10.1016/j.oceaneng.2020.107591.

National Geospatial-Intelligence Agency, Pub. 106- Atlas of Pilot Charts North Atlantic Ocean (including Gulf of Mexico), 2002. Ed.

Passage weather (PW). https://www.passageweather.com/ (accessed on 2021-24-06).

Trozzi, C. (2010) Emission estimate methodology for maritime navigation. USEPA. In Proceedings of the 19th International Emissions Inventory Conference, San Antonio, TX, USA, 20–30 September 2010.

Trozzi, C., De Lauretis, R. (2020) EMEP/EEA air pollutant emission inventory guidebook. Available online: https://www.eea.europa.eu/publications/emep-eea-guidebook-2019/part-b-sectoral-guidance-chapters/1-energy/1-a-combustion/1-a-3-d-navigation/view (accessed on 2021-5-12).

National Oceanic and Atmospheric Administration (NOAA). NOAA releases prototype surface current forecast data for industry testing. Available online: https://nauticalcharts.noaa.gov/updates/noaa-releases-prototype-surface-current-forecast-data-for-industry-testing/ (accessed on 2021-01-06).

International Hydrographic Organization (IHO). S-100 Universal Hydrographic Data Model. Available online: https://iho.int/en/s-100-universal-hydrographic-data-model (accessed on 2021-01-06).

THE SHIP SAFETY FROM SEAFARERS PERSPECTIVE: APPLICATION OF FUZZY AHP FOR DECISION SUPPORT

Luca Braidotti[1,2*], Jasna Prpić-Oršić[2], Marko Valčić[3], Francesco Mauro[4], Vittorio Bucci[1]

Abstract. *In recent years, many studies explored the ship safety enhancement through the application of monitoring systems. Despite their indisputable benefit, the growing number of independent safety and control systems is also increasing the amount of information that masters and officers have to deal with. In order to reduce human error occurrence, decision-making techniques allow developing effective onboard Decision Support Systems (DSSs), capable to assess and measure objectively the overall ship safety during navigation as well as during an emergency. In the present work, the fuzzy analytical hierarchical process is applied to define the weights of importance of a large number of criteria and sub-criteria composing a risk-based framework. The framework is devoted to onboard application as a part of DSS in order to quantify the ship safety level during navigation and emergencies. The structure of the framework has been discussed with a small pool of masters from major shipping companies, while the weights of importance have been evaluated on the base of a large group of masters and officers. The analysis, carried out for different ship types, provides a portrait of the seafarers' safety perception, being a solid base for further development of onboard DSSs.*

Key words: *Fuzzy AHP; risk-based framework; onboard safety; decision support*

[1] Department of Engineering and Architecture (University of Trieste, Trieste, Italy)
[2] Faculty of Engineering (University of Rijeka, Rijeka, Croatia)
[3] Maritime Department (University of Zadar, Zadar, Croatia)
[4] Maritime Safety Research Centre (University of Strathclyde, Glasgow, UK)
[*] Corresponding author: Luca Braidotti (lbraidotti@units.it)

University of Zadar

1 INTRODUCTION

The human factor is the primary factor in order to assure ship safety during navigation and harbour operations. In fact, during the period 2011-2018, 65.8 % of maritime casualties have been attributed to human errors (EMSA, 2019). Therefore, in order to prevent accidents as well as to soften their consequences, acting on the human factor could have the strongest impact on navigation safety. To this end, seafarers' training can be improved and even more safe procedures can be defined, but also the situational awareness and onboard decision support can play a relevant role. Often, in real operations, situational awareness is far from optimal. Seafarers have to deal with partial or unreliable information, especially on old ships complying with outdated regulations having less stringent requirements concerning onboard detection systems, control systems, etc. Recently, exploiting the onboard monitoring systems, more data can be available on bridge. However, the safety state of the ship is dependant on a very large set of heterogeneous information having different relevance, hence the adoption of several different monitoring and alarm systems could be critical and might lead anyway to human error. In such situations, it is likely to neglect some crucial information during the synthesis process, which is, in any case, subjective and based on the master's experience. This issue has been already reported by masters and officers from the latest large passenger ships. To overcome this problem, a viable solution is the onboard application of decision-making techniques, defining rational and objective synthesis procedures to assess ship safety. The information from all crucial systems should be collected in a single Decision Support System (DSS) capable to perform a reliable analysis, providing the outcomes by means of user-friendly interfaces (**Perera *et al.*, 2012**, **Nordström *et al.*, 2016**). A viable solution could be the application of Fuzzy Analytic Hierarchy Process (FAHP) to assess the safety state of the ship through a modular synthesis process (**Trincas *et al.*, 2017**). The FAHP technique is widely applied in the maritime industry field to support Multiple Criteria Decision Making (MCDM) processes related to economic, technical, safety and design issues. However, its application to a global onboard Risk-Based Framework (RBF) has been only hypothesised in a previous explorative study (**Braidotti *et al.*, 2018a**), based on the opinion of a small set of experts mainly from Academic institutions. Here, to enhance previous results, a revised FAHP methodology has been applied to assess the mutual importance of the criteria and sub-criteria included in an onboard RBF. The framework covers the widest range of safety issues and it is applicable to any ship type. Aiming to an onboard application, a functional and effective

structure of the framework cannot be achieved only involving scholars. Therefore, officers and crew members have been inquired to update the RBF's structure, in an initial phase, and then to assess the weights of importance of its criteria and sub-criteria. In this way, multiple subjective experiences are exploited to assess a synthesis process, going beyond the limits related to the assessment based on scholars' opinion only. Finally, the analysis has been carried out highlighting the specific safety issues affecting different ship types.

2 METHODOLOGY

In the present section, the adopted FAHP technique is presented. Namely, the assessment of weights of importance on the base of experts opinion is briefly described. Finally, the group of expert seafarers inquired in the present study is discussed in terms of its composition.

2.1 Adopted Methods. In AHP (**Saaty, 1980**), the problem is decomposed in a hierarchic set of sub-problems subject to the experts' judgement by means of pairwise comparison. For each couple of criteria, sub-criteria or attributes their relative importance is assigned using a linguistic scale. Among MCDC techniques, it provides the methodology to convert those simple comparisons into weights of importance. However, since the experts' opinions are by definition imprecise and vague, the fuzzy set theory has been applied developing FAHP (**van Laarhoven and Pedrycz, 1983**). It is common practice (**Ishizaka and Nguyen, 2013**, **Grošelj and Zadnik Stirn, 2018**) to convert each expert's preference into a triangular fuzzy number $\mathbf{t} = (t^l, t^m, t^u)$ by means of a linguistic scale (**Table 1**). Each expert compares all the couples of criteria via linguistic preferences. Then, all the results are converted into the pairwise comparison matrix containing associated fuzzy numbers:

$$\mathbf{D}^k = \begin{bmatrix} \mathbf{d}_{11}^k & \cdots & \mathbf{d}_{1n}^k \\ \vdots & \ddots & \vdots \\ \mathbf{d}_{n1}^k & \cdots & \mathbf{d}_{nn}^k \end{bmatrix} \tag{1}$$

where $\mathbf{d}_{ij}^k$ is the k-th expert's preference related to the i-th criterion over the j-th criterion.

If more than 7 ± 2 alternatives are considered, the consistency of each pairwise comparison matrix shall be checked and, if necessary, enhanced (**Saaty, 1977**). In the present work, an algorithm based on linear programming (**Zhang *et al.*, 2014**)

has been adopted to reduce inconsistency of all pairwise matrixes having a consistency index *NI* greater than 0.1.

When a number $K > 1$ of experts are taken into account, the group fuzzy preferences have to be evaluated. Several methods have been proposed to deal with multiple expert judgements. Among the others, the geometric mean has been applied, since it is one of the higher quality synthesis techniques according to **Grošelj and Zadnik Stirn (2018)**.

Table 1. Adopted linguistic scale.

	Preference	1st criteria fuzzy number	2nd criteria fuzzy number
1st criteria	Extreme	(9,9,9)	(1/9,1/9,1/9)
	Strong	(6,7,8)	(1/8,1/7,1/6)
	Fair	(4,5,6)	(1/6,1/5,1/4)
	Moderate	(2,3,4)	(1/4,1/3,1/2)
vs	Equal	(1,1,1)	(1,1,1)
2nd criteria	Moderate	(1/4,1/3,1/2)	(2,3,4)
	Fair	(1/6,1/5,1/4)	(4,5,6)
	Strong	(1/8,1/7,1/6)	(6,7,8)
	Extreme	(1/9,1/9,1/9)	(9,9,9)

$$\mathbf{d}_{ij} = \left(\prod_{k=1}^{K} \mathbf{d}_{ij}^{k} \right)^{1/K} \tag{2}$$

Based on averaged preferences, the fuzzy pairwise comparison matrix is updated obtaining the average pairwise comparison matrix **D**. Then, the fuzzy weight $\mathbf{w}_i$ of each criterion is calculated as the normalized geometric mean of all the items from the corresponding row of the average matrix (**Buckley, 1985**):

$$\mathbf{w}_{ij} = \left(\prod_{j=1}^{n} \mathbf{d}_{ij} \right)^{1/n} \otimes \left[\sum_{i=1}^{n} \left(\prod_{j=1}^{n} \mathbf{d}_{ij} \right)^{1/n} \right]^{-1} \tag{3}$$

Since such weights are still triangular fuzzy numbers, they are defuzzified obtaining a mean weight for each criterion evaluated with the centre of area method as:

$$\overline{w}_i = \frac{w_i^l + w_i^m + w_i^u}{3} \tag{4}$$

Eventually, the mean weights are normalized to obtain the final weight for each criterion:

$$w_i = \overline{w}_i \left(\sum_{i=1}^{n} \overline{w}_i \right)^{-1} \tag{5}$$

2.2 Experts inquired in the Study. The present study is based on the opinions of expert seafarers, that have been required to perform pairwise comparisons by means of the linguistic scale preferences. Besides, they commented on the structure of the framework and checked if the adopted nomenclature is suitable for an onboard DSS. Most of them are captains and deck officers engaged in periodic training courses at the University of Rijeka, Faculty of Maritime Studies. In detail, 45 experts (26 from Croatia, 16 from Italy, 2 from Montenegro, and 1 from Slovenia) has been inquired between August and November 2018. Most of them (43) are male and have a long service period (**Figure 1**). The experts provide services on many different vessels' type (**Figure 2**): mainly on container ships, cruise ships and chemical tankers, but also from bulk carriers, oil tankers and a few LNG carriers, RoRo and navy ships.

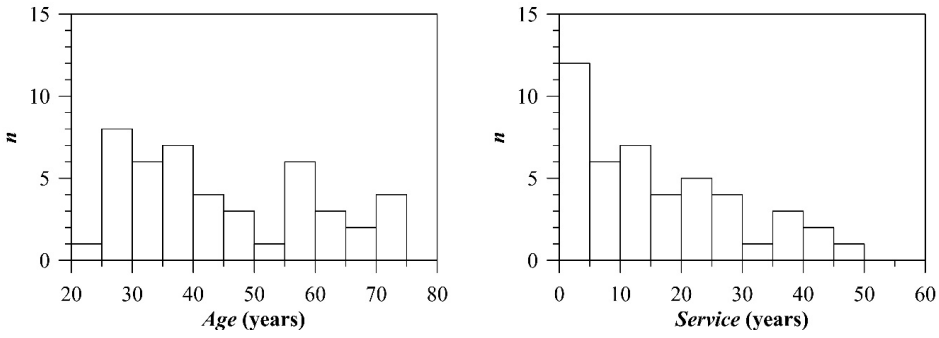

Figure 1. Age and service time of experts.

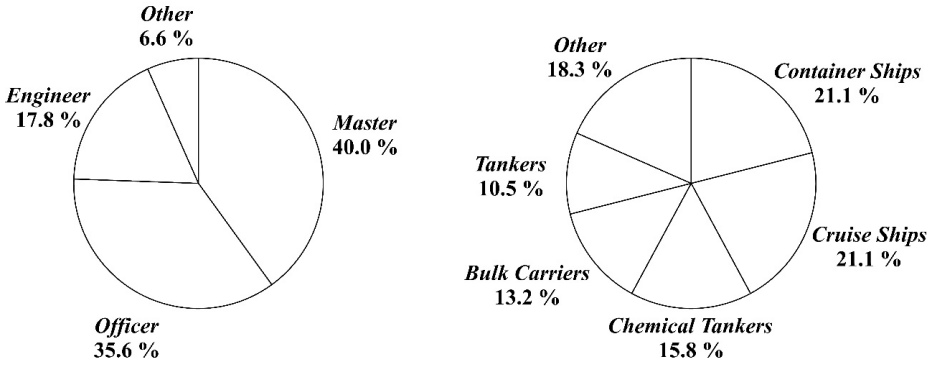

Figure 2. Role in the crew and ship type of subjects.

Considering how difficult is collecting information from onboard personnel, the application of FAHP is particularly suitable since it provided effective results even with very limited sets of experts. Hence, the number of experts inquired in the present work was judged sufficient to carry out the analysis by type of ship and by the role in the crew. Considering all the opinions globally, the set of experts is very large compared to other FAHP applications in the maritime domain present in literature (**Celik *et al.*, 2009**, **Ding *et al.*, 2014**).

3 TEST CASE: THE ONBOARD RBF

The main goal of the RBF is to synthesise all the aspects related to the ship safety with a global risk index r_G, quantifying its safety status by means of an objective process based on multiple experiences from the maritime community. The safety level can be evaluated for a generic ship condition (loading and weather condition, eventual damage, etc.). Following AHP pattern, the MCDM problem is decomposed by means of a hierarchical network (**Figure 3**) with three levels, each one contributing to the r_G through an aggregation process described in (**Trincas *et al.*, 2017**). According to a small group of masters from major shipping companies, the criteria included in the RBF are related to both the rules requirements and the current ship status assessed by means of monitoring systems. In the following, the criteria and their sub-criteria are briefly introduced.

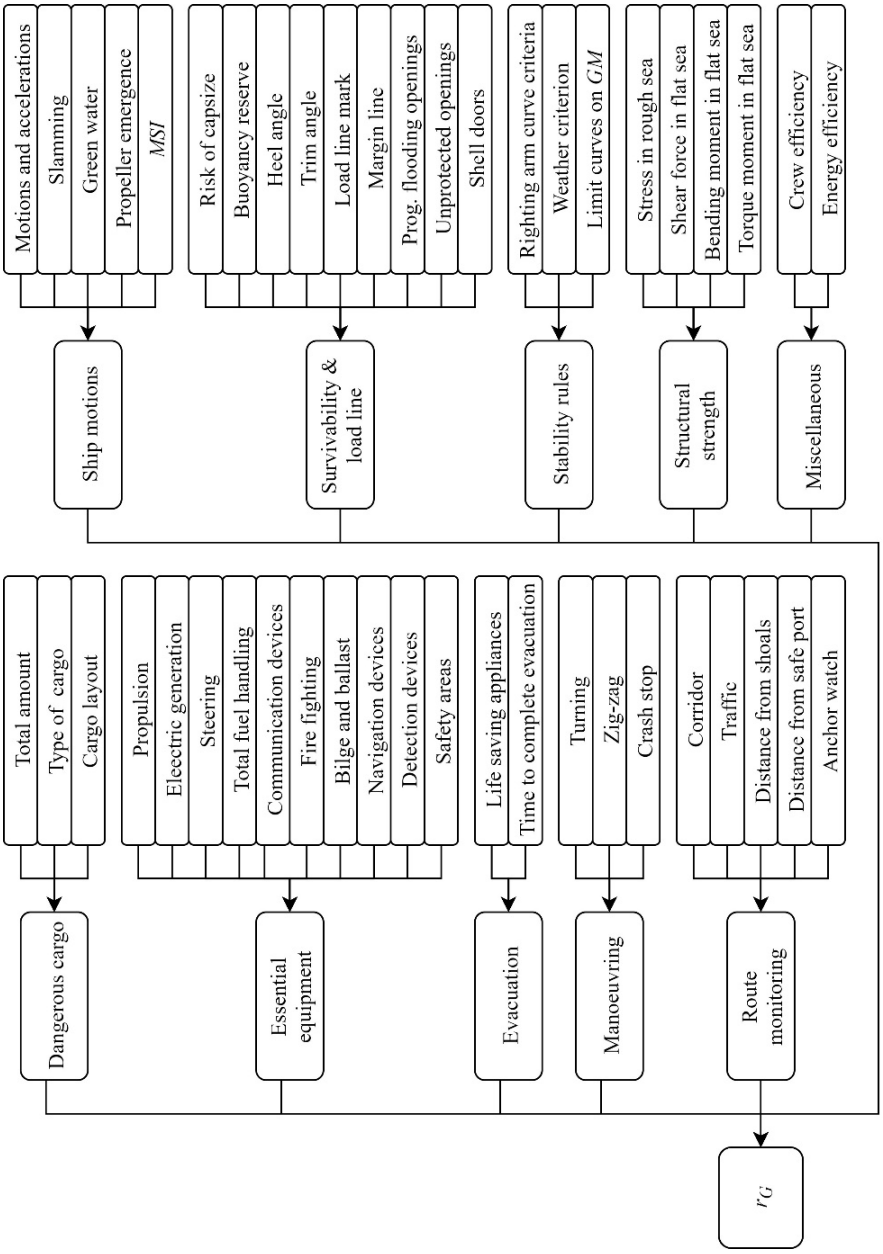

Figure 3. Composition of criteria and sub-criteria.

3.1 Dangerous Cargo. The dangerous cargo criterion is related to the type of cargo defined in *IMDG Code* and its distribution onboard. The total amount of cargo sub-criterion is related to the weight of dangerous cargo versus the allowed amount that can be transported by the ship. The dangerous cargo is classified into classes due to its level of danger providing an intrinsic measure of the risk related to the type of cargo. The cargo layout sub-criterion measures the risk connected to the distance of dangerous cargo from critical spots (essential equipment, heat sources, accommodations, etc.), intervention stations and detection devices, giving a safety measure related to the actual or simulated cargo stowage.

3.2 Essential Equipment. The essential equipment criterion is related to the effective operation of the essential systems as defined by SRtP regulations (*MSC.1/Circ.1214*), considering the effect of shut-down for maintenance, heel/trim angles, fire and/or flooding water. It is worth to notice that the onboard assessment of the operation of essential equipment in case of emergency is recommended by *MSC.1/Circ.1400*.

3.3 Evacuation. The evacuation criterion is related to the effect of a casualty on escape routes and the effect of the ship's list on evacuation time as required by *MSC.1/Circ.1400*. In detail, the number of operative lifesaving appliances is considered, taking into account the effect of fire and/or flooding. The time required to complete the evacuation procedure should be determined, taking into account the effect of the heel, trim, fire, and/or flooding. It can be compared with the time to reach an unsafe condition during progressive flooding (**Braidotti and Mauro, 2019**).

3.4 Manoeuvring. Currently, no rule prescribes to evaluate during navigation the ship's manoeuvring capabilities in the actual loading condition. Anyway, they can affect ship safety, especially in restricted waters and port operations. Hence, manoeuvring has been included in the framework taking into account all the most important manoeuvres defined IMO standards (*MSC 76/23/add.1*).

3.5 Route Monitoring. The route monitoring criterion is related to the main navigational issues to prevent the occurrence of accidents (collisions or grounding). The corridor sub-criterion monitors the deviation from the planned route. The related risk increases as much as the ship approaches the limits of a predefined corridor. Traffic and Distance from shoals sub-criteria are related to the probability of a collision or grounding respectively. This probability could be defined as a function of ship speed, route and distance from other vessels and main obstacles monitored by navigation sensors or provided by sensors and

electronic chart display and information system. The distance from safe port criterion takes into account the risk associated with large distances from search and rescue facilities or from a sheltered anchorage. Finally, the anchor watch is related to distance from anchoring point, in order to early detect a mooring failure and it is not considered during navigation.

3.6 Ship Motions. Nowadays, no rule prescribes to take under control seakeeping during navigation and neither during ship design. Nevertheless, it should be taken into account, especially for passenger ships, having a strong impact on passenger comfort, and for navy ships/offshore vessels (**Mauro and Nabergoj, 2015**), fixing ship's operation limits. Eventually, dynamic phenomena might result also in stress on ship structure (**Mauro and Monacolli, 2018**), reduction of propulsion efficiency or lead to embark seawater. All these considerations led to include seakeeping in the RBF within the ship motions criterion. The Motions and Accelerations sub-criterion deals with the average period of motions, which is compared with the natural periods in order to avoid resonance phenomena. Slamming, green water, and propeller emergence are well-known undesirable phenomena connected to seakeeping (**Prpić-Oršić *et al.*, 2014**), whose occurrence probability shall be considered in the RBF. Finally, the motion sickness index (MSI) measures the passengers' comfort.

3.7 Survivability & Load Line. This criterion is related to all the aspects connected to ship floating position (such as freeboard requirements, submersion of the margin line, unprotected openings, load line mark, etc.). Moreover, it deals with the most important ship survivability issues: buoyancy reserve and risk of capsizing due to actual weather condition. The buoyancy reserve sub-criterion is a function of the difference between the actual displacement and the displacement at unprotected openings or bulkhead deck submersion in intact or damaged condition, respectively. During navigation, a continuous assessment of the risk of capsizing should be also adopted, based on actual loading and weather condition. For this purpose, the extreme values of roll motion (**Mauro and Nabergoj, 2017**), which might lead to capsizing, should be inferred from a record period representative of current weather condition.

3.8 Stability Rules. Stability rules criterion deals with compliance with stability requirements for the intact and damaged condition. In the RBF, a fuzzy satisfaction measurement is adopted, introducing a safe reference condition in addition to the rule threshold. The safe condition could be defined for each attribute as the value providing the larger margin among the values from design loading conditions.

3.9 Structural Strength. The structural strength criterion deals with the compliance with longitudinal strength rules in still water and the assessment of the risk of structural failure in waves. The class rules based on statistical formulation, define the limit curves for shear force, bending moment and, for special types of ships, torque moment. This approach, although included in the framework, is not capable to consider the current weather condition. An approach should be preferred based on extreme values (**Mauro *et al.*, 2019a, b**) inferred from direct stress measurement through an onboard monitoring system.

3.10 Miscellaneous. The miscellaneous criterion is related to the crew efficiency and reduction of emissions. Measuring the crew efficiency onboard is not an easy task. A viable solution could be considering efficiency as a function of Ship Risk Profile (SRP), as defined in the *Paris memorandum of understanding* document. In a given ship condition, a optimal floating position can be defined in order to reduce fuel consumption and, thus, the emissions (**Braidotti *et al.*, 2018b**). The normalized distance between actual and optimal fuel consumption can be assumed as an "environmental risk" to be included in the RBF.

4 RESULTS AND DISCUSSION

In the present study the weight of importance of all the criteria and sub-criteria has been studied. A global analysis of rough data coming from experts' preferences has been performed taking into account all the ship types in order to provide an overall perspective. Moreover, they have been analysed also by ship type, considering only groups composed of three or more experts, highlighting significant differences in weights of importance. The results are reported in Tables 2-12 and, in order to ease the interpretation, their increasing relevance is highlighted with a colour scale ranging from green (less important) to red (most important). In the tables, the judgements according to scholars' opinion (**Braidotti *et al.*, 2018a**) are also reported in a dedicated column ("Old"). As expected, the old outcome often is completely different compared with the seafarers' opinion. In the following, the results are discussed criterion by criterion.

Concerning dangerous cargo (**Table 2**), the cargo layout sub-criterion is widely the most important according to seafarers, whereas the total amount is less important. This trend was obtained mainly from judgements of oil tankers' crewmembers, whilst people from chemical tankers is slightly in countertrend. Personnel from container ships, cruise ships and bulk carriers do not assign significant differences to these sub-criteria.

The results for essential equipment are shown in **Table 3**. Since all these machinery, systems and devices are considered crucial by international rules, it is interesting to study what is really essential from an onboard perspective. Although the judgements differ substantially due to ship type, some common trends can be identified: the fuel handling system is not considered a threat for ship safety, as well as bilge and ballast system, navigation and communication devices. On the other hand, the fire fighting systems are considered of the utmost importance for almost all ship types.

Table 2. Weights of importance of dangerous cargo sub-criteria.

	Container Ships	Cruise Ships	Chemical Tankers	Bulk Carriers	Tankers	Global	Old
Total amount	0.325	0.312	0.383	0.331	0.263	0.279	0.264
Type of cargo	0.346	0.323	0.330	0.338	0.328	0.341	0.093
Cargo layout	0.328	0.365	0.286	0.331	0.409	0.380	0.643

Table 3. Weights of importance of essential equipment sub-criteria.

	Container Ships	Cruise Ships	Chemical Tankers	Bulk Carriers	Tankers	Global	Old
Propulsion	0.104	0.106	0.072	0.099	0.094	0.100	0.131
Electric generation	0.099	0.106	0.061	0.099	0.094	0.102	0.260
Steering	0.102	0.102	0.112	0.099	0.094	0.110	0.166
Total fuel handling	0.097	0.087	0.052	0.099	0.072	0.072	0.100
Communication devices	0.099	0.095	0.080	0.096	0.121	0.086	0.042
Fire fighting	0.101	0.116	0.133	0.104	0.147	0.140	0.121
Bilge and ballast	0.094	0.090	0.112	0.097	0.072	0.091	0.062
Navigation devices	0.104	0.096	0.112	0.101	0.121	0.092	0.035
Detection devices	0.104	0.099	0.133	0.102	0.093	0.112	0.047
Safety areas	0.096	0.103	0.133	0.104	0.093	0.095	0.036

Table 4. Weights of importance of evacuation sub-criteria.

	Container Ships	Cruise Ships	Chemical Tankers	Bulk Carriers	Tankers	Global	Old
Life saving appliances	0.514	0.500	0.544	0.500	0.566	0.532	0.616
Time to comp. evac.	0.486	0.500	0.456	0.500	0.434	0.468	0.384

Table 5. Weights of importance of manoeuvring sub-criteria.

	Container Ships	Cruise Ships	Chemical Tankers	Bulk Carriers	Tankers	Global	Old
Turning	0.341	0.333	0.412	0.327	0.387	0.339	0.237
Zig-Zag	0.314	0.319	0.242	0.320	0.227	0.254	0.332
Crash Stop	0.344	0.348	0.346	0.353	0.387	0.407	0.431

Table 6. Weights of importance of ship motions sub-criteria.

	Container Ships	Cruise Ships	Chemical Tankers	Bulk Carriers	Tankers	Global	Old
Motions and acc.	0.211	0.203	0.159	0.199	0.133	0.217	0.310
Slamming	0.205	0.194	0.183	0.199	0.210	0.213	0.314
Green water	0.206	0.208	0.211	0.204	0.274	0.205	0.044
Propeller emergence	0.210	0.208	0.301	0.204	0.274	0.256	0.265
Motion Sickness Index	0.167	0.186	0.146	0.195	0.108	0.110	0.068

This is not surprising especially on ships carrying flammable products in bulk, e.g. Oil/Chemical tankers. Moreover, the relevance of detection devices enforces this conclusion, being comparable with the one assigned to propulsion, electric generation and steering. It can be concluded that seafarers are more concerned by

means for emergency response and the functionality of the main machinery rather than auxiliary systems. It is worth to notice that the ranking from scholars' opinions is completely different, especially concerning the auxiliaries (considered essential) and emergency response devices (less important).

Table 4 shows the weights of importance of evacuation criterion. Comparable importance has been assigned to availability of lifesaving appliances and to the time required to complete evacuation procedure since both are crucial during ship abandonment. In this case, the seafarers' opinion is considered more reasonable than the one from academic experts.

The analysis of manoeuvring sub-criterion (**Table 5**) highlights a good agreement between people from different ship types. The main manoeuvres defined by IMO, ordered by decreasing importance are crash stop, turning, zig-zag. It could be concluded that from an onboard perspective, crash stop and turning are the most effective to define actual manoeuvring capability, but it could be more representative of the manoeuvres crews are more familiar with. In fact, especially to avoid collisions, the yaw-checking ability, assessed via the zig-zag test, is essential and requires higher importance as was done by scholars.

Ship motions criterion provided surprising results too (**Table 6**). Globally, propeller emergence was always considered a primary concern. Motions and accelerations are also relevant for all ship types other than chemical/oil tankers. On the contrary, slamming is not as important for seafarers, especially for those from cruise ships. Furthermore, green water sub-criterion is inexplicably considered very important for cruise ships, having a much reduced exposed deck, while it is not a primary concern on container ships, where it could cause a cargo loss. The other ship types show more reasonable results for this sub-criterion.

As expected, among survivability and load line sub-criteria (**Table 7**), the ones having the strongest influence on ship safety are the risk of capsizing and the buoyancy reserve, even though the gap with the other sub-criteria is lower than the old one. However, it was unexpected that the risk of capsizing is not considered as one of the most important safety issues on cruise ships. In fact, these vessels are characterized by critical stability: the large wind areas, combined to short free-board, likely drives to serious progressive flooding issues and a probable capsize after major damages. Nevertheless, cruise ships' crews are aware of subdivision issues, assigning high importance to shell doors, unprotected and progressive flooding openings.

Table 7. Weights of importance of survivability & load line sub-criteria.

	Container Ships	Cruise Ships	Chemical Tankers	Bulk Carriers	Tankers	Global	Old
Buoyancy reserve	0.113	0.110	0.139	0.115	0.120	0.135	0.217
Heeling angle	0.110	0.110	0.089	0.115	0.120	0.108	0.147
Load line marks	0.108	0.110	0.139	0.110	0.092	0.091	0.034
Margin Line	0.111	0.106	0.084	0.108	0.092	0.083	0.037
Prog. flooding openings	0.111	0.119	0.117	0.115	0.120	0.132	0.088
Risk of capsize	0.113	0.110	0.117	0.110	0.120	0.135	0.222
Shell doors	0.111	0.124	0.117	0.108	0.120	0.109	0.047
Trim angle	0.105	0.097	0.099	0.105	0.120	0.083	0.103
Unprotected openings	0.118	0.114	0.099	0.113	0.093	0.124	0.105

Table 8. Weights of importance of stability rules sub-criteria.

	Container Ships	Cruise Ships	Chemical Tankers	Bulk Carriers	Tankers	Global	Old
Righting arm c. criteria	0.343	0.324	0.333	0.336	0.287	0.343	0.389
Weather criterion	0.315	0.352	0.333	0.328	0.427	0.339	0.258
Limit curves on KG/GM	0.343	0.324	0.333	0.336	0.287	0.318	0.353

Table 9. Weights of importance of structural strength sub-criteria.

	Container Ships	Cruise Ships	Chemical Tankers	Bulk Carriers	Tankers	Global	Old
Stress in rough sea	0.273	0.268	0.296	0.263	0.266	0.358	0.601
Shear force in flat see	0.247	0.247	0.248	0.246	0.265	0.230	0.172
Bending m. in flat see	0.240	0.247	0.248	0.240	0.265	0.208	0.094
Torque m. in flat see	0.240	0.238	0.208	0.251	0.204	0.204	0.133

The stability rules results (**Table 8**) shows that related sub-criteria are considered almost equally important for all ship types. Only personnel from tankers identified a clear preference for weather criterion.

Concerning structural strength (**Table 9**), for all the types of vessel, more importance has been given to stress in rough sea sub-criterion, based on the assessment of structural stress in the current weather and loading condition, in agreement with scholars' preferences. The still-water rule requirements on the shear force, bending and torque moments are considered less important and their rank differs due to ship type, highlighting the most critical structural issues. In fact, for ships with large deck openings (bulk carriers and container ships), more importance has been assigned to torque moment, confirming that seafarers are aware of risks connected to the structural layout of their ship.

In **Table 10** the results for miscellaneous criterion are provided. The crew efficiency has been considered more important compared to energy efficiency for all ship types other than chemical tankers. The gap is relevant especially for tankers and for other ships like RoRo and navy ships, highlighting the importance of crew training on these ship types.

The route monitoring sub-criterion (**Table 11**) was not present in the previous study since was added in a second time as suggested by onboard personnel. As expected, the risk of collision or grounding, i.e. traffic and distance from shoals sub-criteria, concerns seafarers from any kind of ship other than chemical tankers and bulk carriers. For the latter ship types, traffic is not considered as relevant. The distance from a safe port has been considered the less important by most of the crewmembers frequently engaged in long voyages.

Table 10. Weights of importance of miscellaneous sub-criteria.

	Container Ships	Cruise Ships	Chemical Tankers	Bulk Carriers	Tankers	Global	Old
Crew efficiency	0.521	0.521	0.456	0.506	0.566	0.602	0.892
Energy efficiency	0.479	0.479	0.544	0.494	0.434	0.398	0.108

Table 11. Weights of importance of route monitoring sub-criteria.

	Container Ships	Cruise Ships	Chemical Tankers	Bulk Carriers	Tankers	Global	Old
Corridor	0.192	0.195	0.178	0.199	0.197	0.171	-
Traffic	0.210	0.210	0.178	0.200	0.197	0.239	-
Distance from shoals	0.216	0.196	0.253	0.204	0.257	0.251	-
Distance from safe port	0.182	0.187	0.178	0.196	0.151	0.152	-
Anchor watch	0.200	0.212	0.213	0.201	0.197	0.187	-

Table 12. Weights of importance of all the criteria.

	Container Ships	Cruise Ships	Chemical Tankers	Bulk Carriers	Tankers	Global	Old
Dangerous Cargo	0.106	0.080	0.087	0.102	0.094	0.094	0.087
Essential Equipment	0.098	0.100	0.123	0.102	0.123	0.118	0.118
Evacuation	0.100	0.116	0.123	0.107	0.094	0.126	0.088
Manoeuvring	0.109	0.104	0.086	0.096	0.094	0.096	0.130
Route Monitoring	0.097	0.096	0.086	0.100	0.094	0.086	-
Ship Motions	0.098	0.095	0.072	0.095	0.094	0.078	0.120
Surv. & Load Line	0.100	0.099	0.123	0.100	0.094	0.105	0.117
Stability Rules	0.103	0.104	0.123	0.098	0.094	0.101	0.059
Structural Strenght	0.100	0.099	0.123	0.102	0.094	0.108	0.094
Miscellaneous	0.087	0.107	0.052	0.098	0.123	0.088	0.187

Eventually, **Table 12** provides the weight of importance of all the criteria, highlighting once again a strong dependence on ship type. An overall analysis divides the criteria into three categories. Evacuation and essential equipment were considered the most important, followed by survivability and load line, structural strength, stability rules, manoeuvring, crew and energy efficiency, and dangerous cargo. The least criteria by importance are route monitoring and ship motions. Hence, crewmembers mainly focus on resilience and safety of

essential systems while giving particular attention to real-time monitoring. This trend is also confirmed by the importance given to survivability and structural strength criteria, which are both based on monitoring systems outcomes. This conclusion is in line with the previous results, despite scholars gave more attention to hydrodynamic issues compared to seafarers. In fact, seafarers do not consider essential any mean preventing motions magnification or aiding navigation.

5 CONCLUSIONS

The present work provides an overview of ship safety in the operative condition, according to seafarers' perception. The results are useful not only for the development of an onboard RBF but also to raise some issues concerning rules revision and identify some lacks in masters training. In general, the outcomes show the importance given by masters and officers to the exploitation of monitoring systems. They are considered more effective in assessing ship safety compared with prescriptive rules requirements. This trend, although less evident, confirms the conclusion coming from scholars' opinion.

Moreover, seafarers appear confident on their own navigational capability assigning low importance on criteria and sub-criteria related to route monitoring, navigation and communications devices. These leanings are in sharp contrast with casualties statistics and with scholars and shipowners perspective too. In fact, several shipping companies are recently increasing fleet monitoring in order to gradually reduce the masters' responsibilities in favour of ship operation centres and automation. On the other hand, it can be concluded that ship safety assessment is strongly influenced by ship type. In fact, the results for the analysed ship types are not usually in good agreement. Nevertheless, FAHP provides a viable methodology to assess these preferences, even with a small set of experts. Therefore, for ships categories here not included, a dedicated study is recommended.

The multiple subjective seafarers' experiences, led to define a hierarchical structure to decompose the safety-assessment problem and quantify the relative importance of a very large set of criteria and sub-criteria. Its application as the core of a new DDS could exploit data from monitoring systems to enhance situational awareness and reduce the occurrence of human error in marine operations. Moreover, this framework, due to its modular nature, can be further extended with other criteria/ sub-criteria in order to fit vessels special requirement.

Finally, several judgements collected in the present study were somehow unexpected and not completely justiciable, highlighting some seafarers' lacks of knowledge regarding hydrodynamics. For these topics, further training is advisable for onboard personnel and an assessment of preferences based on naval architects preferences should be preferred.

Acknowledgements

This work has been fully supported by the Croatian Science Foundation under the project IP-2018-01-3739. The authors would like to thank the captains from Grimaldi Lines, CMA CGM and MSC Cruises for their important support.

REFERENCES

Braidotti, L. and Mauro, F. (2019). A new calculation technique for onboard progressive flooding simulation. *Ship Technology Research*, 66 (3), pp. 150–162.

Braidotti, L., Mauro, F., Sebastiani, L., Bisiani, S. and Bucci, V. (2018b). Ballast allocation technique to minimize fuel consumption. In: *Proceedings of The 19th International Conference on Ships and Maritime Research – NAV 2018*, Trieste, Italy.

Braidotti, L., Prpić-Oršić, J., Valčić, M., Trincas, G. and Bucci, V. (2018a). Fuzzy analytical hierarchical process to assess weights of importance in ship operation risk assessment. In: *Proceedings of The 19th International Conference on Ships and Maritime Research – NAV 2018*. Trieste, Italy.

Buckley, J.J. (1985). Fuzzy hierarchical analysis. *Fuzzy Sets and Systems*, 17 (3), pp. 233–247.

Celik, M., Deha Er, I. and Fahri Ozok, A. (2009). Application of fuzzy extended AHP methodology on shipping registry selection: The case of Turkish maritime industry. *Expert Systems with Applications*, 36 (1), pp. 190–198.

Ding, J.F., Jhong, C.H., Huang, W.C. and Taleizadeh, A. (2014). Use of the fuzzy AHP method to evaluate key factors influencing new cross-strait shuttle shipping routes. *Marine Technology Society Journal*, 48 (3), pp. 125–137.

EMSA. (2019). *Annual overview of marine casualties and incidents 2019*. Lisbon. European Maritime Safety Agency.

Grošelj, P. and Zadnik Stirn, L. (2018). Evaluation of several approaches for deriving weights in fuzzy group analytic hierarchy process. *Journal of Decision Systems*, 27 (sup1), pp. 217–226.

Ishizaka, A. and Nguyen, N.H. (2013). Calibrated fuzzy AHP for current bank account selection. *Expert Systems with Applications*, 40 (9), pp. 3775–3783.

Mauro, F. and Monacolli, M. (2018). Evaluation of extreme wave loads for slender tubular structures. In *Proceedings of The 19th International Conference on Ships and Maritime Research – NAV 2018*. Trieste, Italy.

Mauro, F. and Nabergoj, R. (2015). Integrated station-keeping and seakeeping predictions. In: *Proceedings of the 16th International Congress of the International Maritime Association of the Mediterranean – IMAM*. Pula, Croatia.

Mauro, F. and Nabergoj, R. (2017). An enhanced method for extreme loads analysis. *Brodogradnja*, 68 (2), pp. 79–92.

Mauro, F., Braidotti, L., and Prpić-Oršić, J. (2019a). Extreme loads estimation using genetic algorithm approach. In: *Proceedings of the 7th International Conference on Marine Structures – MARSTRUCT 2019*. Dubrovnik, Croatia.

Mauro, F., Braidotti, L., la Monaca, U. and Nabergoj, R. (2019b). Extreme loads determination on complex slender structures. *International Shipbuilding Progress*, 66 (1), pp. 57–76.

Nordström, J., Goerlandt, F., Sarsama, J., Leppänen, P., Nissilä, M., Ruponen, P., Lübcke, T. and Sonninen, S. (2016). Vessel triage: A method for assessing and communicating the safety status of vessels in maritime distress situations. *Safety Science*, 85, pp. 117–129.

Perera, L.P., Rodrigues, J.M., Pascoal, R., and Guedes Soares, C. (2012). Development of an onboard decision support system for ship navigation under rough weather conditions. In: *Sustainable Maritime Transportation and Exploitation of Sea Resources – Proceedings of the 14th International Congress of the International Maritime Association of the Mediterranean – IMAM 2011*. Genova, Italy.

Prpić-Oršić, J., Parunov, J., and Šikić, I. (2014). Operation of ULCS - real life. *International Journal of Naval Architecture and Ocean Engineering*, 6 (4), pp. 1014–1023.

Saaty, T.L. (1977). Scaling method for priorities in hierarchical structures. *Journal of Mathematical Psychology*, 15 (3), pp. 234–281.

Saaty, T.L. (1980). *The Analytical Hierarchy Process*. New York: McGraw-Hill International.

Trincas, G., Braidotti, L. and De Francesco, L. (2017). Risk-based system to control safety level of flooded passenger ship. *Brodogradnja*, 68 (1), pp. 31–60.

van Laarhoven, P.J.M. and Pedrycz, W. (1983). A fuzzy extension of Saaty's priority theory. *Fuzzy Sets and Systems*, 11 (1-3), pp. 199–227.

Zhang, H., Sekhari, A., Ouzrout, Y. and Bouras, A. (2014). Deriving consistent pairwise comparison matrices in decision making methodologies based on linear programming method. *Journal of Intelligent and Fuzzy Systems*, 27 (4), pp. 197–198.

HOLISTIC ENVIRONMENTAL ANALYSIS OF SELECTED ZERO-EMISSION POWERING OPTIONS FOR RO-RO PASSENGER SHIPS IN CROATIA

Maja Perčić*, Nikola Vladimir, Ivana Jovanović, Marija Koričan

Abstract. *Environmental regulations and emissions targets are pushing the shipping industry towards the implementation of alternative decarbonization measures. Among them, the application of zero-emission solutions, such as the use of hydrogen and electricity, are highlighted. Although with their implementation, the exhaust gas while the ship is operating is absent, their environmental performance needs to be investigated from the life-cycle point of view. Therefore, the Life-Cycle Assessment (LCA) is performed, where the emissions released through the life-cycle of the power system with hydrogen and electricity are investigated and compared to the diesel power system configuration. The comparison indicated that the hydrogen produced through the process of electrolysis (green hydrogen) is the best ecological solution with respect to all investigated emission products, while the second-most environmental friendly zero-emission alternative is the full electrification of a ship with a Lithium-ion battery.*

Key words: *environmental assessment; ship power system; hydrogen; battery*

University of Zagreb, Faculty of Mechanical Engineering and Naval Architecture, Ivana Lučića 5, 10000 Zagreb, Croatia

* Corresponding author: Maja Perčić (maja.percic@fsb.hr)

University of Zadar

1 INTRODUCTION

The atmosphere pollution due to excessive use of fossil fuel represents a major environmental problem. The released gas from fossil fuel combustion is a mixture of nitrogen oxides (NO_X), sulphur oxide (SO_X), carbon monoxide (CO), particulate matter (PM) and Greenhouse Gas (GHGs) (Monteiro *et al.* 2018). The latter refers to the emissions of carbon dioxide (CO_2), methane (CH_4), nitrous oxides (N_2O) and fluorinated gases. While the NO_X, SO_X and PM, have an impact on human health by causing respiratory diseases and on the environment in form of its acidification (**Kim and Chae, 2016**; **Toscano and Murena, 2019**), the GHGs causes the Greenhouse effect and, as a consequence of it, global warming (**UNFCCC, 2001**).

In the maritime sector, the emissions regulation is performed by the establishment of emission standards, depending on whether ships are operating in Emission Control Areas (ECAs) or elsewhere. SO_X emissions are regulated by the quality of fuel used in a ship power system, where sulphur content need to meet certain requirements. NOx emission limit depends on the speed of an engine, where Tier I and Tier II are global standards, while Tier III refers to the ECA (**IMO Marine Engine Regulations, 2020**). The CO_2 emissions are regulated within the Energy efficiency regulation (**IMO, 2011**). However, due to the Paris Agreement and other strategies that promote decarbonization of each sector (**Bataille *et al.*, 2018**), including the maritime sector, the International Maritime Organization (IMO) set a goal for international shipping to reduce the total annual GHGs by at least 50 % by 2050, compared to 2008 levels (**IMO, 2020**). The most promising way to accomplish this goal is to replace the conventional ship power system with an alternative one and implementing zero-emissions shipping options.

The electrification of the ship represents one of the zero-emission shipping solutions, which results in the absence of exhaust gases when during ship operation. The fully electrified ship with only a battery implemented onboard offers emissions, noise and maintenance cost reduction, but with a high investment cost. However, commercially available technology can be easily implemented in a ship power system (**Gagatsi *et al.*, 2016**; **Perčić *et al.*, 2020a**).

Reduction in shipping emissions can be achieved by the implementation of fuel cells on board ship. They refer to the electrochemical device that converts chemical energy into electricity which then powers the ship. The ideal fuel for the fuel cell is hydrogen due to its fast kinetics (**van Biert *et al.*, 2016**). However, the investment and fuel cost, but also storage problem and supply chains represent

the main obstacles for its further deployment in the shipping sector (**Bicer and Dincer, 2018**). With the mass production of fuel cells and their commercialization for shipping purposes, hydrogen and hydrogen carriers will be more used as marine fuel (**EMSA, 2017**).

Although the zero-emission options are promoted for reducing the shipping emissions, especially for the coastal vessels, their environmental performance needs to be assessed from the life-cycle point of view. In this paper, the zero-emission shipping options, i.e. electricity-power ship and hydrogen-powered ship are investigated where the results are illustrated for two ships engaged in the Croatian short-sea shipping sector. The Life-Cycle Assessment (LCA) comparison of considered power system configuration is performed, where currently used diesel-powered ship represents a baseline scenario, and the best ecological option is highlighted.

2 METHODOLOGY

2.1 Ship particulars

Consideres vessels are ro-ro passenger ships, i.e. ferries, operating on short (Ship 1) and long route (Ship 2). While Ship 1 connects settlements Prizna and Žigljen, Ship 2 operates on a ferry line connecting Split and island Vis, **Figure 1**.

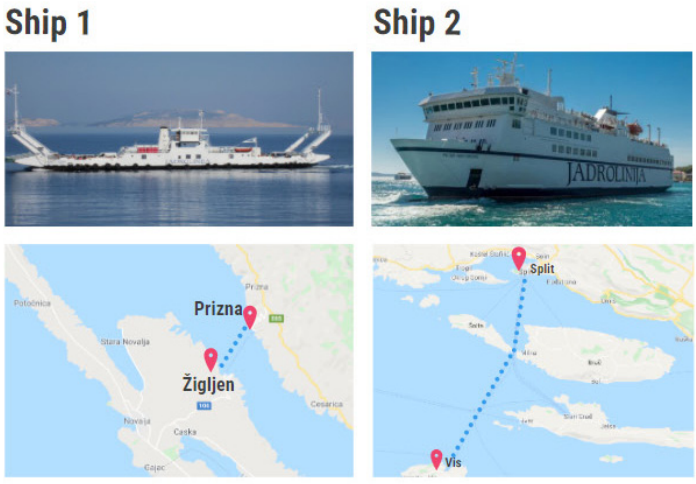

Figure 1. The considered ro-ro passenger ships and their routes.

The ship's main particulars are obtained from the **CRS** (**2020**), while the annual schedule and operating hours are obtained from **Jadrolinija** (**2020**), **Table 1**.

Table 1. The main particulars of the considered ships and their routes. (**CRS, 2020**; **Jadrolinija, 2020**)

	Ship 1	**Ship 2**
Route	Prizna-Žigljen	Vis-Split
Length between perpendiculars, L_{pp} (m)	52.4	80
Breadth, B (m)	11.7	18.0
Draught, T (m)	1.63	3.80
Main engine power, P_{ME} (kW)	792	3,600
Auxiliary engine power, P_{AE} (kW)	84	1,944
Design speed, v_{de} (kn)	8.0	15.75
Trip duration, t (min)	15	140
Route length, l (nm)	1.61	30.2
Annual number of return trips, N_A	1,590	800

Since operating speed usually varies from design speed, it is calculated by dividing the route length by trip duration. Therefore, the average power of the main engine of a ship, $P_{ME,ave}$ (kW), that sails at calculated operating speed, v_{op} (kn), is calculating as follows:

$$P_{ME,ave} = (P_{ME} \cdot 0.8) \cdot \left(\frac{v_{op}}{v_{de}}\right)^3 \quad (1)$$

The average load of the auxiliary engine ($P_{AE,ave}$) is assumed to be 50 %. By summing up $P_{ME,ave}$ and $P_{AE,ave}$ the average ship power (P_{ave}) is calculated.

The energy consumption per distance, EC (kWh/nm), is then calculated according to the following equation:

$$EC = \frac{P_{ave}}{v_{op}} \quad (2)$$

2.2 Environmental analysis

The environmental assessments of the considered power systems are performed through the LCA. This method considers the emissions released throughout each stage of a power system's lifecycle, i.e. from feedstock and production of fuel to manufacturing the main elements of a power system, use of fuel in ship operation up to final disposal and recycling process (**ISO, 2006**).

In this paper, the LCA is performed by LCA software GREET 2020. It offers an investigation of environmental impact through the released emissions from the fuel cycle (i.e. from feedstock extraction, fuel production to distribution of fuel to the pump), i.e. Well-to-Pump (WTP) phase, emissions from the use of the fuel in a power system, i.e. Pump-to-Wake (PTW) phase, and emissions related to certain components of the power system, i.e. Manufacturing (M) phase. The system boundary is placed on the power system and not on the entire ship.

Along with emissions of NO_X, SO_X and PM, in the performed LCAs, the Global Warming Potential (GWP) is investigated. It refers to the measure of GHG's contribute to global warming, regarding the CO_2 emission (EPA 2020). It is expressed in CO_2-eq and calculated according to the following equation:

$$GWP = 1 \cdot E_{CO_2} + 36 \cdot E_{CH_4} + 298 \cdot E_{N_2O} \quad (3)$$

where E refers to the released emissions of a particular gas.

The environmental assessments are performed regarding the lifetime of a ship power system of 20 years.

2.2.1 The LCA of a diesel-powered ship

The processes included in the environmental assessments of the diesel power system configuration are presented in **Figure 2**.

Within the WTP phase, the stationary processes such as crude oil recovery and diesel refining are obtained from the GREET 2020 database, while the transportation processes are modified in order to describe the crude oil and diesel transport pathway for the case of Croatia. Therefore, the crude oil is obtained from the Middle East from which is transported via tankers (4,000 km) up to the Croatian terminal. From there, it is transported via pipeline to the Rijeka refinery where the refining process occurs and diesel is produced. Croatian diesel is further distributed via tank truck up to the required refuelling station.

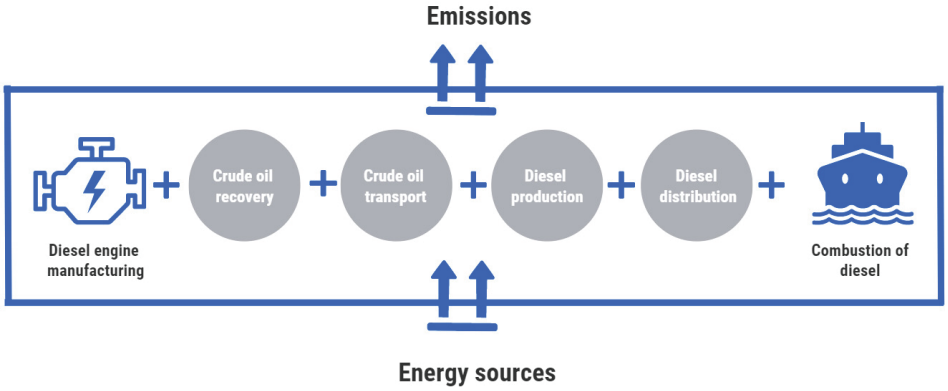

Figure 2. The processed included in the LCA of a diesel-powered ship.

The combustion of diesel in a ship engine results in emissions (*TE*). These emissions refer to the PTW phase and they are calculated by multiplying the energy consumption of a ship (*EC*), specific fuel consumption (*SFC*), and emission factors (*EF*):

$$TE_i = EC \cdot SFC \cdot EF_i \tag{4}$$

where i refers to any emissions, e.g. CO_2, NO_X, SO_X, etc. For high-speed diesel engines, the SFCD is assumed to be 0.215 kg/kWh. The emission factors for particular emission are obtained from the Third IMO GHG study (**IMO, 2014**).

Since the Croatian ro-ro passenger fleet is operating with mostly outdated diesel engine, in this assessment, the implementation of a new diesel engine is investigated where its environmental impact is analysed within the M phase. Its related released emissions are obtained by considered materials embedded in the new engine, such as proposed in the study by **Jeong *et al.*** (**2018**).

2.2.2 The LCA of a hydrogen-powered ship

The implementation of hydrogen as a marine fuel represents an interesting research topic. The processes included in the LCA of a hydrogen-powered ship are presented in **Figure 3**. Although the main feedstock for hydrogen is natural gas (grey hydrogen), it can be obtained from Renewable Energy Sources (RESs) through the process of electrolysis (green hydrogen) (**Dawood *et al.*, 2020**). Therefore, in a stage of the WTP phase, the feedstock preparation for grey hydrogen refers to the natural gas recovery, while for the green hydrogen it

refers to the electricity generation from RESs. It is assumed that the hydrogen is then produced in Western Europe and distributed to the refuelling pump. The Proton Exchange Membrane (PEM) fuel cell with an efficiency of 48 % is selected. The used methodology is presented in the study by **Perčić *et al.*** (**2020b**).

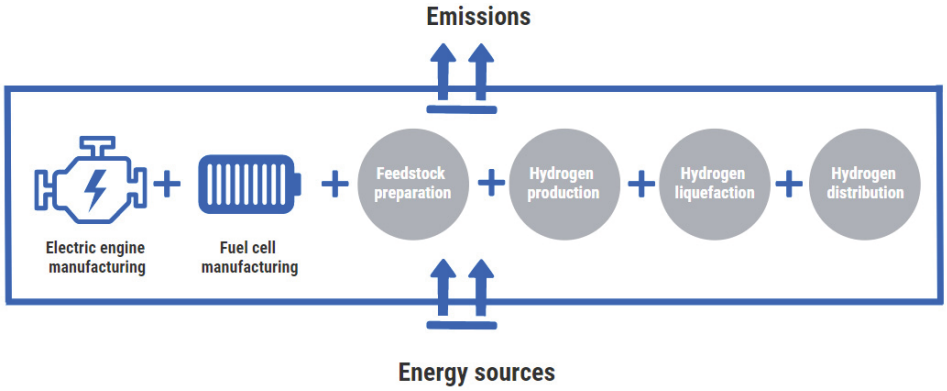

Figure 3. The processes included in the LCA of a hydrogen-powered ship.

While there are no tailpipe emissions released during the ship operation, the manufacturing processes of an electric engine and a fuel cell are considered. The environmental impact of an electric engine is calculated in the same way as for the diesel engine, while the environmental impact of a fuel cell is obtained by calculating the weight of materials used in the manufacturing process for the PEM fuel cell (**Garraín and Lechón, 2014**). It is assumed that the fuel cell is replaced once during the lifetime of 20 years.

2.2.3 The LCA of an electricity-powered ship

While there are different types of electrification of ships (**SPBES, 2021**), in this paper, the assessment is focused on the fully electrified ship with only a battery as a power source. The processes included in the environmental assessment of the fully electric ship are presented in **Figure 4**.

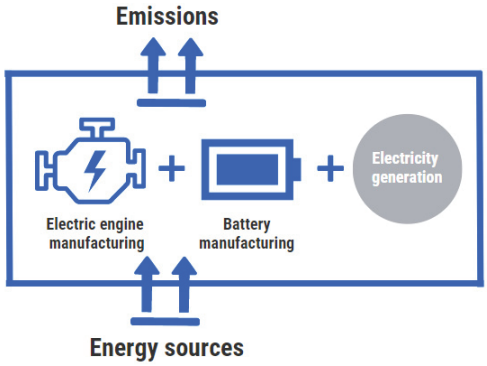

Figure 4. The processes included in the LCA of an electricity-powered ship.

The WTP phase refers to the production of electricity used for charging the battery. In this paper, the European mix from GREET 2020 database is used, which structure is presented in **Figure 5**.

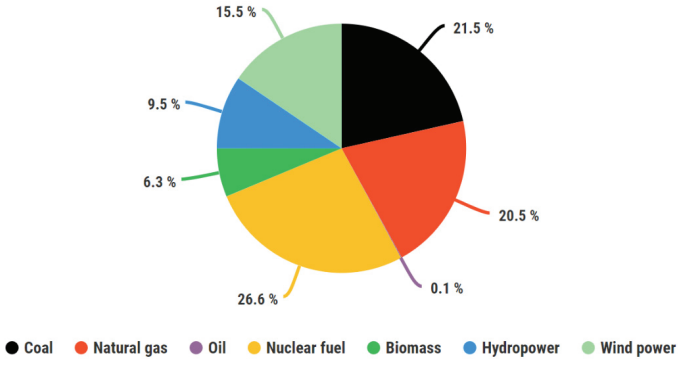

Figure 5. The European electricity mix.

The battery capacity (*BC*) needs to be sufficient enough to supply the ship during the return trip (Ship 1) or one-way trip (Ship 2). It is calculated based on the following equation:

$$BC = 1.5 \cdot EC \cdot l_{BC} \tag{5}$$

where l_{BC} refers to the route length during which the battery needs to supply the ship operation, while *EC* denotes energy consumption of a ship. The capacity is

increased by 50 % due to safety reasons, maintaining the state of charge and gradual degradation (**Pelletier *et al.*, 2017**).

While there are no tailpipe emissions released during the ship operation, the manufacturing processes of an electric engine and a battery are considered. The environmental impact of an electric engine is calculated in the same way as for the diesel engine, while the environmental impact of a battery is obtained by calculating its weight which represents the input parameter for the GREET 2020. Various types of battery can be used in a ship power system. In this paper, the focus is put on two batteries that are familiar and commercially available: Lithium-ion (Li-ion) battery and Nickel-metal hydride (Ni-MH) battery. The weight of a battery is calculated by dividing its capacity with energy density, which for the Li-ion battery is equal to 250 Wh/kg, while for the Ni-MH battery is 80 Wh/kg. The replacement of a battery is taken into account due to its life in cycles of charging and discharging, where for a Li-ion battery, the lifetime is equal to 9,000 cycles, while for Ni-MH, the lifetime is equal to 2,000 cycles (**Wu and Bucknall, 2016**).

3 RESULTS AND DISCUSSION

The results of the performed LCAa are presented in **Figure 6**, where D denotes a diesel-powered ship, H-grey and H-green refer to the power system powered by grey or green hydrogen, while E denotes electrification of a ship with a Li-ion battery (E-Li-ion) and Ni-MH battery (E-Ni-MH).

Hydrogen is usually referred to as a fuel for the green transition and reduction of GHGs. However, the considered ships fuelled with hydrogen produced from the natural gas (grey hydrogen) resulted in higher overall life-cycle CO_2-eq emissions of around 37 %, compared to the diesel power system configuration. Even though this is the zero-emission alternative solution for the ship power system and, therefore, there is the absence of tailpipe emissions in the PTW phase, the main contribution to the atmosphere pollution has the WTP phase. These emissions can be reduced by obtaining the hydrogen from RESs through the process of electrolysis. Moreover, such green hydrogen implemented in a ship power system resulted in around 91% lower CO_2-eq emissions compared to a diesel-powered ship. The green hydrogen represents the most environmentally friendly solution since each considered amount of life-cycle emission is lower than the currently used diesel power system.

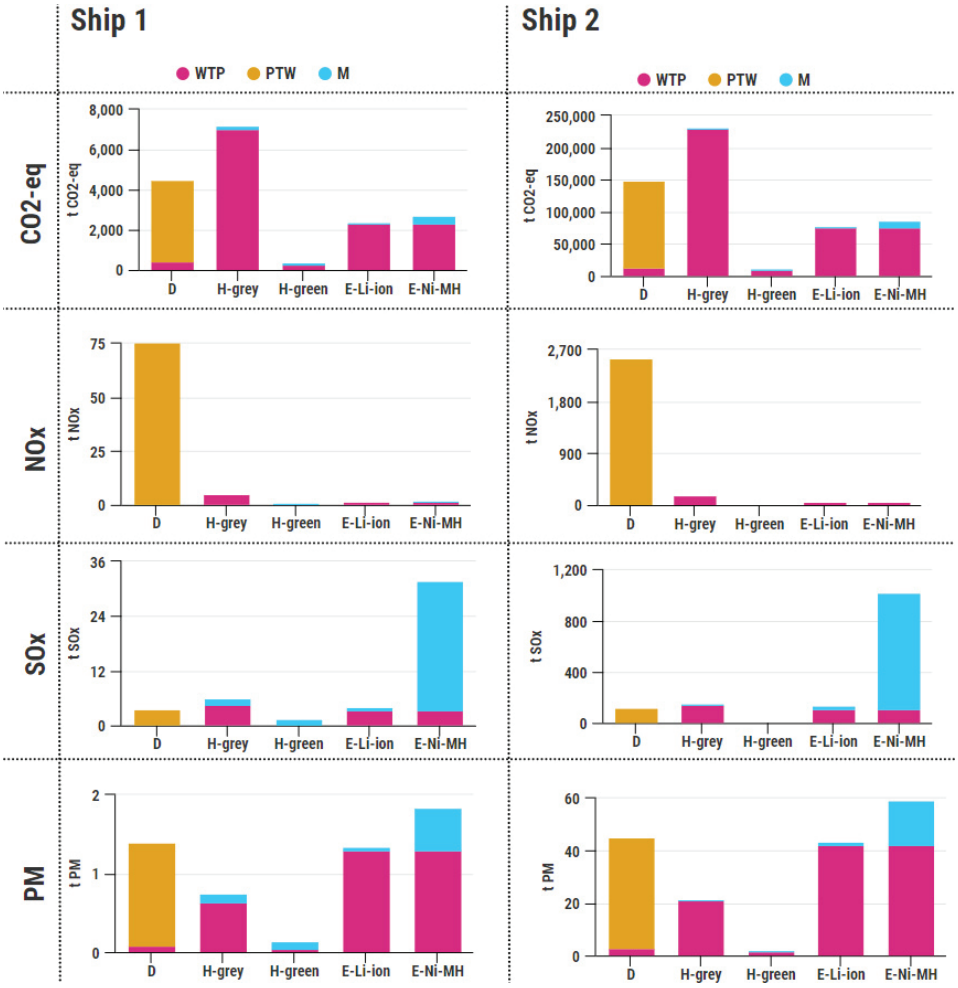

Figure 6. LCA comparison of different power system configurations.

The hydrogen supply chains, refuelling and storage infrastructures in ports and commercialization of fuel cell for ships remain the main obstacles for the greater use of such power system configuration in the shipping sector. When comparing the CO_2-eq emissions of the fully electrified ship with Li-ion battery with the diesel-powered ship, the emissions are lower by 47%, while when using the NI-MH battery, the life-cycle CO_2-eq emissions are around 40% lower. Therefore, both investigated electrification options with different batteries resulted in the reduced GHGs. However, when observing the SO_X and PM emissions, the electrification of ships resulted in higher emissions than they are released from

the diesel power system configuration. Among those electric options, the implementation of a Li-ion battery on board ship is the best solution from the environmental point of view, but also technical point of view since Li-ion battery has higher energy density than the Ni-MH battery, and for the same capacity, it can store more energy.

4 CONCLUSION

Although environmental strategies promote the implementation of zero-emission solutions into the ship power system, these options are not so ecological as they seem. In this paper, the comparison of diesel power system configuration with the hydrogen-powered ship and electricity-powered ship is performed.

The impact of fossil fuel combustion in a ship engine on human health is higher for the local population that live nearby ports. Therefore, the environmental assessments of the considered ship power systems implemented on two Croatian ferries that spend much time in ports and operate between populated settlements were performed.

The LCA highlighted a green hydrogen-powered ship as the most environmental friendly zero-emission solution, which results in the reduction of 91 % of CO_2-eq in comparison to the diesel-powered ship. The second most ecological zero-emission shipping solution regarding the GHGs is the electrification of a ship with a Li-ion battery, resulting in a reduction of 47 %. Although green hydrogen results in the lowest emissions, the electrification of ships with Li-ion battery is probable due to commercially available and familiar technology. At first, the electrification of ships operating near the shore can be fully electrified, but further development of metal-air battery technology opens the pathway towards electrification of ships engaged in international shipping.

Although this paper does not provide insight into the feasibility of a particular power system from an economical point of view, the economic analysis should be taken into the account upon the process of selecting the optimal power system configuration.

Acknowledgements

This research was supported by the Croatian Science Foundation under the project Green Modular Passenger Vessel for Mediterranean (GRiMM), (Project

No. UIP-2017-05-1253). Ivana Jovanović and Maja Perčić, Ph.D. students, are supported through the "Young researchers' career development project – training of doctoral students" of the Croatian Science Foundation.

REFERENCES

Bataille, C., Åhman, M., Neuhoff, K., Nilsson, L.J., Fischedick, M., Lechtenböhmer, S., Solano-Rodriquez, B., Denis-Ryan, A., Steiber, S., Waisman, H., Sartor, O., Rahbar, S. (2018) 'A review of technology and policy deep decarbonization pathway options for making energy-intensive industry production consistent with the Paris Agreement', *Journal of Cleaner Production*, 187, pp. 960–973. doi: 10.1016/j.jclepro.2018.03.107.

Bicer, Y. and Dincer, I. (2018) 'Clean fuel options with hydrogen for sea transportation: A life cycle approach', *International Journal of Hydrogen Energy*, 43(2), pp. 1179–1193. doi: 10.1016/j.ijhydene.2017.10.157.

Croatian Register of Shipping (CRS) (2020) *Web report of a ship*. Available at: http://report.crs.hr/hrbwebreports/Default.aspx (Accessed: 10 December 2020).

Dawood, F., Anda, M. and Shafiullah, G. M. (2020) 'Hydrogen production for energy: An overview', *International Journal of Hydrogen Energy*, 45(7), pp. 3847–3869. doi: 10.1016/j.ijhydene.2019.12.059.

Emission Standards: IMO Marine Engine Regulations (2020). Available at: https://dieselnet.com/standards/inter/imo.php#s (Accessed: 1 November 2020).

European Maritime Safety Agency (EMSA) (2017) *Study on the use of Fuel Cells in Shipping*.

Gagatsi, E., Estrup, T., Halatsis, A. (2016) 'Exploring the Potentials of Electrical Waterborne Transport in Europe: The E-ferry Concept', in *Transportation Research Procedia*. Elsevier B.V., pp. 1571–1580. doi: 10.1016/j.trpro.2016.05.122.

Garraín, D. and Lechón, Y. (2014) 'Exploratory environmental impact assessment of the manufacturing and disposal stages of a new PEM fuel cell', *International Journal of Hydrogen Energy*, 39(4), pp. 1769–1774. doi: 10.1016/j.ijhydene.2013.11.095.

International Maritime Organization (2020) *Fourth IMO GHG Study Executive Summary*.

International Maritime Organization (IMO) (2011) *Resolution MEPC. 203(62)*.

International Maritime Organization (IMO) (2014) *Third IMO Greenhouse Gas Study 2014*.

International Organization for Standardization (ISO) (2006) *ISO 14040*. Available at: https://www.iso.org/standard/37456.html (Accessed: 12 December 2020).

Jadrolinija (2020) *Ferry lines schedule*. Available at: https://www.jadrolinija.hr/red-plovidbe/lokalne-linije-2020- (Accessed: 10 December 2020).

Jeong, B., Wang, H., Oguz, E., Zhou, P. (2018) 'An effective framework for life cycle and cost assessment for marine vessels aiming to select optimal propulsion systems', *Journal of Cleaner Production*, 187, pp. 111–130. doi: 10.1016/j.jclepro.2018.03.184.

Kim, T. and Chae, C. (2016) 'Environmental Impact Analysis of Acidification and Eutrophication Due to Emissions from the Production of Concrete', *Sustainability*, 8(6), p. 578. doi: 10.3390/su8060578.

Monteiro, A., Russo, M., Gama, C., Borrego, C. (2018) 'How important are maritime emissions for the air quality: At European and national scale', *Environmental Pollution*, 242, pp. 565–575. doi: 10.1016/j.envpol.2018.07.011.

Pelletier, S., Jabali, O., Laporte, G., Veneroni, M. (2017) 'Battery degradation and behaviour for electric vehicles: Review and numerical analyses of several models', *Transportation Research Part B: Methodological*, 103, pp. 158–187. doi: 10.1016/j.trb.2017.01.020.

Perčić, M., Ančić, I., Vladimir, N. (2020a) 'Life-cycle cost assessments of different power system configurations to reduce the carbon footprint in the Croatian short-sea shipping sector', *Renewable and Sustainable Energy Reviews*, 131, p. 110028. doi: 10.1016/j.rser.2020.110028.

Perčić, M., Vladimir, N., Fan, A. (2020b) 'Life-cycle cost assessment of alternative marine fuels to reduce the carbon footprint in short-sea shipping: A case study of Croatia', *Applied Energy*, 279, p. 115848. doi: 10.1016/j.apenergy.2020.115848.

Sterling PlanB Energy Solutions (SPBES) (2021) *Electrification of ships*. Available at: https://spbes.com/ (Accessed: 13 January 2021).

Toscano, D. and Murena, F. (2019) 'Atmospheric ship emissions in ports: A review. Correlation with data of ship traffic', *Atmospheric Environment: X*. Elsevier Ltd, p. 100050. doi: 10.1016/j.aeaoa.2019.100050.

Understanding Global Warming Potentials | Greenhouse Gas (GHG) Emissions | US EPA (2021). Available at: https://www.epa.gov/ghgemissions/understanding-global-warming-potentials (Accessed: 8 February 2021).

United Nations Framework Convention Climate Change (UNFCCC) (2021) *Climate Change Information kit*. Available at: https://unfccc.int/resource/iuckit/cckit2001en.pdf (Accessed: 14 January 2021).

van Biert, L., Godjevac, M., Visser, K., Aravind, P.V. (2016) 'A review of fuel cell systems for maritime applications', *Journal of Power Sources*, 327, pp. 345–364. doi: 10.1016/j.jpowsour.2016.07.007.

Wu, P. and Bucknall, R. (2016) 'Marine propulsion using battery power', in *Shipping in Changing Climates Conference 2016*, pp. 1–10.

APPLICATION OF NAVIGATIONAL SIMULATOR IN PORT PLANNING TO DETERMINE VESSEL MOVEMENT IN WORST CASE SCENARIO EMERGENCY BERTH LEAVING

Mate Baric[1*], Djani Mohovic[2], Robert Mohovic[2], Renato Ivce[2]

Abstract. *This paper demonstrates usage of navigational simulator for risk assessment in mooring project of Ploče oil and gas terminal in Croatia. The important part of project was simulation of leaving the berth in emergency situation and determining is there enough sea area with adequate depth to perform such manoeuvre. Analysed emergency situations imply the condition of the vessel or the terminal which demands leaving the berth to prevent or to reduce damage. For the vessel of this kind that situation demands letting go all the mooring ropes and using own engine to leave the terminal. This kind of situation may occur at all times and in any weather condition. In order to properly test the safety of the terminal this simulation has been done for the worst-case scenario when the weather conditions are in its extremes. The result was vessel trajectory which was compared with project sea area configuration to determine the possibility of vessel grounding.*

Key words: *navigational simulator; emergency manoeuvre; risk assessment*

[1] Maritime department (University of Zadar, Zadar, Croatia)
[2] Faculty of Maritime Studies (University of Rijeka, Rijeka, Croatia)
[*] Corresponding author: Mate Baric (mbaric@unizd.hr)

University of Zadar

1 INTRODUCTION

Determining safe port areas for ship manoeuvring is a complex process which beside required area needs risk assessment. Risk assessment can be done qualitatively defining risk without any numerical certainty or quantitatively using data do define numerical probability of event and consequently event consequences. One of the best ways to conduct such risk assessment is by using Navigation simulators. Navigational simulators provide real life ship movement and effect of environmental data on vessel movement. Vessel movement and trajectory of that movement is then used in risk assessment process.

Ship simulators system have been developed to effectively evaluate and optimize the horizontal design of a navigational channel or harbour basin (**McBride *et al.*, 2014**). To minimize any risk of error at the stage of designing, the most advanced technologies, also the research and designing methods should be applied. An example for using simulator for creation navigational infrastructure is the design of the Vistula Spit Cross-out (**Czaplewski *et al.*, 2011**). Beside waterway design, navigational simulator can be used to determine ship movement after adverse event. Authors (**Mohovic *et al.*, 2013**) used the navigational simulator to determine ship movement and worst-case scenario of grounding after steering failure. Some ports use simulators to determine if certain ship can dock, such as port of Koper used detailed case study on simulators to determine admission of post-Panamax container ships (**Twrdy *et al.*, 2013**). The work of authors (**Vidmar *et al.*, 2020**). present usage of simulators for port policy making and risk analysis. The usage of navigational simulators is highly applicable when the effectiveness of safety improvements planning of port and harbour facilities must be assessed (**Perkovic *et al.*, 2016**).

This paper analyses the planned terminal design and determines ship movement in worst case scenario when tugs are not available and vessel must leave terminal in emergency situation. Such movement is then used in risk assessment.

2 PREPARATION OF PROJECT AREA AND VESSELS

Preparing this kind of simulations requires detailed area data. Basic area data was provided through navigational chart and detailed terminal plan was obtained through AutoCAD files of project area. Simulator used in this project was Transas NTPro 5000, version 5.35, and for preparing and modelling area software Transas Model Wizard which allows creation of new simulation areas or modifying

existing areas. In process of determining safety factors of navigation areas and ports, this analysis allows high accuracy and reliability of data, in order to cut costs and increase safety of navigation.

The most important part was determining the size of dredged area around the terminal at nominal depth of 16.5 meters (**Figure 1**). The size of dredged area was determined by port authorities based on vessel size, planned terminal operations and required area for tugs operations. That area was determined keeping in mind that the width of the largest planned vessel is 37 meters and minimum required tugs operation area depth is 5 meters.

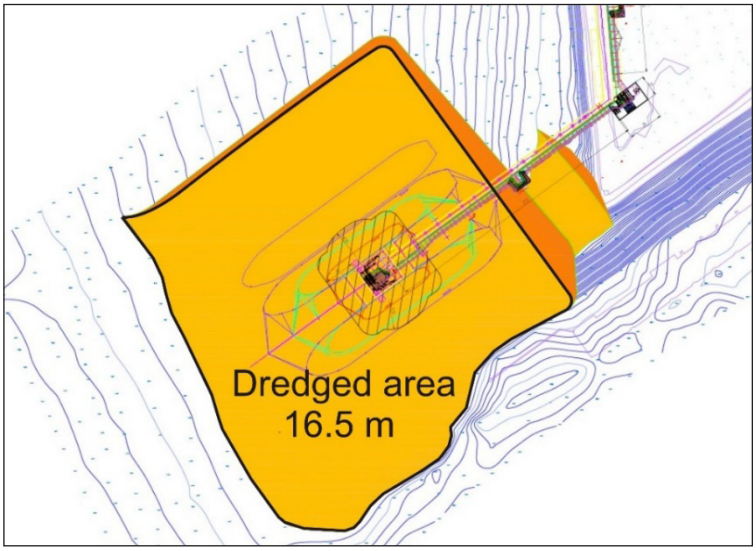

Figure 1. Dredged area around terminal (AutoCAD file).

Comparing present depth from navigational chart with planned depth of project area shows that dredging is required at whole planned area. Planned area is 295 meters wide, northwest part has 165 meters and southeast part 130 meters, measured from terminal (**Figure 2**).

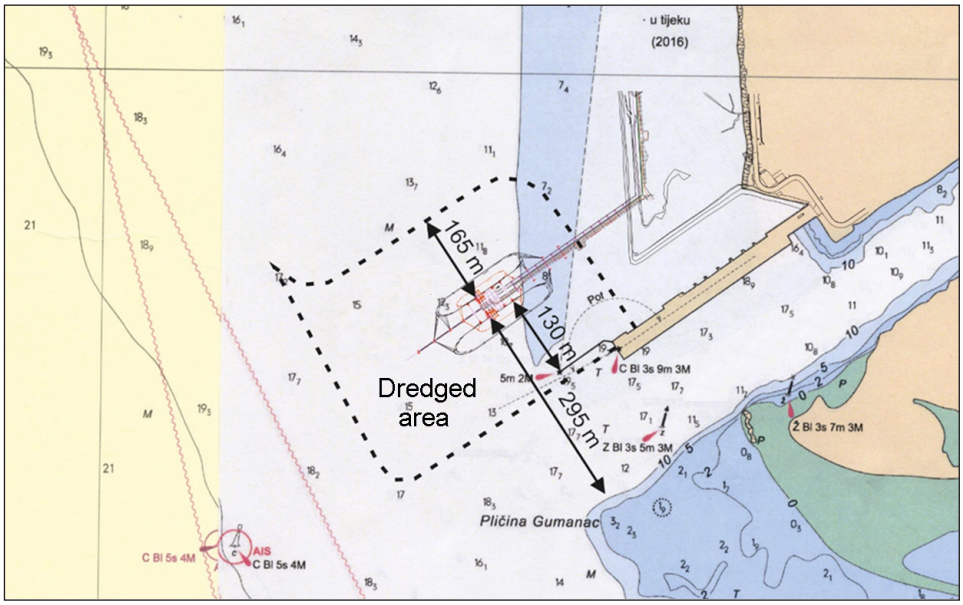

Figure 2. Dimensions of dredged area.

Analysed oil and gas terminal is planned for vessel in range from 90 meters to 230 meters in length. In order to maintain results reliability in simulation are used vessels models which are same or close to planned vessel size, both in loaded and ballast condition. Also, beside size, during initial simulations, vessel models were tested to confirm reliability, like manoeuvrability, unusual responses (to big heel angle, poor engine response, etc.), and according to that test particular vessel models were used. Chosen vessels models are: smaller vessel model with LOA=110 meters, midsize vessel model with LOA=163 meters, and larger size vessel model with LOA=228 meters.

Detailed data of selected vessel model, which are similar to project vessels, are presented in **Table 1**.

Table 1. Selected vessel models data.

Smaller loaded oil tanker	
Length over all (LOA) (m)	110
Breadth (m)	16.1
Draught (m)	6.74
Displacement (t)	6500
Engine power (kW)	2405
Midsize loaded chemical/oil tanker	
Length over all (LOA) (m)	163
Breadth (m)	23.7
Draught (m)	10.1
Displacement (t)	30300
Engine power (kW)	6500
Larger loaded oil tanker	
Length over all (LOA) (m)	228
Breadth (m)	32.2
Draught (m)	13.6
Displacement (t)	82100
Engine power (kW)	9847
Larger oil tanker in ballast condition	
Length over all (LOA) (m)	228
Breadth (m)	32.2
Draught (m)	7.26
Displacement (t)	41900
Engine power (kW)	9847
Midsize loaded LPG tanker	
Length over all (LOA) (m)	183
Breadth (m)	22.6
Draught (m)	10.4
Displacement (t)	33100
Engine power (kW)	8827

3 SIMULATIONS SETTINGS

In simulations worst case weather conditions were used which are acting perpendicular on vessel centerline. Considering terminal orientation, external forces of wind, waves and currents from direction NW and SE are perpendicular on ship centerline. At project site largest external forces are recorded from direction SE, so the vessel berthed at NW side of terminal was chosen as the worst-case scenario.

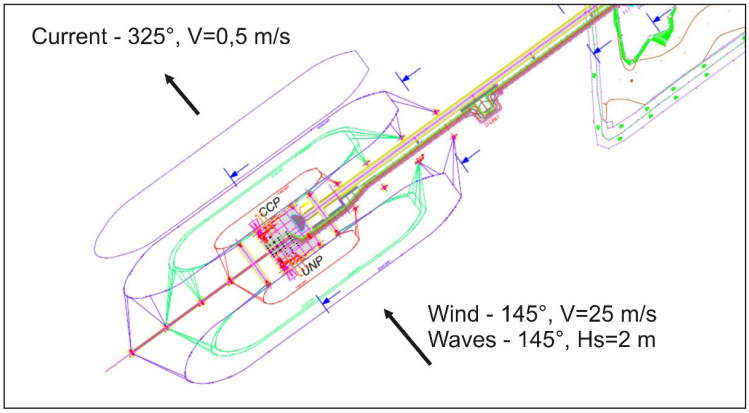

Figure 3. Direction of forces acting on the vessel.

Following external forces (environmental conditions) were used in simulations (**Figure 3**):

- Wind:
  - perpendicular on ship centerline (direction 145°)
  - wind speed 25 m/s (49 knots) based on 50 years return period
  - due to vessel response period, wind starts acting 20 seconds after starting simulation for the vessels smaller than 200m LOA and 30 seconds after starting simulation for vessels larger than 200 meters.
- Waves:
  - perpendicular on ship centerline (direction 145°)
  - waves significant height 2 meters
- Current:
  - perpendicular on ship centerline (direction 325°)
  - current speed 0.5 m/s (1 knot).

Simulations were divided into two groups, simulation without using tug and simulation using tug. At the site in emergency situation there is only one stand by tug with 300 kN bollard pull. In simulations tug with same characteristics was used, which was acting on ship perpendicular at the side opposite to external forces in order to reduce drift.

4 SIMULATIONS RESULTS

Simulations were conducted in full mission Transas simulator with three experts. One was at the instructor position setting up external conditions, while other two were at the navigating bridge manoeuvring the vessel. The manoeuvring consisted of setting the engine to full ahead and controlling the vessel heading using rudder.

Simulations without using tug started at the moment of letting go all of the mooring ropes, setting the engine to full ahead and during the simulation ship heading was controlled and drift recorded. The **Figure 4** represents the drift of smaller oil tanker where the darker colour shows the depth of 16.5 meters.

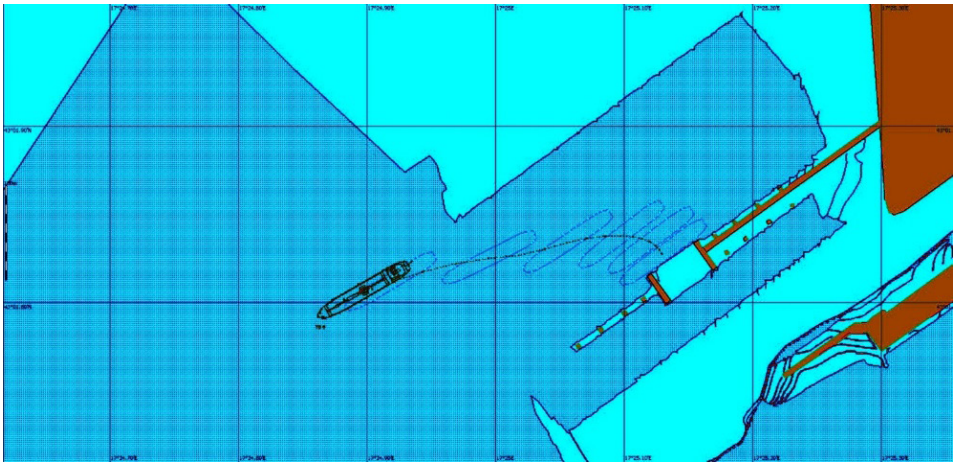

Figure 4. Drift of loaded smaller oil tanker LOA=110 m leaving the berth in emergency without tug; external forces acting perpendicular on ship centerline.

Irrespective of that smaller vessel don't have large lateral underwater and windage area significant drift was recorded. However due to larger UKC (Under Keel Clearance) there is no danger of grounding.

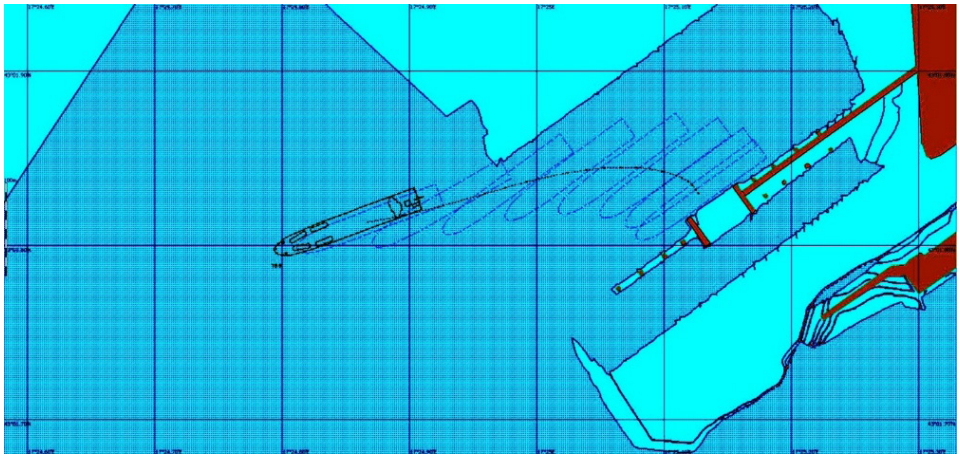

Figure 5. Drift of loaded midsize chemical/oil tanker LOA=163 m leaving the berth in emergency without tug; external forces acting perpendicular on ship centerline.

Model of midsize chemical/oil tanker at loaded condition (**Figure 5**) has significant drift due to slow acceleration which can be ascribed to unfavourable engine power – displacement ratio. However, even in this case this vessel has maximum draft of 10 meters and it was concluded that there is no danger of grounding.

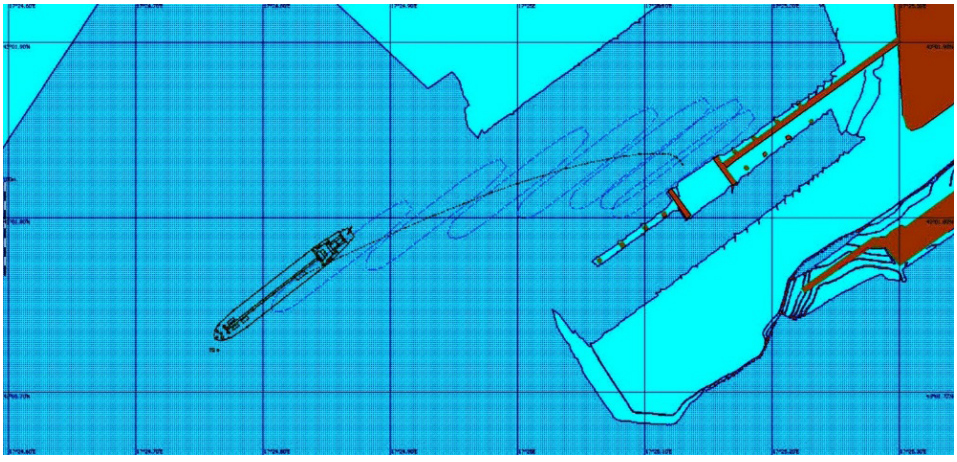

Figure 6. Drift of loaded midsize LPG tanker LOA=183 m leaving the berth in emergency without tug; external forces acting perpendicular on ship centerline.

LPG tankers have a bit larger lateral windage area and smaller draft and underwater area than similar sized oil tankers (**Figure 6**). Loaded midsize LPG tanker vessel model recorded smaller drift than similar oil tanker. However, due to ship draft of 10.7 meters it was concluded that there is no danger of grounding.

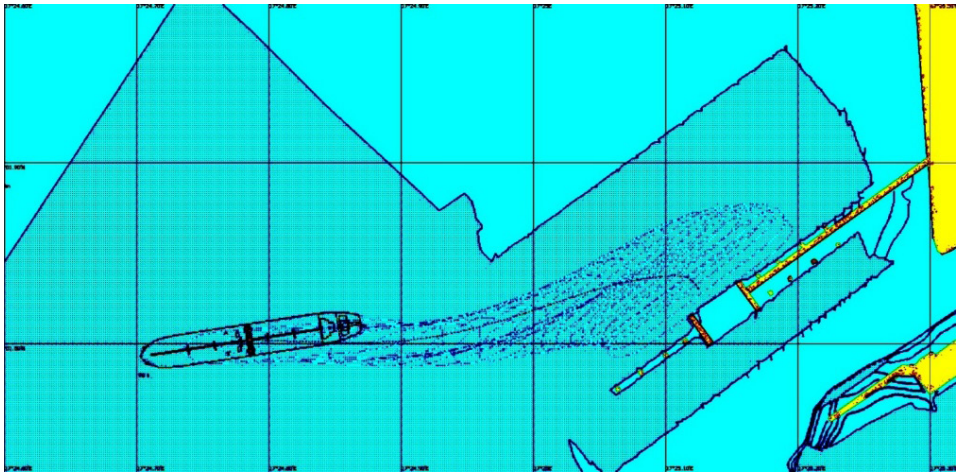

Figure 7. Drift of loaded larger oil tanker LOA=228 m leaving the berth in emergency without tug; external forces acting perpendicular on ship centerline.

Larger oil tankers (**Figure 7**) represent the biggest vessel at planed oil terminal and at full load condition represent the biggest danger of grounding during emergency berth leaving. Due to large displacement this vessel accelerates slowly. However, it has the largest response period on external forces. During these simulations the ship came close to the limit of dredged area and in order to avoid grounding helm was put hard to starboard.

In ballast conditions this type of vessel has larger lateral windage area which causes significant drift compared to fully loaded vessel (**Figures 8** and **9**). However, in ballast condition due to smaller displacement acceleration is better. Also, in this case helm was ordered hard to starboard. If we compare this vessel at different condition the drift is larger in ballast condition. But draft in ballast condition is approximately 8 to 10 meters, so there is less chance of grounding.

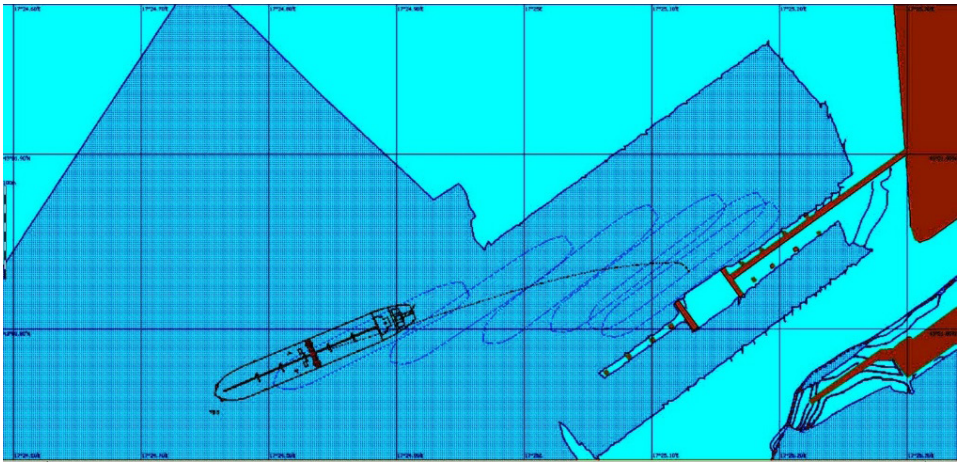

Figure 8. Drift of larger oil tanker LOA=228 m in ballast condition leaving the berth in emergency without tug; external forces acting perpendicular on ship centerline.

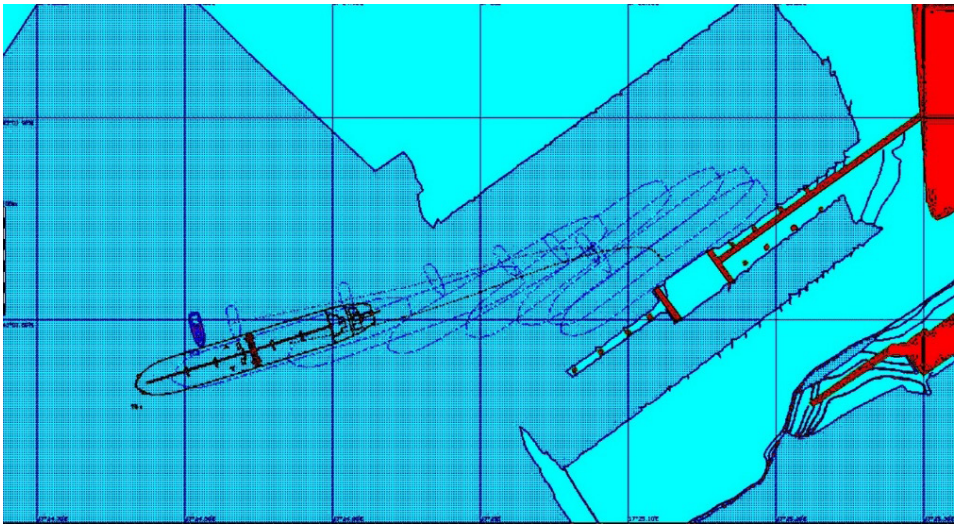

Figure 9. Drift of loaded larger oil tanker LOA=228 m leaving the berth in emergency with tug; external forces acting perpendicular on ship centerline.

Conclusion of all simulations without tug is that the greatest danger of grounding is for loaded larger oil tanker. However, in that case it is possible to use stand by tug. The tug was pushing the vessel away of danger area against external forces with maximum power of 300 kN. The result is significantly smaller drift in comparison with the simulation without using tugs. The limitation of the

terminal is only one available standby tug which in case of poor reaction due to human error may lead to grounding. Also, more available tugs are required to use the berth at southeast terminal side at similar weather conditions.

Using the simulation results, the risk assessment table is prepared (**Table 2**).

Table 2. Grounding risk assessment using the simulation results.

	With tug	Without tug
Smaller loaded oil tanker	Low risk	Low risk
Medium loaded chem/oil tanker	Low risk	Medium risk
Larger loaded oil tanker	Medium risk	Medium risk
Larger oil tanker in ballast	Low risk	Low risk
Midsize loaded LPG tanker	Low risk	Low risk

The input of the data are vessel dimensions and tug requirements. The risk is determined by input data of probability of grounding and the consequences of grounding. For all vessels the consequences of grounding are medium to high impact on environment, lives of personnel and property due to cargo properties. However, the probability of grounding is determined with conducted simulations. Only larger loaded oil tanker, due to its draft, can be in extreme cases of human error grounded outside of dredged area. Using that methodology in **Table 2** are the risks of grounding in simulated weather conditions when vessel leaves berth in emergency, with or without tug assistance.

5 CONCLUSION

Based on all performed simulations it can be concluded that in worst case scenario there is significant drift during emergency berth leaving and it doesn't differ between smaller and bigger vessels. However, smaller vessels due to larger under keel clearance and available sea area have less chance of grounding than bigger vessels.

The proposed dredged area provides for the larger vessels with bigger draught enough sea area and depth to safely leave the berth at emergency situations without danger of going aground. However, at all times at the terminal stand by tug is available, so for all vessels with draught over 12 meters is recommended to use it during emergency berth leaving.

In terms of risk assessment current situation shows that the probability of grounding is very small to medium and even in worst case scenario grounding is unlikely. Such probability combined with the consequence provides good input for risk assessment.

REFERENCES

Czaplewski, K., & Zwolan, P. (2011). Using the software of Navi-Trainer PRO 5000 simulator for assessment of the designed navigational infrastructure. *Annual of Navigation*.

McBride, M., Boll, M., Briggs, M. (2014). Harbour approach channels—Design guidelines. *PIANC Report No. 121*.

Mohović, Đ., Mohović, R., Rudan, I. (2013). Simulation of ship movement after steering system failure to determine the worst case scenario of grounding. *Promet-Traffic & Transportation*, *25*(5), 457–456.

Perkovic, M., Brcko, T., Luin, B., Vidmar, P. (2016). Ship handling challenges when vessels are outgrowing ports. *Proceedings of the IMLA-INSLC*, *19*.

Twrdy, E., Petrovic, M., Batista, M. (2013). Limitation and Restrictions on the Admission of Postpanamax Container Ships in the Port of Koper. *Brodogradnja: Teorija i praksa brodogradnje i pomorske tehnike*, *64*(4), 456–471.

Vidmar, P., Perkovic, M., Gucma, L., Łazuga, K. (2020). Risk Assessment of Moored and Passing Ships. *Applied Sciences*, *10*(19), 6825.

INSIGHT ON THE OFFICER'S WORKLOAD MEASUREMENT IN THE FULL MISSION SIMULATOR DURING COLLISION AVOIDANCE

Dejan Žagar*, Franc Dimc

Abstract. *This paper presents a concept to measure the workload in the full mission simulator during the collision avoidance maneuver based on the biometric data of the officer on watch (OOW). The disturbing factor causes the high workload leading to potentially dangerous human error actions (HEA), which cause a significant number of accidents in the merchant marine despite modern navigation aids on the ship's bridge. HEA, triggered by high cognitive load on the OOW due to unexpected confounding factors, results in a lack of reaction time for safe navigation. Accessing the workload of the OOW with biometric sensor data is difficult due to various reasons such as the environmental conditions in the simulator, the type of task simulated, the type of sensor used, etc. Considering the available literature, an experimental design is proposed for measuring the workload of the OOW during the simulated navigation task.*

Key words: *workload; human factor; human erroneous action; marine simulator; disturbing factor; heart-rate sensor*

University of Ljubljana, Faculty of Maritime Studies and Transport
* Corresponding author: Dejan Žagar (dejan.zagar@fpp.uni-lj.si)

University of Zadar

1 INTRODUCTION

High workload negatively affects Officer On Watch (OOW) cognitive processes, i.e., recognizing information, prioritizing it, and making decisions to avoid collisions. Overload leads to human erroneous action (HEA). According to EMSA, it is the cause of 71 % of all accidents at sea (**EMSA, 2019**). To assess the workload of OOWs during experimental simulations, direct and indirect approaches are used to observe and record the biometric parameters of OOWs, which are later used for post-processing and modeling. Typical observables in the available literature (**Miklody *et al.*, 2017**; **Main, Wolkow and Chambers, 2017**; **Liu *et al.*, 2017**; **Di Nocera *et al.*, 2016**; **Maglić and Zec, 2019**; **Hareide and Ostnes, 2017**; **Kim, Kim and Hong, 2010**; **Barnett, 2005**) include pupil diameter, heart rate, post hoc questionnaire, stress hormone levels, and brain wave intensity. Processing data from invasive sensors is challenging because wearing the sensors negatively affects the biometric parameters in the control phase of the experiment, causing noise, artefacts, and false readings. Machine learning algorithms based on neural networks are usually used for such recordings. During the machine learning phase, you can detect noise.

In this paper, after careful study of the available literature, we devote more attention to indirect approaches and non-invasive types of sensors that are less disruptive to participants. The advantage of using biometric data with less noise is to understand and improve the accuracy of workload assessment of OOWs outside the simulator, where conditions are not as controlled as in the lab-like spaces. A transfer function from biometric data recorded during the experimental task in the simulator to information about the workload of OOWs is performed by the statistical tools (e.g., analysis of variance, regression analysis, etc.) that have recently been supported by machine learning algorithms in the research community.

2 BACKGROUND

As mentioned above, the basic experimental designs usually propose a direct or indirect approach to workload assessment. In the maritime domain, despite the highest technical and financial effort, the direct approach is associated with experimental challenges that lead to noise in the results (**Miklody *et al.*, 2017**; **Main, Wolkow and Chambers, 2017**; **Liu *et al.*, 2017**). The advantage of the indirect approach in the marine simulators lies in the less disruptive methods

and, more recently, wireless sensors to capture the biometric observables of the OOW. This allows participants to move freely port and starboard on the simulated ship's bridge, adding to the reality of the scenario. From this point of view, the carefully designed experimental design consists of a control part in which the biometric data of the participants are collected under normal, typical conditions. In the experimental part, participants are confronted with confounding factors such as bad weather conditions and various nautical or engine alarms, or with the solution of additional tasks (**Di Nocera *et al.*, 2016**; **Maglić and Zec, 2019**; **Hareide and Ostnes, 2017**), in order to increase the cognitive load of OOWs' working memory. The decision-making process of OOWs under increased cognitive load typically reflects an increase in reaction time, which can be measured in the data processing phase and evaluated with statistical significance (**Kim, Kim and Hong, 2010**). According to the available literature, excited biometric observables and reaction time prolongation are standard parameters in the workload assessment algorithm. The standard experimental design usually consists of two parts, as shown in **Figure 1**.

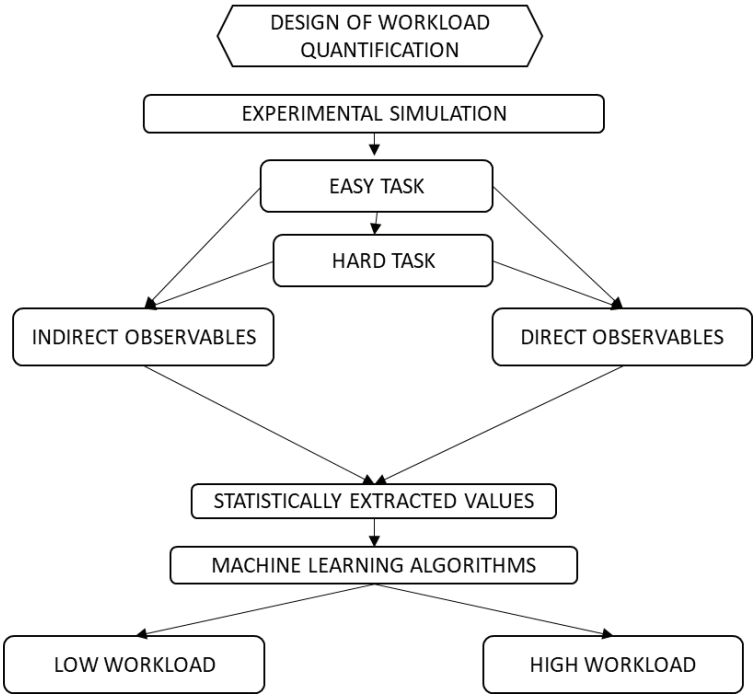

Figure 1. Typical experimental design of workload assessment.

In the control part (easy task), biometric observables are recorded under typical, normal sailing conditions expected in a particular part of the geographical region where the voyage is simulated. The second part of the simulation is the experimental task, during which the disturbing factor is added (hard task) that significantly excites the observables. Post-processing of the data compares the recordings from the experimental phase with those from the control phase, from which the state of the workload of the OOWs is statistically extracted. Statistical tools for data processing are t-test, analysis of variance, support vector method, regression analysis, etc. After statistically extracting the mean values of the participants, the state of workload is defined as low workload or high workload. The literature also mentions a state of excessive workload, where the recorded readings exceed the individually calibrated limits. The behaviour of the OOW at this stage is irrational due to the overload of its working memory and results in a large number of errors, commonly referred to as human erroneous actions (HEA), leading to accident in the worst case (**Barnett, 2005**). The erroneous actions of OOWs also affect substances, e.g., alcohol (**Kim *et al.*, 2007**) and personality (**Orlandi and Brooks, 2018**).

3 METHODOLOGY, RESOURCES AND EXPERIMENTAL PROPOSAL

The scenario used to evaluate the workload of the OOWs compares the assumed standard (normal) navigation and the experimental scenario with introduction of disturbing factors. The biometric observables such as eye tracking and heart rate (HR) are used as parameters for indirect assessment of the workload of the OOWs. This method has been validated and is commonly used in other transport domains, e.g. road transport (**Fridman *et al.***, **Stojmenova and Sodnik, 2018**), where participants typically navigate in a car seat or cockpit. In the maritime domain, similar methods can be used if the technology allows wearable and wireless sensors, e.g. wristbands, chest straps or finger sensors. An advantage of using a full-mission nautical simulator instead of the ship's bridge is safety during the execution of the collision avoidance scenario, even when exposed to disturbing factors such as strong sunlight, high ambient temperature, or disturbing information from social media that can potentially affect biometric readings and consequently workload.

Based on a careful study of the available literature, a case study is proposed. The experiment aims to develop a functional design for HR measuring OOW during

navigation based on the wristband sensor. Five captains volunteered to participate. They were on average 48 years old and had 20 years of navigation experience. The tasks were divided according to their complexity and the workload required. Compared to simpler 'easy' task (control phase), the complex task (experimental phase) consists of avoiding collisions in the traffic separation zone, including the disturbance factor. Participants wear an Empatica E4 multisensor wristband to monitor HR (**Empatica, 2021**). The control phase allows the participant to adapt to the environment and voyage parameters. Adaptation is followed by the experimental phase, which includes disturbances such as fire alarms, severe weather conditions, navigation alarms, etc. The raw data from the sensors are stored on the smartphone in the participant's pocket via Bluetooth, allowing the participant to move freely in the area of the Transas 5000 bridge simulator. In the post-processing phase, the observation values are statistically extracted and the response of the OOWs to the disturbance is evaluated. The result of the evaluation model, e.g., a low HR response or a high HR response, reflects the OOW's cognitive process during a given task (**Haberlandt, 1997**). The results are validated with a post-hoc questionnaire in which participants describe the actual workload during the task.

4 RESEARCH RESULTS

The Empatica wrist sensor consists of several biometric sensors, such as blood volume pulse, electro-dermal activity, body temperature, wrist accelerometer, inter-beat interval, and heart rate. For the present study, we take HR as the primary observable to assess body excitement due to the presence of a simulated disturbance factor. The unwanted disturbance factor was expected during the simulated task due to the wearable equipment and measurement design, but in the post hoc interviews, participants indicated that they forgot they were wearing the sensor a few minutes after the experiment began. The simulated disturbance factor was the sound of the fire alarm with its typical red rotating light. Participants' self-assessment showed that the alarm evoked a stress response that influenced cognitive load during collision avoidance. The average HR rate of participants in the challenging phase was significantly higher than that of participants in the control phase, indicating saturation of high cognitive processes in the brain. However, analysis of individual biometric responses reveals that participants differ in the levels of response captured by the biometric data. The differences correspond to the participants' level of experience in their occupation.

We hypothesise that the biometric response is related to the participant's personality and real-world experience (**Orlandi and Brooks, 2018**). The distance between the upper and lower quartiles represents the interquartile range. The boxplot visualization in Figure 2 shows the 1st (25%) quartile, the median of the sample, the 3rd (75%) quartile, and the maximum line.

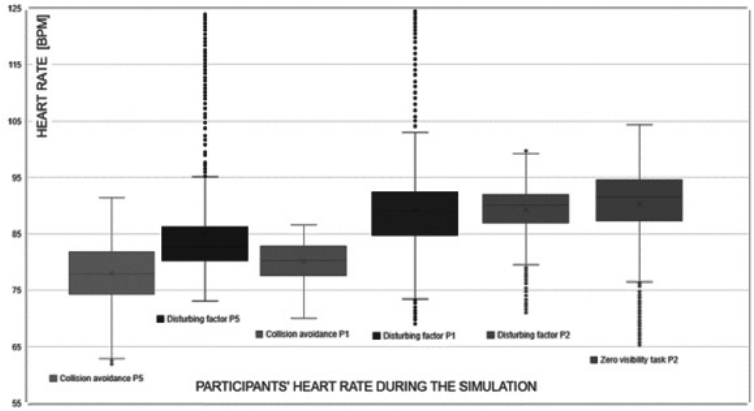

Figure 2. The wrist-band HR measuring design provides non-disturbance and low noise data recording. The processed results show higher HR during cognitive-demanding phase.

The dots below the minimum and above the maximum represent the outliers. The observation of HR rate shows the HR response of a participant during the collision avoidance task (CA), with a median of 79 BPM, which we assume to be a typical condition. During the simulation of the disturbance factor on the scene (experimental phase), the HR median increases to 84 BPM compared to the CA task. For tasks without visibility, the safety of navigation depends only on the user's skill in using navigation devices, and the median increases to 92 BPM.

5 DISCUSSION

The group of participants is homogeneous in terms of age, maritime experience, and personality characteristics. Therefore, the biometric response among the participants is comparable and to some extent expected. Nevertheless, the deeper interpretation of the results is challenging due to the small number of participants (N=5). Compared to typical navigation, the HR shows higher scores due to disturbance factors, indicating a dense cognitive process in working memory. An

interesting observation is the occurrence of the extreme outliers in the participants who experienced the actual fire on board, indicating the post-traumatic response of the participants. The assumption that the zero-visibility task elicits the highest saturation of working memory has not yet been confirmed. The measurement design proved to be appropriate and largely free of interference, which is promising for further research.

6 CONCLUSION

High cognitive load due to disturbing factors that contribute to human error. Available studies of officer workload while manoeuvring ships typically use a variety of biometric sensors. After data processing, low or high workload is determined. Modern technology allows wearable, wireless, low-disturbance biometrical sensors, such as wrist-band heart rate sensors. We intend to use excerpts from the present HR measurement design for the full-scale experiment based on the indirect approach to measure biometric response during collision avoidance in the full-mission simulator. An expected challenge could be the diversity of biometric readings of the participants due to personality traits. The goal is to model the algorithm that detects the high workload condition based on the biometric parameters. We expect that the results will reflect the actual workload of the OOW during the voyage. The next step will be to adapt the model so that it can be used outside the controlled conditions in the laboratory.

REFERENCES

Barnett, M. L. (2005). *Searching for the Root Causes of the Maritime Casualties*, WMU Journal of Maritime Affairs, 2005, pp. 131–145.

Di Nocera, F. *et al.* (2016). *Mental workload assessment using eye-tracking glasses in a simulated maritime scenario*, HFESE-proceedings, pp. 235–248.

Empatica E4 sensor, Available on https://www.empatica.com/research/e4/.

EMSA report (2019). *Annual overview and accident investigation report 2019*, http://www.emsa.europa.eu/emsa-documents/latest/item/3734-annual-overview-of-marine-casualties-and-incidents-2019.html published nov. 2019.

Fridman, L.; Reimer, B.; Mehler, B.; Freeman, W.T. Cognitive Load Estimation in the Wild (2018). In Proceedings of the 2018 CHI Conference on Human Factors in Computing Systems, Montreal, CQ, Canada, 21–26 April 2018; p. 652.

Haberlandt K. (1997). *Cognitive Psychology*. Washington: APA.

Hareide, O. S. and Ostnes, R. (2017). *Maritime Usability Study by Analysing Eye Tracking Data*, Journal of Navigation, 2017, pp. 927–943.

Kim, H. and Kim, H.J. and Hong, S. (2010). *Collision Scenario-based Cognitive Performance Assessment for Marine Officers*, TransNav, the International Journal on Marine Navigation and Safety of Sea Transportation, 2010, pp. 73–77.

Kim, H.; Yang, C.S.; Lee, B.W.; Young, Y.H.; Hong, S.K. Alcohol effects on navigational ability using ship handling simulator. Int. J. Ind. Ergon. 2007, 37, pp. 733–743.

Liu, Y.; Lim, W.L.; Subramaniam, S.C.H.; Liew, S.H.P.; Krishnan GSourina, O.; Konovessis, D.; Ang, H.E.; Wang, L. EEG-based Mental Workload and Stress Recognition of Crew Members in Maritime Virtual Simulator: A Case Study. In Proceedings of the International Conference on Cyberworlds (CW), Chester, UK, 20–22 September 2017.

Maglić L., Zec, D. (2019). *The Impact of Bridge Alerts on Navigating Officers*, Journal of Navigation, 2019.

Main, L. C. & Wolkow, A. & Chambers, T. P. (2017). *Quantifying the Physiological Stress Response to Simulated Maritime Pilotage Tasks: The Influence of Task Complexity and Pilot Experience*, Journal of Occupational and Environmental Medicine, 2017.

Miklody, D. & Uitterhoeve, W. M. & van Heel, D. & Klinkenberg, K. & Blankertz, B. (2017). *Maritime Cognitive Workload Assessment*, Symbiotic Interaction, 2017, Springer International Publishing, pp. 102–114.

Orlandi, L.; Brooks, B. Measuring mental workload and physiological reactions in marine pilots: Building bridges towards redlines of performance. Appl. Ergon. 2018, 69, pp. 74–92.

Stojmenova, K. and Sodnik, J.: Detection-Response Task—Uses and Limitations, *Sensors* 2018 Vol. 18, iss. 2, art. 594, doi: 10.3390/s18020594.

APPLICATION OF MULTIPARAMETER PROBES FOR MARINE POLLUTION MONITORING – INTERREG ADRION PROJECT SEAVIEWS

Marija Koričan[1*], Nikola Vladimir[1], Dario Omanović[2], Loukia Prentza[3], Eirini-Asimina Stamatopoulou[3], Nikolaos P. Ventikos[3]

Abstract. *The Interreg ADRION project "Sector Adaptive Virtual Early Warning System for marine pollution" (SEAVIEWS) aims to develop an early warning system that would help to monitor and control marine pollution, so to tackle vulnerability and fragility of ecosystems in the Adriatic Ionian region. The early warning system consists of a transnational network that receives, stores and analyses real-time data about seawater properties. The network includes a set of stationary and moving sensors, in fixed key-locations in the Adriatic-Ionian Region as well as on the vessels. The network of multi-parameters probes collects data, detects environmental anomalies and transfers this information to the SEAVIEWS platform. Simultaneously, SEAVIEWS will also engage the generic public and widen the sources of information through a mobile application targeting different types of end-users. This paper includes a description of the installation process of a multiparameter probe in the Krka River estuary. The criteria for selecting the installation site, the required specifications of sensors and overall contribution to the project outputs are discussed. The multiparameter probe monitors 9 parameters, 6 directly recorded and 3 calculated indirectly. The*

[1] University of Zagreb, Faculty of Mechanical Engineering and Naval Architecture, Ivana Lučića 5, 10002 Zagreb, Croatia

[2] Ruđer Bošković Institute, Bijenička cesta 54, 10000 Zagreb, Croatia

[3] National Technical University of Athens, School of Naval Architecture & Marine Engineering, Zografou 15772, Athens, Greece

[*] Corresponding author: Marija Koričan (marija.korican@fsb.hr)

University of Zadar

early warning system urges local and national authorities to raise awareness on marine pollution issues, engage civil society in the prevention of marine pollution and most importantly it ensures real-time evaluation of the water quality deviations and enables the mitigation of the marine pollution impacts.

Key words: *marine pollution; early warning system; multiparameter probe; sensors; Adriatic Ionian Region*

1 INTRODUCTION

Pollution is a widespread problem that has a negative effect on the marine ecosystem. In recent decades, this issue has been well approached and awareness has significantly raised. Results from the survey in 15 countries showed that the European and Australian public has a great concern about the effect that marine pollution, especially plastic, has on human health (**Davison *et al.*, 2021**). Therefore, regulations are frequently changing with the goal to prevent marine pollution and many investigations are being funded to achieve a better understanding of the problem.

Marine pollution can be triggered by a variety of sources. Its spreading can be uncontrolled and thus can have a negative impact on the marine culture and tourism of a state. The dominant type of pollution varies depending on the area of investigation. For example, states with a higher level of marine traffic have a greater risk of oil spills, while aquaculture areas have a problem with possible chemical anomalies and biological pollution. Major oil spills in the Adriatic-Ionian Sea aren't a frequent occurrence, but smaller-scale oil spills are being detected (**ITOPF, 2021**). They are usually monitored with remote methods, such as passive observation of the sea surface to detect and map oil spills (GPS trackers, drones, satellites etc.). Marine pollution in the coastal area is often triggered by urban sewer outflows during massive rainy events, resulting in negative consequences on the marine environment and tourism in the coastal area (**Ferrarin *et al.*, 2021**). A numerical simulation of different water circulation scenarios in the coastal area of the Adriatic Sea, taking into account the water level, sea temperature, salinity and E.coli concentration, showed the effect that tidal changes have on the mentioned parameters. Dilution and mixing, induced by tidal action, had a greater effect on bacteria reduction with respect to microbial decay, while estuarine dynamics also affected the microbial concentration. Due to the inevitable dynamics, bacteria concentration monitoring presents a challenging

issue (**Ferrarin *et al.*, 2021**). Since the Adriatic Sea is intensively used for various maritime activities (aquaculture, fishing, tourism), aquaculture and agriculture effluents are common pollutants. The dissolution of fish feed and different supplements causes release of nitrogen and phosphorous, as the main end-product of feeding, leading to eutrophication of the marine area. Agriculture and aquaculture production include various offshore and onshore facilities, which along with the marine ports, discharge wastewater and negatively impact the marine environment and human health. In the end, solid waste is a major marine pollution problem most commonly introduced to the general public.

1.1 Scope of the SEAVIEWS project

The Interreg ADRION project "Sector Adaptive Virtual Early Warning System for marine pollution" is a transnational project aimed at tackling environmental vulnerability and preserving the ecosystem in the Adriatic – Ionian area.

The project brings together partners from six countries: Greece as the lead partner, Italy, Croatia, Albania, Montenegro and Slovenia (**Figure 1**). The main task of each partner is to install stationary and/or moving multiparameter probes in the Adriatic Ionian Sea, that will collect data about the seawater quality. The frequent data collection will be further used to develop an innovative early warning system for preventing and managing marine pollution from various sources.

Figure 1. Interreg ADRION – SEAVIEWS Partner Countries.

Another output of the SEAVIEWS project is the establishment of Marine Pollution Hubs serving as focal points for confronting marine pollution at national level. Their mission will be accomplished by raising awareness for environmental issues, engaging stakeholders and policy makers in the prevention of marine pollution and supporting innovation in this sector.

The final step of the project is developing an action plan for the amendment of national and regional strategies for enhancing marine environmental protection. The seawater quality is being monitored by various organisations, usually a national meteorological and hydrological institute, that collects data about different parameters, issues warnings and produces analyses, forecasts and studies. The gathered data are usually subjected to quality control procedures according to the International standards as these are agreed in the context of EU Projects and International Organizations. The SEAVIEWS transnational network will bring together stakeholders, port authorities, governmental bodies and the civic society from the Adriatic-Ionian area to increase awareness regarding marine pollution and propose protocols of action in case of pollution accidents.

1.2 Aims of the SEAVIEWS project

The first aim of the SEAVIEWS project is to provide detailed monitoring for the water quality within the locations with installed sensors, covering a wide range in the ADRION area. This will be accomplished by collecting real-time data from two sources: installed sensors (scientific database) and SEAVIEWS mobile application (general public database).

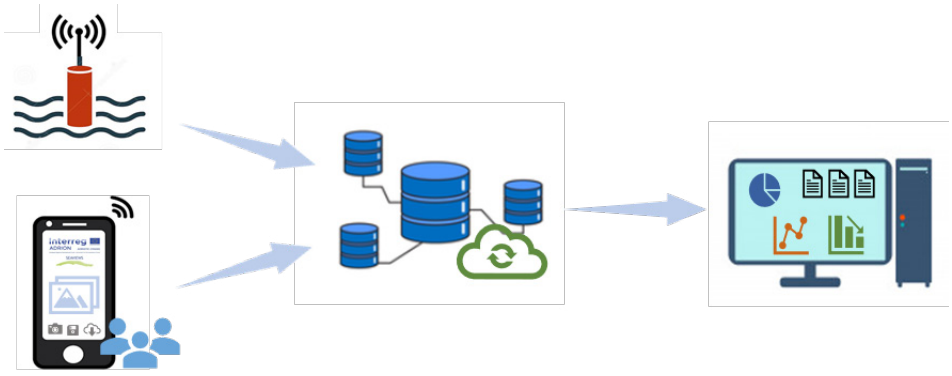

Figure 2. Transnational repository network.

The analysis of the input data will be performed using big data tools and techniques (e.g., machine learning algorithms, trend analysis, gap analysis etc.) as a part of an innovative web-based platform. The goal is to establish a transnational repository network (**Figure 2**) that includes smart sensors, the mobile app, database and servers, control room and the SEAVIEWS platform itself.

The platform will gather information from the sources in the ADRION region and enable sharing and interaction with its users. Therefore, all the data will be analysed to draw necessary conclusions related to potential marine pollution. This enables the achievement of another aim – issuing alerts to relevant stakeholders for potential marine pollution. Early warning on marine pollution enables on-time actions in case of marine pollution incidents.

Raising awareness has a long-term goal to amend the national and regional strategies. The plan is to identify the discrepancies between current and desired levels of environmental safety, and based on the information provided by the SEAVIEWS network, propose improvement actions.

2 METHODOLOGY

The main function of the SEAVIEWS platform is the analysis of data obtained from 18 smart sensors installed across the ADRION area. All partners collect information on 9 different parameters by means of sensors: temperature, salinity, conductivity, pH, dissolved oxygen, ORP (Oxidation-Reduction Potential), turbidity, TDS (Total Dissolved Solids) and depth. Six of the parameters can be directly measured, while others are calculated indirectly.

2.1 Smart sensors network

The multiparameter probe contains several ports (6 to 9, depending on the model) which obtain the required parameters. One of the ports is equipped with an automatic system that cleans the surface periodically, preventing the growth of fouling and organisms that may cause functional impairment of the signal. The probe is additionally characterized by the battery-life length, sampling rate, powering method and other desired specifications.

The remaining ports are used for holding the sensors. The changes of selected parameters can have a highly negative impact on the biological diversity, spreading of bacteria and thermophilic species of tropical algae, and human

activities onshore. For instance, temperature has a significant role in aquaculture and fishing, since it has a great impact on the growth of marine organisms. One example is the effect that warming and ocean acidification have on coral reefs and gastropods, which have an important function in maintaining the stability of the coral reef ecosystem (**Zhang *et al.*, 2021**). A 28-day exposure experiment to acidic (pH 7.6) and/or seawater with a temperature of 30 °C, showed the changes in immune responses, oxidative stress, neurotoxicity and energy metabolism. Higher temperature and acidification caused physiological disturbances in form of weakening the top-shells of gastropods, thus threatening the viability of the species. This could further indulge the proliferation of algae, triggering the degradation of coral reefs (**Zhang *et al.*, 2021**). On the other hand, research on the impact of warming on marine diatoms (type of phytoplankton) showed that the disorders caused a natural adaptation of the species. (**Zhong *et al.*, 2021**). Rise of water temperature can also increase the risk of water-borne diseases. Rising water temperatures in the Baltic Sea due to climate change are also contributing to the further spread of "oxygen-depleted" dead zones, causing the mortality of marine organisms. Salinity variations, due to the inflow of freshwater or increase in precipitation, can also affect the development of marine organisms, especially crustaceans. Another problem is acidification, as a result of absorbing a larger amount of carbon dioxide into the ocean and producing carbonic acid, which prevents crustaceans to build strong shells or skeletal materials making them more vulnerable. Acidification can also affect the photosynthesis of marine plants (**EEA, 2021**).

The pharmaceutical industry also has a negative effect on the marine environment. Pharmaceutical residues, especially antihypertensives, under different acidification scenarios, have a negative biological effect on marine ecosystem (**Pusceddu *et al.*, 2021**). The study showed that losartan, a pharmaceutical compound, has a negative impact on the marine ecosystem and the effect is increased by raising the level of acidification. Further research is needed to evaluate the mutual influence between pharmaceutical residues and acidification, and the level of ecotoxicity (**Pusceddu *et al.*, 2021**).

Sixteen probes are stationary while 2 probes are equipped with a long cable to enable mobility of the sensors. The collected data are sent to a PC located near the installation location. A purpose-developed software is used to receive the data from the multiprobe and the data are sent to the database for further processing. The overall data from the network of multiparameter probes will be collected and

stored in the central database managed by the lead partner. A data backup is stored in a cloud system.

2.2 Data processing

The database stores and manages the information collected from the network with a fine time granularity leading to a vast amount of data. The data, in this case, come from two sources: the sensors and the SEAVIEWS mobile application. The database serves as a central data repository, receiving and transferring the appropriate data to the appropriate location. Therefore, it enables data interchanging between the SEAVIEWS platform and the two other components (sensors and mobile application).

The sensors will collect values of 9 water quality parameters and send them to the platform every 15 minutes. The parameter values will be accompanied by a timestamp, the location of the sensor and the name of the sensor. Through the database, this information will be sent to the platform for further analysis. At first level, the developed software of the platform will perform data consolidation and analysis in order to serve the different user queries (figures, datasets for specific periods and parameters). This information will be also illustrated in an interactive map where the current values of the different parameters will be depicted.

The warnings will be executed by issuing real-time alerts in case of marine pollution incidents by considering out of limit parameter values from the sensors. The early warning algorithm is based on normal, abnormal and reference values and recognize unusual patterns in the parameters value distribution from the existing data. A machine learning algorithm will be used to make marine pollution predictions and issue early warning alerts. Before its implementation, detailed research of possible options will be performed to find the optimal solution for the project. The early warning system will warn users of three types of pollution, namely oil spill incident, eutrophication and effluents through data from the mobile app.

The data gathered by SEAVIEWS mobile app include photos of marine pollution incidents, short descriptions, GPS coordinates and timestamps of the entry, sent by public users. The information collected through the mobile app will be also sent to the platform for further analysis. The photos sent by public users will be checked and validated prior to their uploading.

3 PROJECT IMPLEMENTATION IN CROATIA

The Croatian coastline (**Croatia.eu, 2021**) occupies most of the eastern Adriatic shoreline. The Adriatic Sea is relatively shallow, the north part is shallower than 100 m and the deepest part equals 1,228 m in the south. The Croatian part of the Adriatic area is characterized by the Dalmatian type of shoreline, which has a significant impact on marine culture and tourism. Five main rivers drain towards the Adriatic Sea – Neretva, Lika, Zrmanja, Krka and Cetina. Due to the inflow of fresh water from rivers and springs, the salinity of the Adriatic Sea is slightly lower than the salinity of the eastern Mediterranean (average 38.30%). The mouths of the rivers are often used for the development of aquaculture. Except for aquaculture production, there are numerous fishing grounds of white and blue fish, offshore and around islands, while the water is rich in different types of crustaceans. The natural characteristics of the Adriatic Sea, such as clarity and transparency of the sea and mild Mediterranean climate, enabled Croatia to develop a strong tourist-oriented industry. The increase in the number of tourists every year also increases the level of maritime traffic, especially in summer when tourism is at its peak (**Europe.eu, 2021**). The frequent traffic of a variety of ships makes the Adriatic sea an environmentally sensitive area and the possibility of pollution increases with the advancement of the industry.

For the SEAVIEWS project, the mouth of the Krka River, near Šibenik, has been chosen for the study location (**Figure 3**). The Krka River estuary is a Natura 2000 site under the name "Krka Mouth" and it is also a Marine Protected Area (MPA) region. It is characterised by brackish surface water and the bottom seawater layer. Many aquaculture plants for mussels and fish farming are mainly located in the lower part of the estuary. There are three main reasons for choosing an aquaculture field for the SEAVIEWS study area:

- the low salinity is not tolerable for the mussels and fish and mortality can occur,
- the increased copper concentration can be harmful to the mussel embryos as well as for the fish,
- the monitoring of water quality is essential for the growth and reproduction of species.

The Croatian partner has a task to install one multiparameter probe in the location of interest (**Figure 4**). The study location incorporates a small platform with electricity, which facilitates the problem of the connection of sensors with a

Figure 3. The location of the SEAVIEWS study area in Croatia.

Figure 4. Aquaculture farm, Krka River, Croatia.

PC and internet connectivity. Since the platform is protected with a roof, the problem of protection in bad weather conditions has also been eliminated. The aquaculture farm and the platform are permanently protected by a guard-person. Also, a marine station is located nearby, which serves as a logistic support. The areas are well connected and easily approachable by a research vessel.

Figure 5. EXO2 Multiparameter sonde. (**YSI**, **2021**)

The EXO2 multiparameter sonde is used (**YSI, 2021**), presented in **Figure 5**. The EXO2 sonde is a multiparameter water quality sonde with 7 sensor ports, including a central wiper port. The available 6 ports hold the sensors for temperature, conductivity, pH/ORP, dissolved oxygen, turbidity and depth. Other parameters will be calculated indirectly. The data will be collected and exported in various formats, thus adapting the format to the needs of the project.

4 RESULTS

First measurements have been performed in August 2021 (**Figure 6**). This paper brings measurement results from October to November 2021 (**Figure 7**) and compares them to the results in summer time.

The water temperature in August ranged from 24 °C to 28 °C, while in November the temperature dropped to a minimum of 16 °C, as expected for winter months. According to **FAO** (**1993**), the optimum performance for the majority of fish species is at 15 °C. At temperatures below 20 °C fishes consume more food. The pH in November is slightly higher, with an average 8.06. In August the average pH was 7.8. The optimal pH range is 6.5 – 8.5 (**FAO, 1993**) so the results still show good

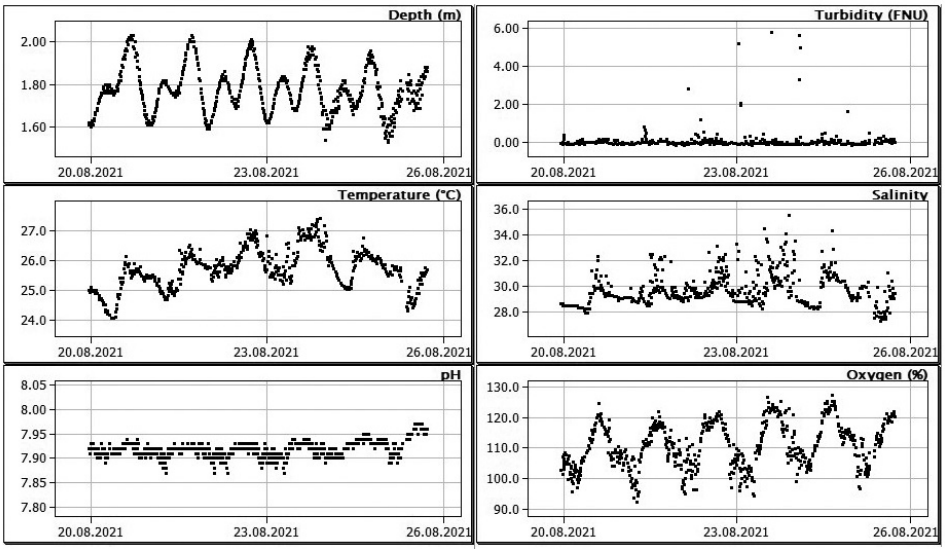

Figure 6. Water quality parameters – August 2021.

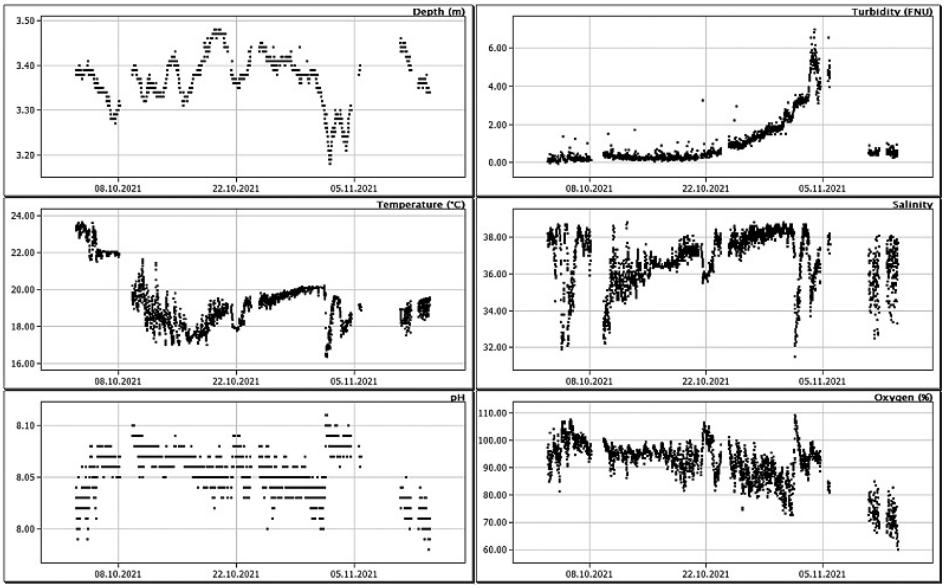

Figure 7. Water quality parameters – October/November 2021.

values. Oxygen requirements depend on the species and the concentration increases at a higher temperature. Therefore, it was expected to achieve lower values in colder weather. In August the oxygen concentration ranged from 90 % to 130 %, while in November these values were significantly lower, with a maximum of 110 %. In October these values ranged from 85 % to 105 %, while in November, at lower temperatures, they were ranging from 60 % to 85 %. Salinity is a major issue in the study area and its value depends mainly on the inflow of freshwater. The results in October and November are similar to the ones from August. Salinity presents a critical parameter in the aquaculture farm since it can increase the mortality of species (**FAO, 1993**). The greatest disturbances are visible in turbidity. In August, the turbidity values ranged from 0.01 FNU to 0.78 FNU (Formazin Nephelometric Unit). At the end of October, the values start to increase. At the beginning of November, the values reached a maximum at approximately 6 FNU, after which the values dropped to 0.70 FNU. The changes in turbidity may be triggered by the increase in measuring depth, fouling of the multiprobe, silt and mud due to bad weather, etc. The maximum in November was reached at the same time the depth decreased from 3.50 m to 3.20 m. Graphs from October and November show short gaps in the measurements. The first gap, visible in the first part of October, was the result of removing the multiprobe from the water due to cleaning from fouling. The second gap, at the begging of November, is the result of short-term electricity loss.

Based on the gathered data, it can be concluded that the measuring system is fully functional and it can provide useful information on water quality at a target location over a longer period. Therefore, it is fully integrable into the SEAVIEWS platform.

5 CONCLUSIONS

In the first phase of the project, a network of sensors was established and the foundations were laid for the development of the SEAVIEWS platform. A project plan has been set up, which includes the technical and promotional parts of the project implementation. The next step is data collecting and analysis, which will further be used for the development of the SEAVIEWS mobile application and preparation of improvement actions which will be issued at the end of the project. The results gathered in summer and winter showed the effect that temperature changes have on water quality parameters. Since the multiparameter probe is installed on an aquaculture area, it is reasonable to assume that the results are also affected by the movements of marine organisms, the dissolution of food and other chemicals. A larger database will enable us to observe which disruptances

are triggered by changes in environmental conditions, and which are caused by human activities. The key part of the project is promoting the results of the project to raise general awareness and enhance marine environmental protection.

Acknowledgements

This research was co-funded by a European transnational programme INTERREG V-B Adriatic-Ionian ADRION Programme 2014-2020, under the project Sector Adaptive Virtual Early Warning System for marine pollution (SEAVIEWS), (Project No. ADRION-951).

Disclaimer

REFERENCES

Croatia.eu (2021). https://www.croatia.eu/index.php?view=article&id=11&lang=2, accessed 09 April 2021.

Davison S.M.C, White M.P., Pahl S., Taylor T., Fielding K., Roberts B.R., Economou T., McMeel O., Kellett P., Fleming L.E. (2021). Public concern about, and desire for research into, the human health effects of marine plastic pollution: Results from a 15-country survey across Europe and Australia. *Global Environmental Change.* Volume 69. 102309. ISSN 0959-3780. https://doi.org/10.1016/j.gloenvcha.2021.102309.

Europe.eu (2021). https://ec.europa.eu/info/sites/info/files/economy-finance/eb036_en.pdf, accessed 09 April 2021.

European Environmental Agency (2021). https://www.eea.europa.eu/, accessed 10 April 2021.

Ferrarin C., Penna P., Penna A., Spada V., Ricci F., Bilić J., Krzelj M., Ordulj M., Šikoronja M., Đuračić I., Iagnemma L., Bućan M., Baldrighi E., Grilli F., Moro F., Casabianca S., Bolognini L., Marini M. (2021). Modelling the Quality of Bathing Waters in the Adriatic Sea. *Water*. 13(11):1525. https://doi.org/10.3390/w13111525.

Food and Agriculture Organization (FAO) (1993). Water quality and fish health, http://www.fao.org/3/t1623e/t1623e.pdf (accessed 08 November 2021).

ITOPF website, Countries and Territories Documentation (2021). https://www.itopf.org/knowledge-resources/countries-territories-regions/, accessed 10 April 2021.

OTT. Hydrolab HL7 sonde (2021). https://www.ott.com/products/water-quality-2/hydrolab-hl7-multiparameter-sonde-2338/, accessed 09 April 2021.

Pusceddu F.H., Guimarães M.M., Lopes L.O., Souza L.S., Cortez F.S., Pereira C.D.S., Choueri R.B., Cesar A. (2021). Biological effects of the antihypertensive losartan under different ocean acidification scenarios. *Environmental Pollution.* 118329. ISSN 0269-7491. https://doi.org/10.1016/j.envpol.2021.118329.

YSI. EXO2 Multiparameter sonde (2021). https://www.ysi.com/exo2, accessed 09 April 2021.

Zhang T., Qu Y., Zhang Q., Tang J., Cao R., Dong Z., Wang Q., Zhao J. (2021). Risks to the stability of coral reefs in the South China Sea: An integrated biomarker approach to assess the physiological responses of Trochus niloticus to ocean acidification and warming. *Science of The Total Environment*. Volume 782. 146876. ISSN 0048-9697. https://doi.org/10.1016/j.scitotenv.2021.146876.

Zhong J., Guo Y., Liang Z., Huang Q., Lu H., Pan J., Li P., Jin P., Xia J. (2021). Adaptation of a marine diatom to ocean acidification and warming reveals constraints and trade-offs. *Science of The Total Environment*. Volume 771. 145167. https://doi.org/10.1016/j.scitotenv.2021.145167.